

**Cyclic Dynamics of Spatially Heterogeneous
Populations**
—
From Biodiversity to Disease Prevalence

Dissertation
zur Erlangung des mathematisch-naturwissenschaftlichen Doktorgrades

“Doctor rerum naturalium”

der Georg-August-Universität Göttingen

vorgelegt von
David Lamouroux
aus Köln

Göttingen 2012

Mitglied des Betreuungsausschusses: Prof. Dr. Theo Geisel (Referent)
MPI für Dynamik und Selbstorganisation, Göttingen &
Georg-August-Universität Göttingen

Mitglied des Betreuungsausschusses: Prof. Dr. Fred Wolf
MPI für Dynamik und Selbstorganisation, Göttingen

Mitglied des Betreuungsausschusses: Prof. Dr. Marc Timme
MPI für Dynamik und Selbstorganisation, Göttingen

Mitglied der Prüfungskommission: Prof. Dr. R. Kree (Korreferent)
Georg-August-Universität Göttingen

Mitglied der Prüfungskommission: Dr. Oskar Hallatschek
MPI für Dynamik und Selbstorganisation, Göttingen

Mitglied der Prüfungskommission: Prof. Dr. U. Parlitz
MPI für Dynamik und Selbstorganisation, Göttingen

Tag der mündlichen Prüfung: 14.12.2012

Hiermit versichere ich, dass ich die vorliegende Arbeit selbstständig und nur mit den angegebenen Quellen und Hilfsmitteln angefertigt habe.

Göttingen, November 2012

David Lamouroux

List of abbreviations

CGLE	– complex Ginzburg-Landau equation	– see Sec. 2.2.3
c.d.f.	– cumulative distribution function	– see Sec. 2.3
FPE	– Focker-Planck equation	– see box Interlude II on page 8
LBPM	– lattice-based population model	– see Sec. 2.2
ME	– master equation	– see box Interlude II on page 8

Contents

Contents	v
1 Introduction	1
2 The Rock-Paper-Scissors Game	5
2.1 Introduction	5
2.2 A Lattice-based Population Model	11
2.2.1 Deterministic Dynamics	12
2.2.2 Pattern Formation in 2-dimensional Systems	16
2.2.3 The Spiraling State and the Complex Ginzburg-Landau Equation	19
2.2.4 The Well Stirred State and its Stochastic Mean Field Dynamics	23
2.3 Pathes to Extinction	25
2.3.1 Traveling Planar Waves vs. Traveling Spiral Waves	27
2.3.2 Scaling with the System's Size N	29
2.3.3 Scaling with the Carrying Capacity C	32
2.4 Sequential and Parallel Update Schemes	35
2.5 More than Three Species	37
2.6 Discussion	44
3 Immunity Eliciting Diseases	47
3.1 Introduction	47
3.2 A Metapopulation Model for Spatially Varying Infectiousness	49
3.2.1 Nonspatial Compartmental Model	49
3.2.2 Metapopulation Model	51
3.2.3 Paradoxical Effects of Coupling	53
3.2.4 Reduction of Spatial Complexity	64
3.2.5 Effective Coupling, Migration, and Home Locations	69
3.3 Waning Immunity	74
3.4 Discussion	76
4 Conclusions and Outlook	81
Acknowledgments	87
Bibliography	89

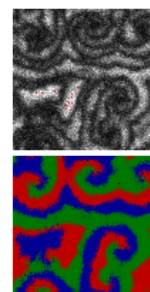
CONTENTS

Chapter 1

Introduction

The field of population dynamics is concerned with the composition and size of populations and their temporal evolution. This applies to ecosystems where different species compete with each other for limited resources as well as to epidemics, whose temporal evolution is determined by the interaction of healthy and ill individuals. In fact, ecology and epidemiology treat basically the same questions: How is the population influenced by environmental and biological factors? How does the interaction of subpopulations or species shape their respective temporal evolution? A common phenomenon is that the interaction of subpopulations or species leads to oscillations of their population sizes: This *cyclic population dynamics* is of central importance both for ecological systems (Murray, 1993; Kaitala et al., 1996) and epidemiological systems (Anderson and May, 1991) – albeit with fundamentally different causes.

In epidemiology, cyclic population dynamics is almost self-evident for diseases like measles or mumps, where infected individuals acquire life-long immunity upon recovery. For these diseases susceptible individuals become infectious individuals by contracting the disease and once they are infectious, they recover and become immune. The susceptible population is constantly replenished since all newborns are susceptible to the disease (Anderson and May, 1991). On the population level this induces a cycle where a population goes through a susceptible phase, enters an infectious phase, recovers to an immune phase and eventually returns to the susceptible phase. Cyclic population dynamics, hence, ensures the persistence – or recurrence – of the infectious population. In ecology, one instance where cyclic population dynamics emerges is when different species cyclically compete with each other. Cyclic competition was identified as a mechanism that acts as to preserve the equilibrium of different populations (Gilpin, 1975; May and Leonard, 1975). Until then (Hardin, 1960) and even afterwards (den Boer, 1986), it was believed that any ecological niche can only sustain a single species because any albeit small fitness difference of two species will eventually lead to the extinction of the inferior one. The idea that species do not necessarily dominate each other in a hierarchical manner, provides a mechanism that explains the preservation of greater biodiversity (Gilpin, 1975): If three species dominate each other cyclically, i.e., species A is superior to species B, which is superior to species C, but species C in turn is superior to species A, all three species are cyclically predominant in the ecosystem



and can persist in coexistence (May and Leonard, 1975).

A core issue in ecology and epidemiology consequently is the persistence of populations, i.e., the stability of equilibrium states. In this regard, Earn et al. (1998) have emphasised how valuable research in one field has been for the respective other field – although the objectives oppose one another: In ecology, the survival of populations is a major goal and the loss of biodiversity is a danger (Schipper et al., 2008). The purpose of understanding the population dynamics in ecosystems is thus to devise strategies that prevent extinction events (see Sahasrabudhe and Motter, 2011, and references therein). In epidemiology, on the contrary, the survival of potentially harmful infectious populations is the danger and eradication the goal. The purpose of understanding the population dynamics is thus to design control strategies that eradicate a disease or stem its proliferation (May and Anderson, 1984; Lloyd and Jansen, 2004; Ferguson et al., 2006).

A fine example of an aspect that was first introduced in ecological research and that is valuable in the field of epidemiology is spatial heterogeneity. It was first recognised for ecological populations that the spatial segregation of subpopulations plays an important role for the persistence of the overall population. The idea of a “population of populations” (Hanski and Gilpin, 1991) was first conceptualised as a *metapopulation* by Levins (1969). It accounts for the fact that animals interact with one another on a local scale in their subpopulation (like swarms, herds, or flocks) while they occasionally relocate to a different region or different subpopulation. This concept could be readily applied to epidemiological models since human populations naturally segregate into well-defined subpopulations like villages, cities, or any other social aggregations (Grenfell, 1992; Bolker and Grenfell, 1995; Hagensaaers et al., 2004). This conjunction of cyclic population dynamics and spatial heterogeneity has substantially contributed to the explanation of the high level of persistence of diseases, which could not be explained in non-spatial models (Bartlett, 1957; Nåsell, 1999).

In both epidemiology and ecology, spatial heterogeneity reduces the likelihood of extinction of the global population (of infectious individuals or a certain biological species) because this requires that all subpopulations become extinct simultaneously. It comes therefore as no surprise that epidemiologists consider synchronous dynamics of all subpopulations as desirable (Grenfell et al., 1995; Lloyd and May, 1996) whereas ecologists seek means to prevent synchronous dynamics (Heino et al., 1997; Keeling, 2000).

In ecology, the interplay of cyclic competition and a spatially extended environment attracted a lot of attention when Czárán et al. (2002) and Kerr et al. (2002) found non-hierarchical competition experimentally between three strains of *E. coli* bacteria. They observed that the three strains can coexist when their dispersal is only local whereas coexistence is quickly lost when they disperse on a much larger scale. Reichenbach et al. (2007a) then found that the dispersal of individuals is critical to the emergence of spiral patterns in a lattice-based model system of three cyclically competing species. These patterns, in turn, induce a transition from unstable coexistence to stable coexistence, whose characterisation becomes better the larger the population size. In their study, however, the population size and the spatial size of the system is identical because the

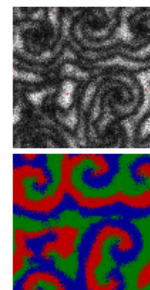
scale at which individuals interact and the scale at which individuals disperse is the same. Yet this equality restricts the capability to characterise the transition, while it is of central importance in ecology to understand under which conditions a biodiverse ecosystem collapses to a monocultural system.

In Chapter 2, I therefore introduce a lattice-based population model for three cyclically competing species that separates the local scale at which individuals interact from the meta-scale at which they migrate, following the idea of a “population of populations” (Hanski and Gilpin, 1991). This model allows to study stability properties of the coexistence separately in dependence on the population size and the spatial size. In contrast to earlier works (Reichenbach et al., 2007a), I show that the emergence of spiral patterns is related but not equivalent to the emergence of stable coexistence. Instead, I demonstrate that the scale separation allows to sharply determine the conditions at which the emergence of patterns merely begins to stabilise biodiversity.

In order to study the *emergence* of cyclic competition among three species, I also consider in Chapter 2 a system of four species that spatially compete. For this purpose, the lattice-based population model can be easily extended to more than three species. Since the four species cannot coexist in equilibrium (as shown in Chapter 2), one species quickly becomes extinct and leaves behind a system of three species. I thus determine under which conditions the competition among the remaining three species is either cyclic or hierarchical. I show that cyclic competition emerges when the four species disperse on a local scale while a hierarchical competition emerges when individuals disperse on a larger scale. Local dispersal is thus not only critical to the stability but also to the emergence of cyclic competition among species.

In epidemiology, the conjunction of spatial heterogeneity and cyclic population dynamics is long known to, e.g., alter the demands on control measures like vaccination strategies (May and Anderson, 1984; Hethcote and van Ark, 1987). Yet the recent threat of different pandemics has triggered a lot of attention to epidemiological models that consider large spatial scales (Hufnagel et al., 2004; Ferguson et al., 2006; Epstein et al., 2007; Bajardi et al., 2011). In a modern world, which becomes ever more connected, the impact of different regional climatic conditions or health regulations on disease properties like the infection rate becomes ever more important. However, only rarely have studies accounted for this variation (Grassly et al., 2005) and most epidemiological models assume a spatially homogenous infection rate (May and Anderson, 1984; Hethcote and van Ark, 1987; Grenfell, 1992; Lloyd and May, 1996; Keeling, 2000; Xia et al., 2004; Hagenaars et al., 2004). Studying the impact of a spatially varying infection rate, however, is not only essential for the understanding of disease dynamics on a larger scale. It is also crucial for the design of containment measures such as vaccination strategies or travel restrictions.

In contrast to existing studies, I consider – in Chapter 3 – a metapopulation model for an epidemic in which the risk of infection explicitly depends on the location where the disease is contracted. This framework takes thus a regionally varying infection rate into account that arises when societal, cultural, or environmental differences are relevant for local disease properties. I analyse how coupling influences the different subpopulations



to demonstrate that the impact is fundamentally different from the situation in which the infection rate is constant throughout the metapopulation. I show that the level of infection can paradoxically increase upon coupling to a region with a lower level of infection.

Furthermore, I study in Chapter 3 whether the influence of a group of populations on a focal population – like a group of satellite villages surrounding a central city – can effectively be modelled as the influence of a single ‘surrounding’ population. This pertains to the question: Which degree of heterogeneity has to be taken into account to capture the relevant dynamics of the system? I demonstrate that the heterogeneity of the satellite populations can be absorbed into the parametrisation of a substitute surrounding population if the levels of infection are either all smaller or all larger than that in the focal population. Allowing for a regional variation of disease properties is, hence, substantial for epidemiological models of a modern world.

Chapter 2

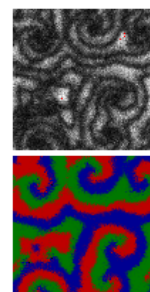
The Rock-Paper-Scissors Game

2.1 Introduction

The question “Why are there so many species?” is posed in many ecosystems where the explanation of the high number of species presents a long standing challenge (cf. Hutchinson, 1959; Ranta and Vepsäläinen, 1981), which is still subject to investigations (cf. Dykhuizen, 1998; Novotny et al., 2006). Biological studies have devised plenty and some quite specific explanations, including but not limited to a high speciation rate, the lack of competition due to spatial heterogeneity, or the almost manifest explanation that there are simply unexpectedly many ecological niches. A principle that coined the early debate during the second half of the last century is called the *competitive exclusion principle* (Hardin, 1960; Armstrong and McGehee, 1980; den Boer, 1986). It basically states that the number of sustainably coexisting species cannot exceed the number of abiotic resources or more generally the number of ecological niches. The rationale behind this principle is the idea that any difference between species in the ability to exploit a certain resource will inevitably lead to the eventual extinction of the inferior one. In quite similar studies, Gilpin (1975) and May and Leonard (1975) established that the *competitive exclusion principle* only applies to special cases and that a single resource allows even more than two species to coexist. The crucial aspect of their model was a non-hierarchical (or cyclic) competition between the species, which – depending on the set of parameters – can lead to either stable, marginally stable or unstable coexistence (see box **Interlude I: Deterministic linear stability**).

To illustrate this kind of non-hierarchical relationships, Gilpin uses the following example: “In pure exploitation competition for a single resource, species 1 is the best, 2 is next best, and 3 the worst. Species 1 eliminates 2 in pairwise competition, and 2 eliminates 3 in pairwise competition, but 3 excretes a substance that is uniquely and completely poisonous to 1. Species 3 can therefore eliminate 1. That is, 1 better than 2, 2 better than 3, but 3 better than 1” (Gilpin, 1975). This example of three species that compete cyclically corresponds to the well known Rock-Paper-Scissors Game.

Although the theoretical basis was provided quite early and non-hierarchical relations were suggested as explanations for the high level of diversity in coral reef invertebrates



Interlude I: Deterministic linear stability

Consider a dynamical system that is described by its state vector $\mathbf{x} \in \mathbb{R}^d$ and its temporal evolution

$$\dot{\mathbf{x}} = \mathbf{f}(\mathbf{x}) \quad (2.1)$$

where $f : \mathbb{R}^d \mapsto \mathbb{R}^d$. A *fixed point* \mathbf{x}_s of the dynamical system is a state in which the system remains unchanged unless a perturbation occurs, i.e. $\mathbf{f}(\mathbf{x}_s) = 0$. The fixed point can be further characterised by its response to infinitesimal perturbations. If the system returns to the fixed point after a small perturbation, it is said to be *stable*. If the perturbation grows and the system moves away from the fixed point, it is said to be *unstable*. If the perturbation neither grows nor decays, the fixed point is said to be *marginally stable*. To determine the stability of the fixed point, the equations for the temporal evolution are linearised around the fixed point, i.e. the quantity

$$\mathcal{L}_s = \left. \frac{\partial \mathbf{f}(\mathbf{x})}{\partial \mathbf{x}} \right|_{\mathbf{x}=\mathbf{x}_s} \quad (2.2)$$

is considered, which describes the temporal evolution in the vicinity of the fixed point. Defining $\mathbf{y} := \mathbf{x} - \mathbf{x}_s$ the temporal evolution in the vicinity of \mathbf{x}_s (i.e. for small $|\mathbf{y}|$) is thus governed by:

$$\dot{\mathbf{y}} = \mathcal{L}_s \mathbf{y} \quad (2.3)$$

Since this is a linear differential equation, the behavior of its solutions can be classified by the eigenvalues of \mathcal{L} (see Strogatz, 1994, for an inclusive description): If the real part of all eigenvalues is negative, \mathbf{x}_s is a *stable* or attracting fixed point. If the real part of any single eigenvalue is positive, \mathbf{x}_s is an *unstable* or repelling fixed point. If the real parts of the eigenvalues are all negative except for at least one that is zero, \mathbf{x}_s is a *marginally stable* fixed point.

(Jackson and Buss, 1975), the field only gained new momentum when empirical studies observed non-hierarchical relations in nature. To this day, cyclic competition has been observed in a wide range of ecosystems, including *E. coli* bacteria (Czárán et al., 2002; Kerr et al., 2002), parasite-grass-forb communities (Cameron et al., 2009) and lizard populations (Sinervo and Lively, 1996; Corl et al., 2010). Nonetheless, cyclic competition might seem to be a peculiarity of these systems. Allesina and Levine (2011), however, have recently shown that cyclic competition is the rule rather than the exception if species compete for several resources instead of a single one.

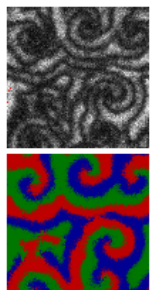
Yet cyclic competition is not limited to biological systems of competing species. The well-known Prisoner's Dilemma is a game theoretical paradigm for cooperative situations between two agents in which the dominant strategy keeps the agents from receiving the maximum pay-off (Nowak, 2007). Hauert et al. (2002) and Szabó and Hauert (2002) proposed to ease the Prisoner's Dilemma by the introduction of a third

strategy that does not partake in the game but rather resorts to a fixed payoff. This third strategy basically turns the Prisoner's Dilemma into a Rock-Paper-Scissors game. It was not until the 1990s in the field of evolutionary game theory that spatial aspects and stochasticity were recognised to play an important role concerning the persistence of coexistence of strategies or species (Nowak and May, 1992, 1993; Nowak et al., 1994a,b; Durrett and Levin, 1994). Spatial and stochastic models for three cyclically competing species (Hassell et al., 1994; Durrett and Levin, 1997, 1998; Zhang et al., 2006) and more (Szabó and Czárán, 2001b,a; Szabó and Sznaider, 2004; Szabó et al., 2008) were subsequently studied, establishing that space can have a stabilising influence on the population dynamics.

The inclusion of stochasticity – arising from the finite number of individuals and the stochastic interaction between them – introduced, however, the new problem to properly characterise the stability of coexistence in such systems. In any stochastic birth-death process with a per capita birth and death rate the only *absorbing state* – i.e. a state that cannot be left (even not by chance) – is the state where all individuals have died out (see box **Interlude II: Stochastic description of birth-death processes** on page 8). A stochastic system of cyclically competing species will thus at some point always reach the state where only one species prevails.

Frey and Reichenbach (2011) have thus devised new definitions of what stability in stochastic population systems mean. They categorise the stability of stochastic systems by the dependence of the average time τ_{ex} it takes to reach the absorbing state on the size of the system N . They argue that in an *unstable* system, which is systematically driven towards the absorbing state, τ_{ex} grows logarithmically with the system size, i.e. $\tau_{\text{ex}}(N) \propto \ln(N)$. In a *marginally stable* system, in which the birth and death processes balance each other on average, such that there is no drift in any direction, any time scale in such a system is proportional to the system size, i.e., $\tau_{\text{ex}}(N) \propto N$. In a *stable system*, which is driven away from the absorbing state, τ_{ex} will grow exponentially with N , i.e. $\tau_{\text{ex}}(N) \propto \exp(N)$. While this is certainly not a mathematically strict definition of stability, it provides a classification that can serve to reasonably distinguish different stability regimes in stochastic population dynamics.

The stabilising influence of space on the dynamics of the Rock-Paper-Scissors game was known to be related to the formation of rotating spiral waves from the first spatial models (Hassell et al., 1991; Nowak et al., 1994a). Yet it was only conjectured that there must be a connection between the characteristic length of the spatial patterns and the stability of the coexistence of the three species (Hassell et al., 1994). Reichenbach et al. (2007a) found this connection when they were studying a spatial and stochastic system of three cyclically competing species that also form spiral patterns. In their model, individuals move diffusively in a square lattice while they compete with other individuals and reproduce. The central quantity in their study is the mobility of individuals. They find that the wavelength of the spirals (their characteristic length scale) grows with the individual's mobility as $\lambda \propto \sqrt{M}$. This implies that the extent of the spirals outgrows the extent of any finite system with growing mobility. When the wavelength becomes larger than the system size, the spirals collapse or cannot form and thus not maintain coexistence. The mobility M is therefore a pivotal quantity



Interlude II: Stochastic description of birth-death processes

The temporal evolution of the state of a stochastic system is not predictable as opposed to deterministic systems where the temporal evolution can be perfectly predicted. It is rather of interest to ask for the probability of the stochastic system $P(\mathbf{s}, t)$ to be in a certain state $\mathbf{s} \in \mathbb{R}^d$ at time t . The temporal evolution of $P(\mathbf{s}, t)$ is then given by the **Master Equation** (abbreviated with ME in the following) (the description in this Interlude closely follows Gardiner, 2009):

$$\partial_t P(\mathbf{s}, t) = \sum_{\Delta \mathbf{s}} [W(\mathbf{s} | \mathbf{s} + \Delta \mathbf{s}, t) P(\mathbf{s} + \Delta \mathbf{s}, t) - W(\mathbf{s} + \Delta \mathbf{s} | \mathbf{s}, t) P(\mathbf{s}, t)] \quad (2.4)$$

Here, $W(\mathbf{s} + \Delta \mathbf{s} | \mathbf{s}, t)$ is the transition probability, which is the scaled limit of the *jump probability* $p(\mathbf{s} + \Delta \mathbf{s}, t + \Delta t | \mathbf{s}, t)$:

$$W(\mathbf{s} + \Delta \mathbf{s} | \mathbf{s}, t) = \lim_{\Delta t \rightarrow 0} \frac{1}{\Delta t} p(\mathbf{s} + \Delta \mathbf{s}, t + \Delta t | \mathbf{s}, t), \quad |\Delta \mathbf{s}| \geq \varepsilon > 0 \quad (2.5)$$

$p(\mathbf{s}_2, t_2 | \mathbf{s}_1, t_1)$ denotes the conditional probability that the system changes its state by $\Delta \mathbf{s}$ during the time interval $[t, t + \Delta t]$. The ME describes jump processes, which means that the state variable of any realization, i.e. actual observed process, typically remains unchanged until it is abruptly changed by a finite value. Any sample path $\mathbf{s}(t)$ will thus be non-continuous in time. If \mathbf{s} describes a stochastic birth-death process, only jumps of finite and integer order occur and $\mathbf{s} \in \mathbb{N}_+^d$. The temporal evolution of the stochastic process is then governed by a discrete set of reactions \mathcal{M} and we can rewrite the ME in a more intuitive form:

$$\begin{aligned} \partial_t P(\mathbf{s}, t) = \sum_{m \in \mathcal{M}} [& t_m^+(\mathbf{s} - \mathbf{r}_m) P(\mathbf{s} - \mathbf{r}_m, t) - t_m^-(\mathbf{s}) P(\mathbf{s}, t) \\ & + t_m^-(\mathbf{s} + \mathbf{r}_m) P(\mathbf{s} + \mathbf{r}_m, t) - t_m^+(\mathbf{s}) P(\mathbf{s}, t)] \end{aligned} \quad (2.6)$$

t_m^+ and t_m^- denote the transition probability per unit time (similar to $W(\mathbf{s}_2 | \mathbf{s}_1, t)$ in Eq. (2.4)) of the m^{th} reaction and its inverse counterpart, respectively (see Gardiner, 2009, for more details). \mathbf{r}_m is the difference by which the m^{th} reaction changes the state of the stochastic system. The only stable states of stochastic systems are those that cannot be left. Mathematically speaking, an absorbing state \mathbf{s}_A is defined by the property $t_m^\pm(\mathbf{s}_A) = 0 \forall m \in \mathcal{M}$.

The ME is, in general, not analytically solvable. An equation that is analytically more tractable is the **Fokker-Planck Equation** (abbreviated with FPE in the following). As opposed to the ME, it describes diffusion processes, which have continuous but nowhere differentiable sample paths. Although the two equations describe basically different stochastic processes, the FPE can be considered to be an approximation of the ME for large systems.

In the following, the size of the stochastic system (or the thermodynamic volume) is denoted by Ω . If the transition probabilities t_m^\pm are proportional to Ω , it is

possible to perform van Kampen's system size expansion as well as the Kramers-Moyal expansion, whose first two terms are asymptotically the same (see Gardiner, 2009, for details). Truncating these expansions to second order, yields the FPE:

$$\partial_t P(\mathbf{s}, t) = - \sum_{i=1}^d \frac{\partial}{\partial s_i} [A_i(\mathbf{s}) P(\mathbf{s}, t)] + \frac{1}{2} \sum_{i,j=1}^d \frac{\partial^2}{\partial s_i \partial s_j} [B_{ij}(\mathbf{s}) P(\mathbf{s}, t)] \quad (2.7a)$$

$$\text{with } A_i(\mathbf{s}) = \sum_{m \in \mathcal{M}} r_{m,i} [t_m^+(\mathbf{s}) - t_m^-(\mathbf{s})] \quad (2.7b)$$

$$\text{with } B_{ij}(\mathbf{s}) = \sum_{m \in \mathcal{M}} r_{m,i} r_{m,j} [t_m^+(\mathbf{s}) + t_m^-(\mathbf{s})] \quad (2.7c)$$

This FPE can equivalently be written for the densities $\mathbf{x} := \frac{\mathbf{s}}{\Omega}$.

The diffusion processes whose probability densities obey Eq. (2.7) can be described by the *stochastic differential equation*

$$d\mathbf{x} = \frac{1}{\Omega} \mathbf{A}(\Omega \mathbf{x}) dt + \frac{1}{\Omega} \underline{\mathbf{B}}(\mathbf{x}) d\mathbf{W}(t), \quad (2.8)$$

where $d\mathbf{W}(t)$ is a d-dimensional Wiener process, which is a diffusion process with Gaussian distributed increments. The matrix $\underline{\mathbf{B}}(\mathbf{x})$ must fulfill $\underline{\mathbf{B}}(\mathbf{x}) \underline{\mathbf{B}}(\mathbf{x})^T = \underline{\mathbf{B}}(\mathbf{s})$. Since this relation is not unique, the relation between the FPE Eq. (2.7) and the corresponding stochastic differential equation Eq. (2.8) is neither. It is important to note, that all t_m^\pm were required to be $\propto \Omega$ and thus \mathbf{A} and $\underline{\mathbf{B}}$ are also $\propto \Omega$. The first term in Eq. (2.8) is therefore independent of the system size and the second term is proportional to $\Omega^{-\frac{1}{2}}$, since $\underline{\mathbf{B}} \propto \sqrt{\Omega}$. In the large Ω limit the deterministic temporal evolution is thus recovered:

$$\frac{\partial}{\partial t} \mathbf{x} = \frac{1}{\Omega} \mathbf{A}(\Omega \mathbf{x}) \quad (2.9)$$

for the stability of coexistence of cyclically competing species: Reichenbach et al. (2007a) identify a critical mobility M_c above which coexistence is rapidly lost while “a low mobility $M < M_c$ guarantees coexistence of all three species” (see Fig. 2.1).

Their work stimulated a lot of further research, including studies of the effect of species specific reaction rates (Berr et al., 2009, confirming earlier results by Frean and Abraham (2001)), the generalisation to networks (Zhang et al., 2009), studies of the influence of the initial conditions (Shi et al., 2010), of intra- and interspecies spreading of lethal diseases (Wang et al., 2010), of intraspecific competition (Yang et al., 2010), of mutations among species (Mobilia, 2010), and of the interplay between intra- and inter-patch migration (Wang et al., 2011).

When discriminating a parameter regime (such as $M < M_c$) for which a stochastic birth-death system exhibits stable coexistence from a regime for which coexistence is unstable (according to Frey and Reichenbach, 2011), the decisive part is to reliably measure the dependence of τ_{ex} on the system size N . However, when the parameters approach the stable regime and the system size N becomes large, τ_{ex} and thus the

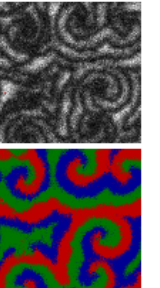
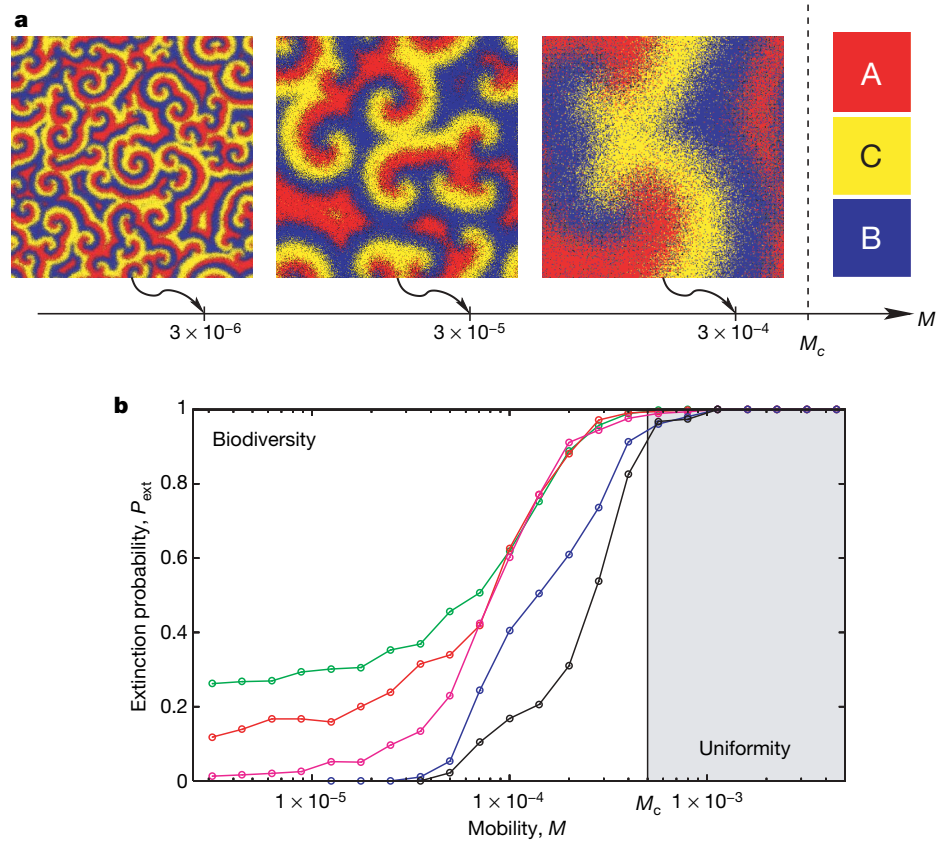


Figure 2.1: Simulations of a latticed based model of the Rock-Paper-Scissors game by Reichenbach et al. (2007a). **a:** Snapshots of typical states of the system after a long transient time and for different values of the mobility (or diffusion constant) M . **b:** The probability P_{ext} that only one species has prevailed after a fixed waiting time $t = L \times L$ (where L is the linear extent of the lattice) for different lattice sizes, $L = 20$ (green), $L = 30$ (red), $L = 40$ (purple), $L = 100$ (blue) and $L = 200$ (black). Reprinted by permission from Macmillan Publishers Ltd: Nature (London) **448**, 1046 (2007).



computation time of the simulations become extremely large. This severely limits the range of system sizes that can be feasibly analysed (Reichenbach et al., 2007a; He et al., 2010) and as a result the determination of critical parameters such as M_c is impeded. In the model by Reichenbach et al. (2007a), the population size (i.e. the overall number of individuals) and the spatial size (i.e. number of lattice sites) are approximately identical since every lattice site is either accommodated by one individual or by none. The relaxation of this restriction allows to enlarge the population size without altering the spatial size. This is a promising approach to mitigate the increase of the computation time of the simulations when studying the dependence of τ_{ex} on large population sizes. It thus almost suggests itself to relax this restriction to overcome the limitation when determining critical parameters.

Apart from overcoming limitations, relaxing the restriction of one individual at maximum per lattice site also appears to be biologically the more general framework. The approximate identity between spatial size and population size also implies that the scale at which migration takes place and the scale at which interaction takes place are the same as both take place between adjacent lattice sites. Corl et al. (2010) studied isolated populations of lizards in which different mating strategies dominate each other cyclically (Sinervo and Lively, 1996). While their study focused on the prevalence of the three species in different populations, it is illustrative for the more general setting where the competition between individuals takes place on a local scale (inside the population) while the populations are globally separated.

In the next section of this dissertation, I therefore introduce a spatial and stochastic model for cyclic competition among species that allows to tune the number of individuals that can be accommodated on a single lattice site by introducing a variable per site carrying capacity. In this model, individuals migrate between adjacent sites but interact only on a local scale with individuals at the same lattice site. This allows to study the dependence of the typical time of coexistence separately on the (spatial) system size and on the population size. In Sec. 2.3, I show that this extended model provides a feasible way to sharply discriminate the spiralling regime and the non-spiralling regime by considering the dependence of the typical time of extinction on the carrying capacity and thus on the population size.

In Sec. 2.5, I adapt this model to competition among four species to study under which conditions cyclic competition among three species arises by natural selection. It turns out that the mobility of individuals is not only pivotal to the stability but also to the emergence of cyclic competition.

2.2 A Lattice-based Population Model

The extended model that is introduced in this section has in principle no restriction on the number of individuals that can be accommodated by a single lattice site. Most of the results obtained from this *lattice-based population model* (abbreviated as LBPM in the following) are published in Lamouroux et al. (2012). In this model, three species S_0 , S_1 , and S_2 compete cyclically, meaning that S_0 has a competitive advantage over S_1 , S_1 has a competitive advantage over S_2 and S_2 has in turn a competitive advantage over S_0 (see Fig. 2.2). The strength of competition σ is equally large for all relations. σ is the rate with which an individual dies when encountering a member of the corresponding superior species. This gives the three reactions of competition

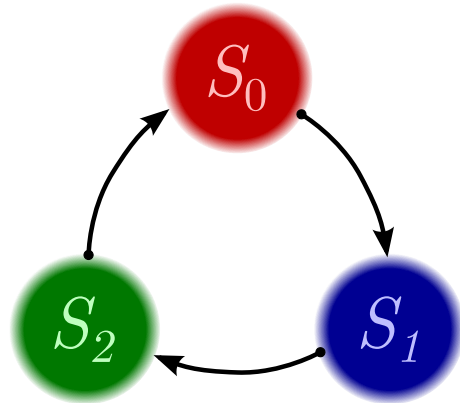


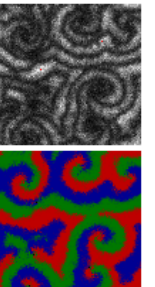
Figure 2.2: RPS dominance scheme

of competition

$$S_i \xrightarrow{\sigma_i^*} \emptyset \quad \sigma_i^* = \sigma s_{i+2} \quad (2.10)$$

where s_i denotes the absolute number of individuals of species S_i in a population. As throughout this chapter, indices have to be taken modulo three. Competition thus only reduces the number of individuals. Reproduction, on the other side, serves to increase the number on individuals and occurs equally likely for all three species with rate μ^* :

$$S_i \xrightarrow{\mu^*} 2S_i \quad \mu^* = \mu \left(1 - \frac{s}{C}\right) \quad (2.11)$$



s denotes the overall number of individuals in a population, i.e. $s = \sum_i s_i$. C is the *carrying capacity* that serves to vary the overall population size independently from the spatial size. It constitutes an upper limit to reproduction and thus denotes the maximal number of individuals that can coexist in a population. If $s = C$ the rate of reproduction becomes zero. If $s = 0$ the reproduction rate becomes maximal. Since fluctuations allow the local population to exceed C , the reproduction rate must be defined for $s > C$ in which case it is set to $\mu^* = 0$.

The populations are arranged on the sites of a square lattice of size $N = L \times L$ with continuous boundary conditions. The reactions Eq. (2.10) and Eq. (2.11) only take place inside the individual populations and do not affect the neighbouring sites. The only spatial process is migration (see Fig. 2.3). With a rate ε any individual moves to one of the four neighbouring sites. It is important to note that the movement of an individual to an adjacent site does not require empty space on the target site. More than that, ε is neither dependent on the density at the starting site nor at the target site (this property will be important in Sec. 2.2.1).

The temporal evolution of the system is accomplished by successive updates of the entire lattice. Prior to each update step $\sigma_i^*(x, y)$ and $\mu^*(x, y)$ are calculated, where (x, y) denote the integer coordinates on the lattice. Consecutively, all individuals in all populations simultaneously either reproduce, die or migrate to one of the neighbouring sites with the respective probabilities

$$p_{\mu,i}(x, y) = \frac{\mu^*(x, y)}{\varepsilon + \mu^*(x, y) + \sigma_i^*(x, y)} \quad (2.12a)$$

$$p_{\sigma,i}(x, y) = \frac{\sigma_i^*(x, y)}{\varepsilon + \mu^*(x, y) + \sigma_i^*(x, y)} \quad (2.12b)$$

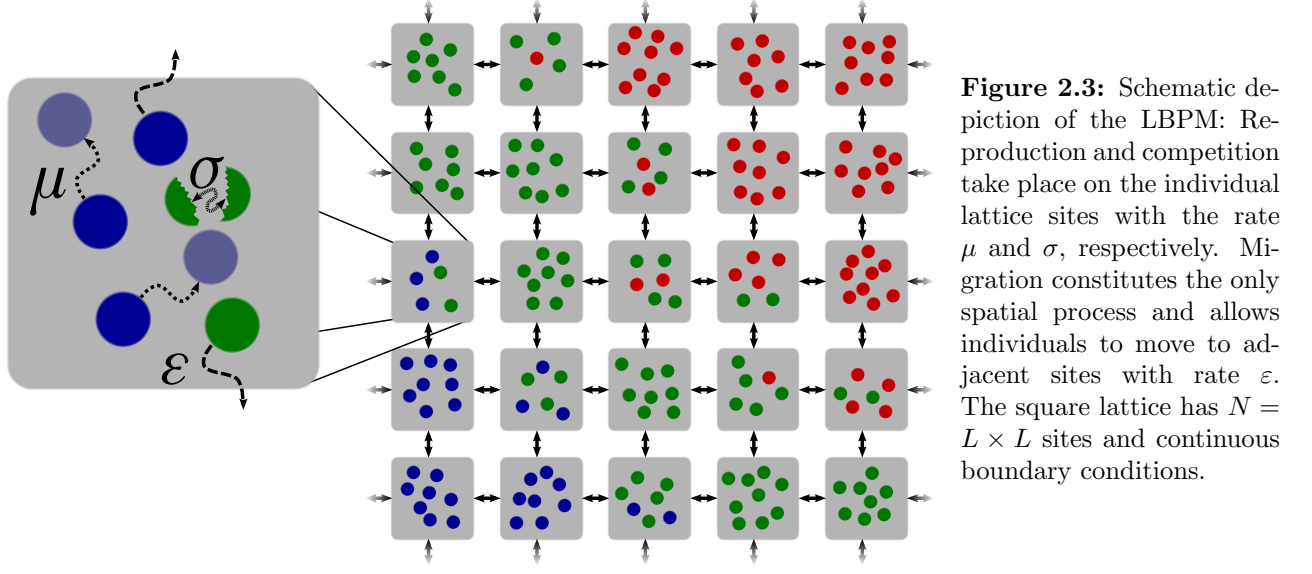
$$p_\varepsilon = \frac{\varepsilon}{\varepsilon + \mu^*(x, y) + \sigma_i^*(x, y)}. \quad (2.12c)$$

Since exactly one reaction occurs per individual and per update and since the number of reactions per unit time is roughly proportional to $\kappa = \varepsilon + \sigma + \mu$, κ updates define one unit of time. One update thus corresponds to $\delta t = \frac{1}{\varepsilon + \sigma + \mu}$.

A measure for the mobility of the individuals that is independent from the lattice spacing L^{-1} is the mobility (Reichenbach et al., 2007a) or diffusion constant (Gardiner, 2009) $M := \frac{\varepsilon}{2N}$. The linear extent of the lattice is then defined to be unity.

2.2.1 Deterministic Dynamics

To learn more about the dynamics of the LBPM, it is instructive to derive the deterministic reaction diffusion equation that would govern the temporal evolution if stochastic fluctuations due to the discrete nature of the population number were neglected. In what follows, the reaction equation for an isolated population is derived and it is argued that the reaction diffusion equation of the spatially extended system follows by adding a Laplacian. To derive the deterministic reaction equation, the transition probabilities per unit time t_m^\pm for all reaction channels, labeled by $m \in \mathcal{M}$, need to be known (see box **Interlude II: Stochastic description of birth-death processes** on page 8).



The form Eq. (2.6) of the ME is thus derived from the general form Eq. (2.4) to obtain the set $\{t_m^\pm\}$.

First note that for large system sizes or large mobilities, σ and μ are much smaller than the migration rate ε and thus the time that corresponds to one update becomes approximately $\delta t \approx \varepsilon^{-1}$ and the reaction probabilities then become $p_{\mu,i} = \mu^* \delta t$ and $p_{\sigma,i} = \sigma_i^* \delta t$. During the time interval δt each individual of species i can cause a change in the population of $+1$, -1 or 0 with the respective probability $p_\mu = \mu^* \delta t$, $p_{\sigma,i} = \sigma_i^* \delta t$, and $1 - p_\mu - p_{\sigma,i}$. In general, the population of each species i can therefore change by any value $\Delta s_i \in \{-s_i, s_i\}$ during δt . The probability $p(s_i + \Delta s_i, t + \delta t | s_i, t)$ that the population s_i changes by a value Δs_i different from ± 1 and 0 is, however, at least $\propto \delta t^2$. Since the limit $\delta t \rightarrow 0$ is eventually performed (which corresponds to the limit $L \rightarrow \infty$, since $\delta t \approx \varepsilon^{-1} = (2ML^2)^{-1}$ for fixed mobility M), the jump probability becomes

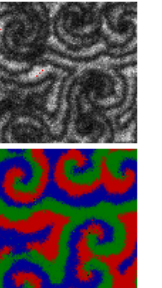
$$p(s_i + \Delta s_i, t + \delta t | s_i, t) = s_i (1 - p_\mu - p_{\sigma,i})^{s_i - 1} (\delta_{-1, \Delta s_i} p_{\sigma,i} + \delta_{1, \Delta s_i} p_\mu) + \delta_{0, \Delta s_i} (1 - p_\mu - p_{\sigma,i})^{s_i} \quad (2.13)$$

where $\delta_{k,\ell}$ denotes the Kronecker-Delta. The changes of s_i of the different species are statistically independent and thus the probability that the state \mathbf{s} changes by $\Delta \mathbf{s}$ is:

$$p(\mathbf{s} + \Delta \mathbf{s}, t + \delta t | \mathbf{s}, t) = \prod_{i=0}^2 p(s_i + \Delta s_i, t + \delta t | s_i, t) \quad (2.14)$$

$$= \sum_{i=0}^2 s_i (\delta_{-e_i, \Delta \mathbf{s}} p_{\sigma,i} + \delta_{e_i, \Delta \mathbf{s}} p_\mu) \prod_{k=0}^2 \frac{(1 - p_\mu - p_{\sigma,k})^{s_k}}{(1 - p_\mu - p_{\sigma,i})} \quad (2.15)$$

In the last step, terms at least $\propto \delta t^2$ have been disregarded. e_i denotes the standard basis vector. Since $\frac{p_\mu}{\delta t} = \mu^*$, $\frac{p_{\sigma,i}}{\delta t} = \sigma_i^*$ and $\lim_{\delta t \rightarrow 0} (1 - p_\mu - p_{\sigma,i}) = 1$, the scaled limit



of the jump probability is:

$$\lim_{\delta t \rightarrow 0} \frac{1}{\delta t} p(\mathbf{s} + \Delta \mathbf{s}, t + \delta t | \mathbf{s}, t) = \sum_{i=0}^2 s_i (\delta_{-\mathbf{e}_i, \Delta \mathbf{s}} \sigma_i^* + \delta_{\mathbf{e}_i, \Delta \mathbf{s}} \mu^*) \quad (2.16)$$

With the scaled limit of the jump probability the ME Eq. (2.4) can be recast in the form Eq. (2.6)

$$\begin{aligned} \partial_t P(\mathbf{s}, t) = & \sum_{i=0}^2 \{ t_i^-(\mathbf{s} + \mathbf{e}_i) P(\mathbf{s} + \mathbf{e}_i, t) - t_i^+(\mathbf{s}) P(\mathbf{s}, t) \\ & + t_i^+(\mathbf{s} - \mathbf{e}_i) P(\mathbf{s} - \mathbf{e}_i, t) - t_i^-(\mathbf{s}) P(\mathbf{s}, t) \} \end{aligned} \quad (2.17)$$

with $t_i^-(\mathbf{s}) = s_i \sigma_i^*(\mathbf{s})$ and $t_i^+(\mathbf{s}) = s_i \mu^*(\mathbf{s})$. $P(\mathbf{s}, t)$ is the probability that the populations of an *isolated* lattice site are of size s_0 , s_1 and s_2 , respectively, at time t . It seems tempting to consider the scaled population numbers $\mathbf{z} := \frac{\mathbf{s}}{C}$ and to perform a system size expansion in C to obtain the corresponding FPE. However, this requires the transition probabilities t_i^\pm to be proportional to C (Gardiner, 2009). While $t_i^+(\mathbf{z}) = z_i C \mu (1 - z_0 - z_1 - z_2)$ indeed fulfils this requirement, $t_i^-(\mathbf{z}) = z_i z_{i+2} C^2 \sigma$ is quadratic in C . Hence, there is no FPE that corresponds asymptotically to Eq. (2.17) for the individual lattice sites.

However, this only means that there is no appropriate limit in which the relative fluctuations vanish. This is because the number of competitive reactions grow quadratically with C . It is, nonetheless, possible to use Eq. (2.17) to calculate the temporal evolution of the mean $\langle \mathbf{s} \rangle$ around which fluctuations occur:

$$\partial_t \langle s_j \rangle = \partial_t \sum_{\mathbf{x} \in \mathbb{N}_+^3} x_j P(\mathbf{x}, t) \quad (2.18)$$

$$\begin{aligned} = & \sum_{\mathbf{x} \in \mathbb{N}_+^3} \sum_{i=0}^3 x_j [t_i^+(\mathbf{x} - \mathbf{e}_i) P(\mathbf{x} - \mathbf{e}_i) - t_i^+(\mathbf{x}) P(\mathbf{x}) \\ & + t_i^-(\mathbf{x} + \mathbf{e}_i) P(\mathbf{x} + \mathbf{e}_i) - t_i^-(\mathbf{x}) P(\mathbf{x})] \end{aligned} \quad (2.19)$$

$$\begin{aligned} = & \sum_{\mathbf{x} \in \mathbb{N}_+^3} x_j [t_j^+(\mathbf{x} - \mathbf{e}_j) P(\mathbf{x} - \mathbf{e}_j) - t_j^+(\mathbf{x}) P(\mathbf{x}) \\ & + t_j^-(\mathbf{x} + \mathbf{e}_j) P(\mathbf{x} + \mathbf{e}_j) - t_j^-(\mathbf{x}) P(\mathbf{x})] \end{aligned} \quad (2.20)$$

$$= \sum_{\mathbf{x} \in \mathbb{N}_+^3} [(x_j - 1) t_j^-(\mathbf{x}) P(\mathbf{x}) - x_j t_j^-(\mathbf{x}) P(\mathbf{x})] \quad (2.21)$$

$$+ (x_j + 1) t_j^+(\mathbf{x}) P(\mathbf{x}) - x_j t_j^+(\mathbf{x}) P(\mathbf{x})] \quad (2.22)$$

$$\partial_t \langle s_j \rangle = \langle t_j^+(\mathbf{x}) \rangle - \langle t_j^-(\mathbf{x}) \rangle \quad (2.23)$$

In the second step we have used that for $i \neq j$ the consecutive summands in the summation over x_i on the right hand side cancel out and thus only the $i = j$ terms survive. Neglecting correlations, i.e., $\langle s_i s_{i+2} \rangle = \langle s_i \rangle \langle s_{i+2} \rangle$, the deterministic temporal evolution of the mean $\langle \mathbf{s} \rangle$ is governed by

$$\partial_t \langle s_j \rangle = \mu \langle s_i \rangle \left(1 - \frac{\langle s \rangle}{C} \right) - \sigma \langle s_i \rangle \langle s_{i+2} \rangle. \quad (2.24)$$

The reaction rate equation Eq. (2.24) is valid only for the temporal evolution of an isolated population – just like Eq. (2.17), which was the starting point of the derivation. The dynamical system described by Eq. (2.24) has four fixed points apart from the trivial solution $\langle \mathbf{s} \rangle = 0$. Three fixed points describe the monocultural states where two species are extinct and one species prevails. The fourth reactive fixed point describes coexistence of all three species, i.e., $\langle s_i \rangle \neq 0 \forall i$. The four fixed points are

$$\mathbf{s}_m = \begin{pmatrix} C \\ 0 \\ 0 \end{pmatrix}, \begin{pmatrix} 0 \\ C \\ 0 \end{pmatrix}, \begin{pmatrix} 0 \\ 0 \\ C \end{pmatrix} \quad \text{and} \quad \mathbf{s}_r = \frac{\mu C}{3\mu + \sigma C} \begin{pmatrix} 1 \\ 1 \\ 1 \end{pmatrix} \quad (2.25)$$

To determine the stability of the fixed points, Eq. (2.24) is linearised around the respective fixed point. Representative for the three monocultural fixed points, the stability for the fixed point given by $(C, 0, 0)^T$ is determined by:

$$\partial_t \tilde{\mathbf{s}} \simeq \underline{\mathcal{A}} \tilde{\mathbf{s}} \quad \text{with} \quad (2.26)$$

$$\underline{\mathcal{A}}(\mathbf{s}_m) = \begin{pmatrix} -\mu & -\mu & -\mu - \sigma C \\ 0 & -\sigma C & 0 \\ 0 & 0 & 0 \end{pmatrix} \quad (2.27)$$

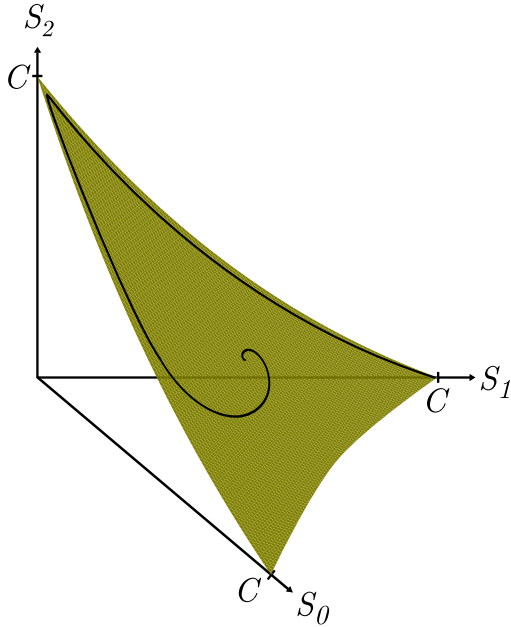
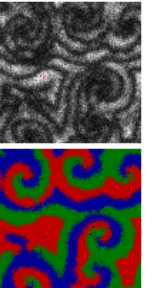


Figure 2.4: Phase Space of the non-spatial dynamics: Trajectories spiral outwards from the reactive fixed point and oscillate with ever growing period from one edge to the other.

for the translated variable $\tilde{\mathbf{s}} := \mathbf{s} - \mathbf{s}_{m/r}$. The stability of the fixed point is determined by the eigenvalues of $\underline{\mathcal{A}}$ (see box **Interlude I: Deterministic linear stability**). For the monocultural fixed points, the eigenvalues are $\{-\mu, -\sigma C, 0\}$. Since the largest eigenvalue is zero, the linear stability analysis does not allow for a proper characterisation of the fixed point. However, the monocultural state can easily be seen to be unstable because an infinitesimal small fraction of s_{i+2} introduced to the monocultural state $s_i = C$ will grow at the cost of the population s_i . However, in a finite stochastic system, the monocultural fixed point is an absorbing point that cannot be left without interaction from outside.



fixed point is an absorbing point that cannot be left without interaction from outside.

The linearisation around the reactive fixed point is described by the matrix

$$\underline{\mathcal{A}}(\mathbf{s}_r) = -\frac{\mu}{3\mu + \sigma C} \begin{pmatrix} \mu & \mu & \mu + \sigma C \\ \mu + \sigma C & \mu & \mu \\ \mu & \mu + \sigma C & \mu \end{pmatrix} \quad (2.28)$$

The eigenvalues of this matrix reveal that the dynamics around the reactive fixed point has one stable and two unstable directions (i denotes the imaginary unit):

$$\eta_0 = -\mu \quad (2.29a)$$

$$\eta_{1/2} = \frac{1}{2} \frac{\mu\sigma C}{3\mu + \sigma C} (1 \pm i\sqrt{3}) \quad (2.29b)$$

The reactive fixed point is thus also unstable. This results is a special case of the models by May and Leonard (1975), who studied the nonspatial version of cyclic competition in great detail. They showed that the solutions of Eq. (2.24) perform oscillations with ever growing period. Starting from any point in the phase space, the trajectories spiral away from the reactive fixed point, quickly approach the boundaries of the phase space (being defined by $s_i = 0$ for at least one species) and converge to one of the absorbing monocultural fixed points \mathbf{s}_m . However, they never reach these edges, but start to approach the edge of the superior counter-part $\mathbf{s} = C\mathbf{e}_{i+2}$ (see Fig. 2.4). These transitions from one species dominating the system to another species dominating the system take ever longer the older the system.

An important property of the LBPM is that individuals diffuse without hindrance over the lattice as it is not required that there is empty space on the site to which the individual migrates. Lugo and McKane (2008) have shown that in models where this requirement is made the diffusion of the individuals is not described by a simple diffusion description. Instead, a cross-diffusion term arises that accounts for the density dependent motion of individuals. In the present model however, migration of individuals can simply be accounted for by a diffusion description. The reaction diffusion equation for the space dependent state $\langle \mathbf{s}(x, y) \rangle$ is thus (omitting the brackets $\langle \cdot \rangle$ for readability)

$$\partial_t s_i(x, y) = M\nabla^2 s_i(x, y) + \mu s_i(x, y) \left(1 - \frac{s(x, y)}{C}\right) - \sigma s_i(x, y) s_{i+2}(x, y) \quad (2.30)$$

where ∇ acts on the spatial dimension (x, y) and $s(x, y)$ again denotes the local overall population.

2.2.2 Pattern Formation in 2-dimensional Systems

In the spatially extended system of cyclically competing species, the dynamics at every point in the plane is governed by Eq. (2.24). Hence, the spatially homogenous state $\mathbf{s}(x, y) = \mathbf{s}_r$ is a solution of Eq. (2.30). As this solution is unstable at every point, infinitesimal fluctuations will determine towards which absorbing state \mathbf{s}_m the local states evolve. Since mobility acts as to locally stir the populations, this evolution is

not expected to lead to a completely uncorrelated distribution of the three populations. The question at stake is thus what kind of pattern emerges from cyclic competition among species in a spatially extended environment.

In general, the instability of spatially homogenous but unstable states can be classified into three categories with two subcategories each (the description presented here follows Cross and Greenside (2009)). This classification bases on the linear response of the homogenous and unstable state to perturbations. A general perturbation, defined as $\mathbf{p}(x, y) := \mathbf{s}(x, y) - \mathbf{s}_r$, can be seen as a superposition of Fourier modes. The linear response of the system to

$$\mathbf{p}(\mathbf{x}) = \mathbf{p}_0 e^{\sigma_q t} e^{i\mathbf{q}\mathbf{x}}, \quad (2.31)$$

hence, classifies the response to a general perturbation. Here, \mathbf{x} denotes the position in the plane, \mathbf{q} is the wave vector of the perturbation and σ_q determines the temporal evolution of the perturbation and is in general a complex number and depends on \mathbf{q} . For a spatially homogenous solution to be unstable, the real part of σ_q , denoted by $\text{Re}(\sigma_q)$, has to be positive so that the perturbation grows. The classification scheme uses the qualitative dependence of $\text{Re}(\sigma_q)$ on $|\mathbf{q}|$. The instability of the homogenous state is called a Type-I instability if the maximal growth rate occurs for some $|\mathbf{q}| \neq 0$ and if the range for which the homogenous state is unstable against perturbations ($\text{Re}(\sigma_q) > 0$) does not extend to $|\mathbf{q}| = 0$. If the maximal growth rate occurs for some $|\mathbf{q}| \neq 0$ but the growth rate $\text{Re}(\sigma_q)$ is always zero for $|\mathbf{q}| = 0$, the instability is called a Type-II instability. When the maximal growth rate is in contrast maximal at $|\mathbf{q}| = 0$, the instability is called Type-III instability (see Cross and Greenside, 2009, for more details and examples). This classification can be further refined by the imaginary part of σ_q , denoted by $\text{Im}(\sigma_q)$. If the imaginary part is zero, the emerging pattern will be stationary and thus a ‘s’ is added to the classification. If, on the other hand, the imaginary part is unequal zero, the emerging pattern will oscillate and thus a ‘o’ is added to the classification.

In the present case, the linearised equations for $\mathbf{p}(\mathbf{x})$ of Eq. (2.30) are

$$\partial_t \mathbf{p}(\mathbf{x}) = M \nabla^2 \mathbf{p}(\mathbf{x}) + \underline{\mathcal{A}}(\mathbf{s}_r) \mathbf{p}(\mathbf{x}) \quad (2.32)$$

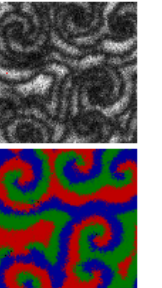
with $\underline{\mathcal{A}}$ as defined in Eq. (2.28). The ansatz of the Fourier mode then transforms this equation into

$$\sigma_q \mathbf{p}_0 = (-M |\mathbf{q}|^2 \mathbb{1} + \underline{\mathcal{A}}(\mathbf{s}_r)) \mathbf{p}_0 \quad (2.33)$$

where $\mathbb{1}$ denotes the identity matrix. This equation shows that σ_q is the eigenvalue of the matrix $-M |\mathbf{q}|^2 \mathbb{1} + \underline{\mathcal{A}}(\mathbf{s}_r)$ and the homogenous state is unstable if at least one the eigenvalues is larger than zero. Fortunately, the eigenvalues can be easily obtained because the eigenvalues of $\underline{\mathcal{A}}(\mathbf{s}_r)$ are already known:

$$\sigma_{q,0} = -M |\mathbf{q}|^2 - \mu \quad (2.34a)$$

$$\sigma_{q,1/2} = -M |\mathbf{q}|^2 + \frac{1}{2} \frac{\mu \sigma C}{3\mu + \sigma C} \left(1 \pm i\sqrt{3} \right) \quad (2.34b)$$



As expected from the analysis of the nonspatial system, the homogenous state has one stable direction, corresponding to the eigenvalue $\sigma_{q,0}$, and is unstable in the two remaining directions. As μ , σ , C , and M are strictly positive parameters, $\text{Re}(\sigma_{q,1})$ and $\text{Re}(\sigma_{q,2})$ are both maximal at $|\mathbf{q}| = 0$ and thus the spatially homogenous state constitutes a Type-III instability. Since $\text{Im}(\sigma_{q,1/2}) \neq 0$ the instability is of Type-III-o. Eqs. (2.34) yield furthermore two interesting observations: First, the maximum of the growth rate $\text{Re}(\sigma_q)$ is always positive irrespective of the set of parameters (μ, σ, M, C) . Hence, there is no critical parameter set at which the system exhibits a transition from a stable homogeneous state to a pattern forming state. The system is always in a pattern forming state. Second, Eqs. (2.34) show that the wave vectors of the perturbations against which the homogeneous state is unstable lies in the interval

$$|\mathbf{q}| \in \left[0, \sqrt{\frac{1}{2M} \frac{\mu\sigma C}{3\mu + \sigma C}} \right]. \quad (2.35)$$

The wavelength of a perturbation with wave vector $|\mathbf{q}|$ is defined by $\lambda := \frac{2\pi}{|\mathbf{q}|}$. The minimal wavelength of a potential pattern can thus be determined from the interval of wave vectors and yields

$$\lambda_{\min} = 2\pi \sqrt{\frac{6\mu + 2\sigma C}{\mu\sigma C}} \sqrt{M}. \quad (2.36)$$

Implicit in the derivation of these results is the assumption of an infinitely large system or periodic boundary conditions of a system whose extent is large compared to the typical length scale of the expected patterns. In the LBPM, the linear extent of the system is normalised to unity and periodic boundary conditions are imposed. The results thus only remain valid as long as $\lambda < 1$.

In particular, the finding that patterns will emerge irrespective of the mobility and the remaining parameters is only true for comparably small patterns.

Until here, the analysis was restricted to a linear approximation and the requirement that the growth rate $\text{Re}(\sigma_q)$ is larger than zero. However, this requirement alone implies that perturbations grow indefinitely. If patterns are supposed to be stable, nonlinearities must act as to saturate this growth and stabilise the process of pattern formation. In more detail, the amplitude of the perturbation was denoted by $z := p_0 e^{\sigma_q t}$ (see Eq. (2.31)), which is the solution to the linear approximation $\partial_t z = \sigma_q z$. If higher order terms are included, the temporal evolution of the amplitude of patterns arising from a Type-III-o instability is described by the complex Ginzburg-Landau equation. To further analyse the patterns that the LBPM is expected to exhibit, it is thus necessary to approximate the full spatial model Eq. (2.30)

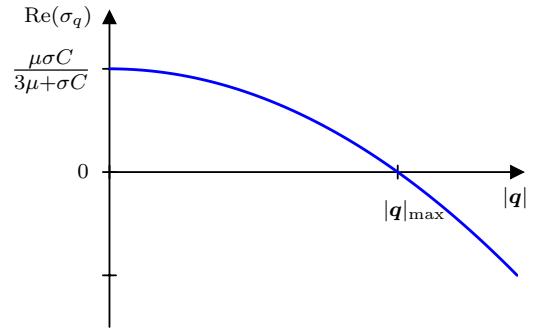


Figure 2.5: Growth rate $\text{Re}(\sigma_q)$ of a perturbation with wave vector $|\mathbf{q}|$ for the spatially extended system of three cyclically competing species.

by the complex Ginzburg-Landau equation. Reichenbach et al. (2007a) performed this approximation for their model (see Fig. 2.1) with a unit carrying capacity. In the next section, their approximation is applied to the LBPM.

2.2.3 The Spiraling State and the Complex Ginzburg-Landau Equation

The spatially homogenous, time independent solution of the spatially extended system Eq. (2.30) that is studied in the last section corresponds to the reactive fixed point of the non-spatial system Eq. (2.25), $\mathbf{s}(x, y) = \mathbf{s}_r$. Just like in the non-spatial case, however, this configuration is not stable against perturbations. The Type-III-o instability leads to pattern forming fronts, where the three species spatially segregate to form entangled spiral arms that rotate around a common vertex. Reichenbach et al. (2007a, 2008) could show that Eq. (2.30) can be transformed into a Complex Ginzburg-Landau Equation (abbreviated by CGLE in the following). The CGLE describes the temporal evolution of the amplitude of patterns arising from a Type-III-o instability and describes a range of phenomena, including the formation of traveling spiral waves (van Saarloos, 2003; Cross and Greenside, 2009).

The starting point of the transformation of Eq. (2.30) into the CGLE (as detailed in Reichenbach et al., 2008) is the observation that the non-spatial dynamics foremostly evolves on a two-dimensional sub-manifold in phase space (see Fig. 2.4). In the vicinity of the fixed point Eq. (2.25) this manifold is perpendicular to the eigenvector \mathbf{v}_{η_0} of the negative eigenvalue:

$$\mathbf{v}_{\eta_0} = \frac{1}{\sqrt{3}} \begin{pmatrix} 1 \\ 1 \\ 1 \end{pmatrix} \quad (2.37)$$

Here, the derivation by Reichenbach et al. (2008), which consists of two crucial steps, is only sketched to focus on the subsequent derivation of the prediction of the wavelength of the travelling spiral waves:

First, the variables \mathbf{s} are linearly transformed to a new set of variable $\mathbf{y}^{(\ell)}$, such that in the new frame \mathbf{v}_{η_0} corresponds to the z -direction and the fixed point \mathbf{s}_{fix} becomes the new origin. In order to describe the dynamics in the two-dimensional manifold, $y_2^{(\ell)}$ is approximatively expressed in terms of the remaining two variables, $y_0^{(\ell)}$ and $y_1^{(\ell)}$. This results in a two-dimensional non-linear system.

Second, the new variables $y_0^{(\ell)}$ and $y_1^{(\ell)}$ are non-linearly transformed to obtain the normal form of the two-dimensional system. Ignoring nonlinearities that arise from the application of the non-linear transformation to the diffusion term in Eq. (2.30) allows to keep the diffusion term also for the nonlinearly transformed variables. By interpreting the two variables as the real and imaginary part of one complex variable z , its temporal evolution is described by the CGLE (see Reichenbach et al., 2008):

$$\partial_t z = M \nabla^2 z + (\alpha_1 - i\beta) z - \alpha_2 (1 - i\alpha_3) |z|^2 z \quad (2.38)$$

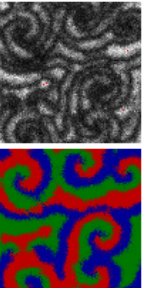
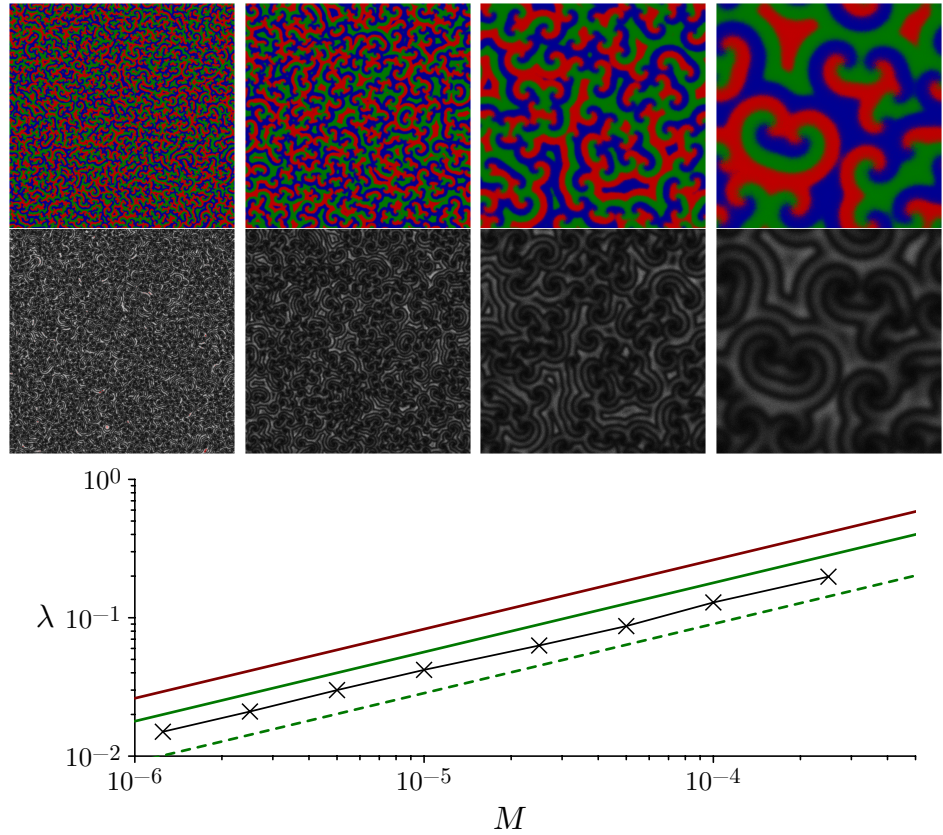


Figure 2.6: Upper part: Snapshots from the spiralling state for different mobilities $M = 2.5 \cdot 10^{-6}$, 10^{-5} , $5 \cdot 10^{-5}$ and $2.5 \cdot 10^{-4}$ (from left to right). Red, green and blue values of the colour code in the upper part correspond to the respective fraction of species at the lattice sites. Lower part shows the population fraction $z = \sum_i s_i / C$ from $z = 0$ (black) to $z = C$ (white). **Lower part:** Dependence of λ on M measured from simulations (\times) and analytical predictions according to Reichenbach et al. (2008) (—) and according to Eq. (2.48) (—) together with the prediction for the minimal possible wavelength Eq. (2.36) (---). Parameters are $L = 1000$, $C = 100$, $\mu = \sigma = 1$.



Since the LBPM is described by a reaction diffusion equation Eq. (2.30) that slightly differs from the one scrutinised by Reichenbach et al. (2007a, 2008) due to the introduction of the carrying capacity C , the parameters α_1 , α_2 , α_3 , and β yield

$$\begin{aligned} \alpha_1 &= \frac{1}{2} \frac{\mu\sigma C}{3\mu + \sigma C} & \alpha_2 &= \frac{\sigma(3\mu + \sigma C)(48\mu + 11\sigma C)}{56\mu(3\mu + 2\sigma C)} C \\ \alpha_3 &= \frac{\sqrt{3}(18\mu + 5\sigma C)}{48\mu + 11\sigma C} & \beta &= \frac{\sqrt{3}}{2} \frac{\mu\sigma C}{3\mu + \sigma C} \end{aligned} \quad (2.39)$$

To obtain the properties of the rotating spiral waves, the velocity of the wave fronts has to be determined first (van Saarloos, 2003). To this end, the linearised version of the CGLE has to be considered, which means that the cubic term in Eq. (2.38) is neglected. Considering the spatio-temporal Fourier transformation

$$\mathcal{F}[z](\mathbf{k}, \Omega) = \int_{\mathbb{R}} dt \int_{\mathbb{R}^2} d\mathbf{r} z(\mathbf{r}, t) e^{-i\mathbf{k}\mathbf{r} - i\Omega t} \quad (2.40)$$

yields the dispersion relation between the spatial and the temporal frequency of solutions of Eq. (2.38). In accordance with Reichenbach et al. (2008) this relation is:

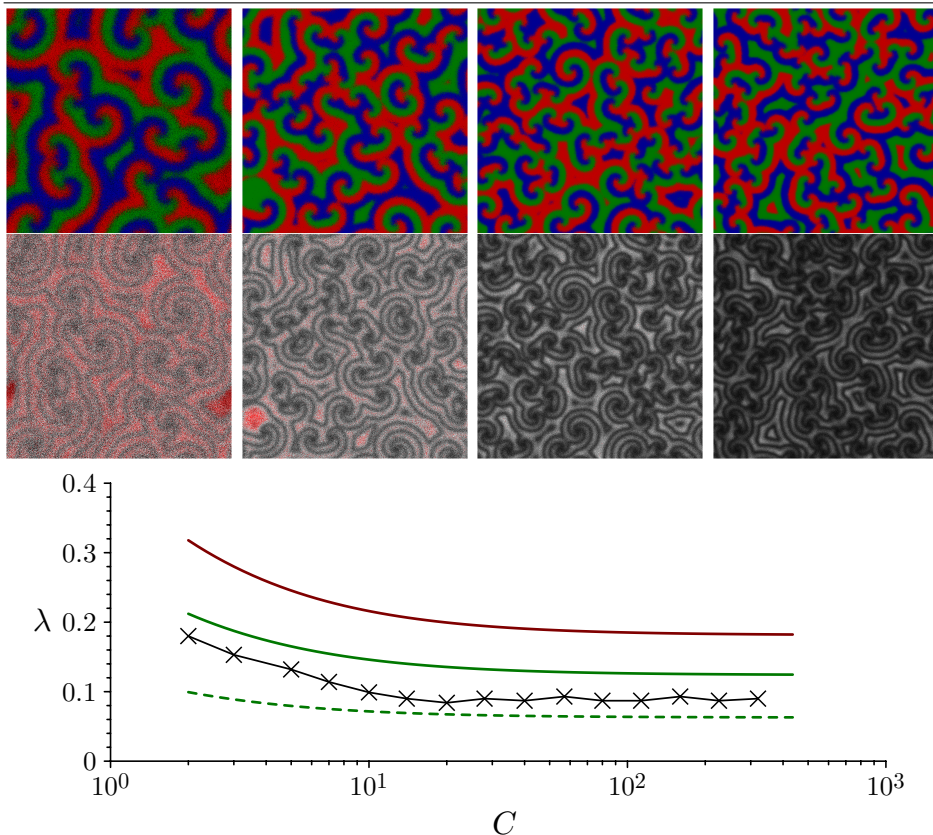


Figure 2.7: Snapshots from the LBPM from the spiraling state for different capacities $C = 3$, $C = 10$, $C = 28$ and $C = 57$ (from left to right). **Upper row:** Colours as before. Grey shades as before, overpopulated sites ($z > C$) are indicated as red. **Lower row:** Dependence of λ on C measured from simulations (\times) and analytical prediction according to Reichenbach et al. (2008) (—) and according to Eq. (2.48) (—) together with the prediction for the minimal possible wavelength Eq. (2.36) (---). Parameters are $L = 1000$, $M = 5 \cdot 10^{-5}$, $\mu = 1$, and $\sigma = 1$.

$$\Omega = \beta + i(\alpha_1 - M|\mathbf{k}|^2) \quad (2.41)$$

Note that $|\cdot|$ denotes the absolute value of the vector and is not to be confused with the absolute value of a complex number, since $|\mathbf{k}|$ can, in general, have a real and an imaginary part. Consistently, $\Omega = -i\sigma_{q,1}(|\mathbf{k}|)$ (as is seen by inserting the definition of α_1 and β), confirming that the CGLE exhibits the same linear response to Fourier modes as the original system Eq. (2.30).

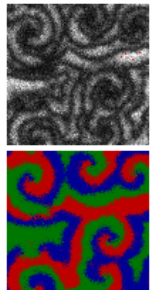
Following van Saarloos (2003), the front velocity v^* can be found to obey

$$v^* = \left. \frac{d\Omega}{dk} \right|_{|\mathbf{k}^*|} \quad (2.42)$$

with a yet to find wavevector \mathbf{k}^* . From the requirement that the fronts neither grow nor decay in a co-moving frame, the condition

$$v^* = \frac{\text{Im}(\Omega)}{\text{Im}(|\mathbf{k}^*|)} \quad (2.43)$$

can be derived, which implies that v^* is real. Using the the first relation, Eq. (2.41) returns $v^* = -i 2M|\mathbf{k}^*|$, implying that $|\mathbf{k}^*|$ is purely imaginary to ensure that v^* is



real. The second relation then yields:

$$2M \operatorname{Im}(|\mathbf{k}^*|) = \frac{\alpha_1 - M \operatorname{Im}(|\mathbf{k}^*|)^2}{\operatorname{Im}(|\mathbf{k}^*|)} \Leftrightarrow \operatorname{Im}(|\mathbf{k}^*|) = \sqrt{\frac{\alpha_1}{3M}} \quad (2.44)$$

In contrast to Reichenbach et al. (2008), here, this calculation returns

$$v^* = \sqrt{\frac{4}{3}\alpha M}. \quad (2.45)$$

Equipped with the velocity of the wave fronts, it is now possible to determine the wavelength of the traveling spiral waves from the full nonlinear CGLE Eq. (2.38). Far from their vertices, spiral solutions are similar to traveling planar waves. Following Reichenbach et al. (2008), it is thus appropriate to choose the corresponding ansatz $z(\mathbf{r}, t) = z_0 e^{-i\Omega t - i\mathbf{q}\mathbf{r}}$. This leads to the full dispersion relation

$$\Omega = \beta + i(\alpha_1 - M|\mathbf{q}|^2) - \alpha_2(i + \alpha_3)z_0^2. \quad (2.46)$$

Since Ω is defined to be real, the imaginary part on the right hand side must yield zero, $\alpha_1 - M|\mathbf{q}|^2 = z_0^2\alpha_2$. With this, Eq. (2.46) becomes

$$\Omega = \beta + \alpha_3(M|\mathbf{q}|^2 - \alpha_1). \quad (2.47)$$

The eigenvalues of the non-spatial system Eq. (2.29) show that β is the temporal frequency of the oscillation that stems from the intrinsic dynamics. Ω is thus a superposition of the non-spatial frequency and the frequency that originates from the wave fronts, traveling with the velocity v^* . Since oscillations that emerge from traveling waves have a frequency of $v^*|\mathbf{q}|$, the superposition equals $\Omega = \beta - v^*|\mathbf{q}|$ (see van Saarloos, 2003). Together with the front velocity Eq. (2.45), this determines the absolute value of the wave vector $|\mathbf{q}|$. The wavelength of the spirals is then given by $\lambda := \frac{2\pi}{|\mathbf{q}|}$ and thus is:

$$\lambda = \frac{2\sqrt{3}\pi\alpha_3}{\sqrt{\alpha_1}(\sqrt{3\alpha_3^2 + 1} - 1)}\sqrt{M} \quad (2.48)$$

Apart from the modified parameters Eqs. (2.39), this result deviates from the result by Reichenbach et al. (2007a, 2008) due to the different front velocity Eq. (2.45). The crucial prediction, however, which is shared by both results, is that the wavelength of the spirals grows with the mobility as \sqrt{M} .

Fig. 2.6 shows snapshots from the LBPM after sufficiently long transient times, for different values of the mobility M . The measured wavelength $\lambda(M)$ is also shown together with the predicted wavelength according to Reichenbach et al. (2007a, 2008), according to the prediction presented here, Eq. (2.48), and the prediction of the minimal

possible wavelength, Eq. (2.36), derived in Sec. 2.2.2. The prediction by Reichenbach is computed by employing the parameters Eqs. (2.39) to account for the carrying capacity C . The wavelength was determined directly by measuring the thickness of the spiral arms and finding the mode of the resulting statistical distribution. The qualitative dependence on M is very well captured by the prediction of a square root dependence. The quantitative prediction, however, seems to systematically deviate by a constant factor. This deviation was already observed by Reichenbach et al. (2007a) and was attributed to the imperfect mapping from the full three-dimensional system Eq. (2.30) to the CGLE Eq. (2.38). The prediction that was derived in this section seems to capture the quantitative observation better than the original analytical prediction derived in Reichenbach et al. (2008), though. Together with the prediction for the minimal wavelength Eq. (2.36), the analytical prediction of this section present an upper and lower bound for the measured wavelength shown in Fig. 2.6.

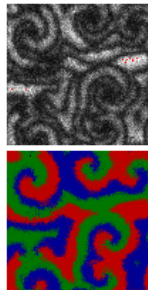
Fig. 2.7 shows snapshots of the LBPM for different values of the carrying capacity C together with the measured wavelength and the analytical predictions. For small C it is common that the sites become overpopulated, i.e. that more than C individuals are accommodated by one lattice site. This can occur since the carrying capacity C is an upper limit to reproduction but does not restrict mobility. Again, the qualitative dependence of $\lambda(C)$ is well captured by both, the analytical prediction Eq. (2.48) and the one by Reichenbach et al. (2007a) while the prediction derived in this section appears to quantitatively agree better. As before, the prediction by Reichenbach is adapted to account for the carrying capacity C by using the parameters Eqs. (2.39). As for the dependence of the wavelength λ on the mobility M , the prediction of the minimal wavelength in dependence on C constitutes a lower bound to the measured wavelength.

2.2.4 The Well Stirred State and its Stochastic Mean Field Dynamics

For very large mobilities M , migration becomes so frequent that every individual moves a large distance in between any two competition or reproduction events. Any individual thus interacts equally likely with any other individual on the lattice as correlations decay faster than they emerge due to the fast diffusion. This limit is referred to as the *well stirred state*.

In Sec. 2.2.1, it was argued that the ME that describes the stochastic dynamics of a *single* population on the lattice cannot be expanded in the carrying capacity C to obtain a FPE because the transition probabilities do not scale linearly with C . In the well stirred state, however, the overall population behaves like one single large population in which the transition probabilities scale linearly in N . In this case, the stochastic dynamics of the overall population $\mathbf{w} := \sum_{x,y} \mathbf{s}(x, y)$ can be described by a FPE in the large N limit.

The starting point of the derivation is again the calculation of the jump probability for



the overall population,

$$p(\mathbf{w} + \Delta\mathbf{w}, t + \Delta t | \mathbf{w}, t) = \prod_{i=0}^2 p(w_i + \Delta w_i, t + \Delta t | \mathbf{w}, t), \quad (2.49)$$

which factorizes since the increments in the different population are stochastically independent. As in the derivation of Eq. (2.17), any change of the overall population of the single species w_i that is different from ± 1 and 0 will at least have a probability that is $\propto \Delta t^2$. The limit $\Delta t \rightarrow 0$ corresponds, as before, to the limit $N \rightarrow \infty$. By keeping terms up to linear order in Δt , the jump probability can be expressed in terms of the reaction probabilities p_μ and $p_{\sigma,i}$ (see Eq. (2.12)):

$$\begin{aligned} p(\mathbf{w} + \Delta\mathbf{w}, t + \Delta t | \mathbf{w}, t) &= \prod_{i=0}^2 [\delta_{\Delta w_i, 0} (1 - p_\mu - p_{\sigma,i})^{w_i} \\ &\quad + \delta_{\Delta w_i, 1} w_i p_\mu (1 - p_\mu - p_{\sigma,i})^{w_i-1} \\ &\quad + \delta_{\Delta w_i, -1} w_i p_{\sigma,i} (1 - p_\mu - p_{\sigma,i})^{w_i-1}] \end{aligned} \quad (2.50)$$

Here, it is implicitly assumed that $\mathbf{s}(x, y) = \langle \mathbf{s} \rangle$, i.e. that the well stirred state is spatially homogeneous. Thus, p_μ and $p_{\sigma,i}$ are identical for every individual on the lattice, whereas originally they depend on the location (x, y) .

Recalling that $\frac{p_\mu}{\Delta t} = \mu^*(\frac{\mathbf{w}}{N})$, $\frac{p_{\sigma,i}}{\Delta t} = \sigma_i^*(\frac{\mathbf{w}}{N})$ and $\lim_{\Delta t \rightarrow 0} (1 - p_\mu - p_{\sigma,i}) = 1$ (note that $\frac{\mathbf{w}}{N} \equiv \langle \mathbf{s} \rangle$ by definition), the scaled limit of the jump probability $W(\mathbf{w} + \Delta\mathbf{w} | \mathbf{w}, t) = \lim_{\Delta t \rightarrow 0} \frac{1}{\Delta t} p(\mathbf{w} + \Delta\mathbf{w}, t + \Delta t | \mathbf{w}, t)$ becomes

$$W(\mathbf{w} + \Delta\mathbf{w} | \mathbf{w}, t) = \sum_{i=0}^2 w_i \left(\delta_{\Delta w, \mathbf{e}_i} \mu^* \left(\frac{\mathbf{w}}{N} \right) + \delta_{\Delta w, -\mathbf{e}_i} \sigma^* \left(\frac{\mathbf{w}}{N} \right) \right). \quad (2.51)$$

Equipped with this equation, the ME of the overall population can be cast into the form

$$\begin{aligned} \partial_t P(\mathbf{w}, t) &= \sum_{i=0}^2 [\tau_i^-(\mathbf{w} + \mathbf{e}_i) P(\mathbf{w} + \mathbf{e}_i, t) - \tau_i^+(\mathbf{w}) P(\mathbf{w}, t) \\ &\quad + \tau_i^+(\mathbf{w} - \mathbf{e}_i) P(\mathbf{w} - \mathbf{e}_i, t) - \tau_i^-(\mathbf{w}) P(\mathbf{w}, t)] \end{aligned} \quad (2.52)$$

with $\tau_i^-(\mathbf{w}) = w_i \sigma^*(\frac{\mathbf{w}}{N})$ and $\tau_i^+(\mathbf{w}) = w_i \mu^*(\frac{\mathbf{w}}{N})$. These transition probabilities are proportional to N , since $\tau_i^-(\mathbf{w}) = \sigma \langle s_i \rangle \langle s_{i+2} \rangle N$ and $\tau_i^+(\mathbf{w}) = \mu \langle s_i \rangle N \left(1 - \frac{\langle s \rangle}{C} \right)$. It is therefore possible to derive the FPE that is valid the large N limit. According to Eq.

(2.7), the FPE for the overall population \mathbf{w} reads:

$$\partial_t P(\mathbf{w}, t) = - \sum_{i=0}^2 \frac{\partial}{\partial w_i} [\tau_i^+(\mathbf{w}) - \tau_i^-(\mathbf{w})] P(\mathbf{w}, t) \quad (2.53)$$

$$\begin{aligned} &+ \frac{1}{2} \sum_{i=0}^2 \frac{\partial^2}{\partial w_i^2} [\tau_i^+(\mathbf{w}) + \tau_i^-(\mathbf{w})] P(\mathbf{w}, t) \\ &= - \sum_{i=0}^2 \frac{\partial}{\partial w_i} w_i \left[\mu \left(1 - \frac{w}{NC} \right) - \frac{\sigma}{N} w_{i+2} \right] P(\mathbf{w}, t) \quad (2.54) \\ &+ \frac{1}{2} \sum_{i=0}^2 \frac{\partial^2}{\partial w_i^2} w_i \left[\mu \left(1 - \frac{w}{NC} \right) + \frac{\sigma}{N} w_{i+2} \right] P(\mathbf{w}, t) \end{aligned}$$

By defining the quantity $\mathbf{u} := \frac{\mathbf{w}}{N}$, which equals the average occupation number $\langle \mathbf{s} \rangle$ and becomes a continuous variable for $N \rightarrow \infty$, the FPE takes the analogous form

$$\begin{aligned} \partial_t P(\mathbf{u}, t) &= - \sum_{i=0}^2 \frac{\partial}{\partial u_i} u_i \left[\mu \left(1 - \frac{u}{C} \right) - \sigma u_{i+2} \right] P(\mathbf{u}, t) \quad (2.55) \\ &+ \frac{1}{2N} \sum_{i=0}^2 \frac{\partial^2}{\partial u_i^2} u_i \left[\mu \left(1 - \frac{u}{C} \right) + \sigma u_{i+2} \right] P(\mathbf{u}, t). \end{aligned}$$

This FPE describes the diffusion process of the scaled variable \mathbf{u} of the overall population in the well stirred state. The temporal evolution of a single realisation of this diffusion process is governed by the corresponding stochastic differential equation. According to Eq. (2.8) it takes the form

$$\partial_t u_i = \mu u_i \left(1 - \frac{u}{C} \right) - \sigma u_i u_{i+2} + g_i(\mathbf{u}) \Gamma_i(t) \quad (2.56)$$

where $\Gamma(t)$ is three-dimensional Wiener process (see box **Interlude II: Stochastic description of birth-death processes**) and the *noise amplitude* is

$$g_i(\mathbf{u}) = \frac{1}{\sqrt{N}} \sqrt{\mu u_i \left(1 - \frac{u}{C} \right) + \sigma u_i u_{i+2}}. \quad (2.57)$$

The noise amplitude gives an estimate of the fluctuations around the deterministic motion of the well stirred state.

2.3 Pathes to Extinction

Any finite population in which individuals die and reproduce randomly to a certain degree can be described as a stochastic birth-death system. Once this has been realized, the question “Why are there so many species?” translates to “What period of time can species coexist?”. Coexistence can be lost through different mechanisms: (i)

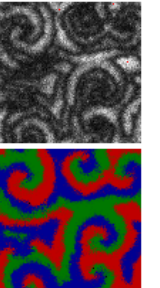
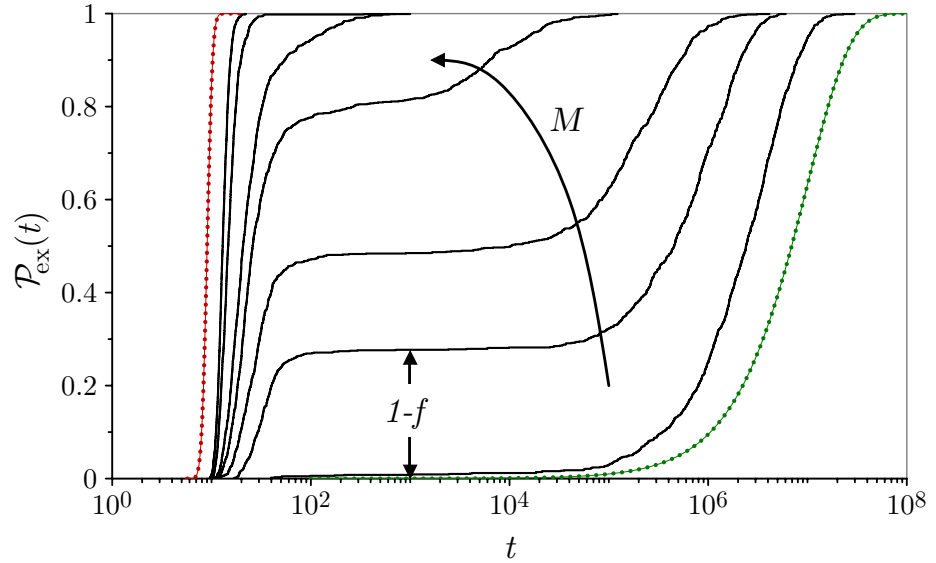


Figure 2.8: $\mathcal{P}_{\text{ex}}(t)$ for different values of the mobility M (black lines, from bottom to top: $M = 7 \cdot 10^{-4}$, $2 \cdot 10^{-3}$, $2.8 \cdot 10^{-3}$, $4 \cdot 10^{-3}$, $5.2 \cdot 10^{-3}$, $9 \cdot 10^{-3}$, $1.6 \cdot 10^{-2}$). The green and the red line are the (guessed) limiting cases for orientation and correspond to an exponential and a log-normal cumulative distribution function, respectively. Parameters are $\mu = \sigma = 1$, $L = 70$ and $C = 25$.



The coexisting species drive each other towards extinction, (ii) the coexisting species act as to support coexistence but by chance one of them eventually dies out, or (iii) the coexisting species interfere only weakly but stochasticity again dictates eventual extinction.

Reichenbach et al. (2007a) have shown that in a spatially extended system where species cyclically compete for dominance, the stability of coexistence crucially depends on the individual's mobility M . They identified a stable regime for low mobilities and an unstable regime for high mobilities. These two regimes are found to correspond to the two states described above: The spiralling state is stable while the well-stirred state is not. In order to find a critical mobility that separates these two regimes, Reichenbach et al. (2007a) use the auxiliary quantity $\mathcal{P}_{\text{ext}}(t = N)$, the probability that only one species has prevailed after a time t that equals the system size N . With this quantity, they are able to define a critical mobility M_c that separates the well-stirred and the spiralling state (see Fig. 2.1).

However, much information is lost when evaluating $\mathcal{P}_{\text{ext}}(t)$ only at $t = N$ instead of considering the entire function. Using a slightly different definition, I consider the probability $\mathcal{P}_{\text{ex}}(t)$ that at least one of the three species has gone extinct after a time t . $\mathcal{P}_{\text{ex}}(t)$ is the cumulative distribution function (c.d.f.) of the stochastic variable τ_{ex} , which is the time of the first species going extinct. $\mathcal{P}_{\text{ex}}(t)$ contains all the information about the extinction process. It can be obtained by evolving the LBPM until the first species goes extinct and measuring the age of the system τ_{ex} at that time. Repeating this procedure n times (giving $\tau_{\text{ex}}(j)$ for $j = 1, \dots, n$), $\mathcal{P}_{\text{ex}}(t)$ can be estimated as

$$\mathcal{P}_{\text{ex}}(t) = \sum_{j=1}^n \frac{\Theta(t - \tau_{\text{ex}}(j))}{n} \quad (2.58)$$

with the Heaviside stepfunction $\Theta(x)$, which is 1 for $x > 0$ and 0 for $x < 0$. $\mathcal{P}_{\text{ex}}(t)$ is thus the fraction of realizations that have gone extinct at time t .

Apparently, this approach has been rarely used due its computationally excessive time consumption. Exceptions in this field are Rulands et al. (2011) and He et al. (2010, 2011), who studied the probability density function of τ_{ex} , which is the derivative of $\mathcal{P}_{\text{ex}}(t)$, and Schütt and Claussen (2010) who derive approximations for $\langle \tau_{\text{ex}} \rangle$ for a non-spatial model. However, any auxiliary quantity like $\mathcal{P}_{\text{ex}}(t = N)$ (Reichenbach et al., 2007a) or the mean $\langle \tau_{\text{ex}} \rangle$ can be directly inferred from $\mathcal{P}_{\text{ex}}(t)$ – or more precisely from the set $\{\tau_{\text{ex}}(j)\}$.

Fig. 2.8 shows $\mathcal{P}_{\text{ex}}(t)$ for the LBPM for different values of the mobility M . All simulations in this chapter were initialised with random initial conditions, viz. each lattice site is initially populated by 0 to 5 individuals of each species. Fig. 2.8 captures the transition from the spiralling state (Sec. 2.2.3) to the well-stirred state (Sec. 2.2.4): For low mobilities $\mathcal{P}_{\text{ex}}(t)$ resembles an exponential c.d.f. with extremely long life times ($\sim 3.5 \cdot 10^6$ for $M = 7 \cdot 10^{-4}$). This is the regime where all realisations exhibit traveling spiral waves and extinction occurs due to large and rare fluctuations. For high mobilities, the system becomes well-stirred and no realisation exhibits spiral solutions. In this regime, the extinction times $\tau_{\text{ex}}(j)$ are narrowly distributed around a small value and $\mathcal{P}_{\text{ex}}(t)$ best resembles a log-normal c.d.f.. In all realisations the first species goes extinct at approximately the same time as no spirals emerge to maintain coexistence. In between these two clear regimes, there is an interesting intermediate regime, which seems to be a combination of the two c.d.f.'s of the extreme cases. Indeed, depending on the mobility, spirals form in the LBPM with a certain probability f or the system remains in the well-stirred state with probability $1 - f$. A fraction $1 - f$ of the realisations thus dies out quite early while the remaining fraction f of realisations survives until rare fluctuations drive one species to extinction. This explains the “plateau” in Fig. 2.8 for intermediate values of M . The probability f to form entangled spiral waves would be an excellent quantity to characterise the transition between the two states. However, the timescales of the c.d.f.'s describing the two states come very close to each other in the relevant mobility regime. The quantity f is thus impossible to determine for the relevant parameter sets. It is necessary to devise a different quantity to characterise the transition between the two regimes. Frey and Reichenbach (2011) have devised general criteria to classify the coexistence properties of stochastic birth-death systems (see Sec. 2.1). They characterise the stability by the dependence of τ_{ex} on the system size N . Whether this dependence is suitable to discriminate the spiralling and the non-spiralling regime for the LBPM is studied in this section.

Most of the results presented here have also been published in Lamouroux et al. (2012).

2.3.1 Traveling Planar Waves vs. Traveling Spiral Waves

To gain intuition for the behaviour of $\langle \tau_{\text{ex}} \rangle$ it is helpful to consider its dependence on the mobility M . Fig. 2.9 shows $\langle \tau_{\text{ex}} \rangle$ as a function of M for different system sizes N . For large mobilities, where the system is in the well-stirred state, the mean extinction time is largely independent of M at a small value of $\langle \tau_{\text{ex}} \rangle$. Intuitively, this is clear: When the system is well-stirred, intensifying the stirring mechanism cannot stir the system any further. Reducing the mobility M leads to a sharp increase in the mean extinction

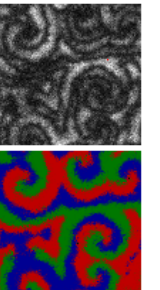
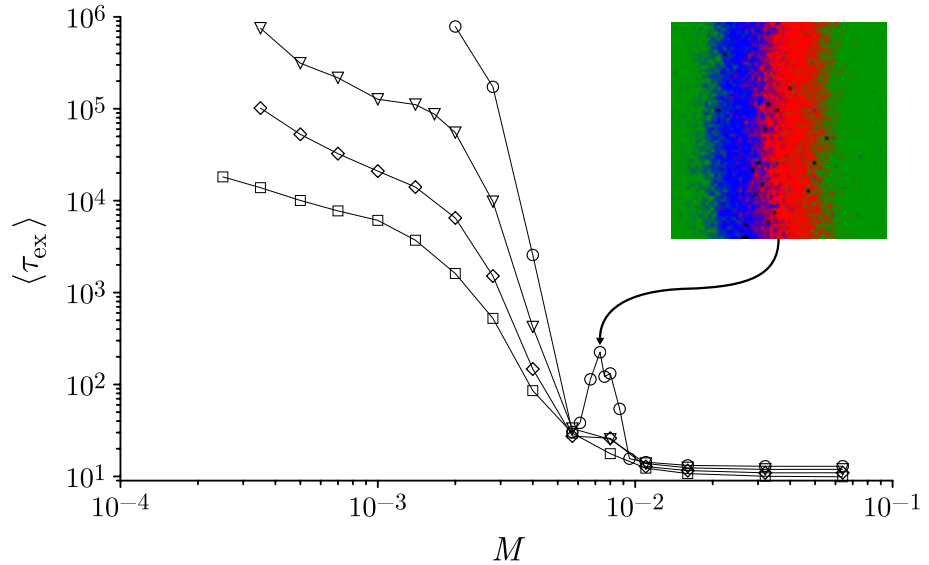


Figure 2.9: Mean extinction time $\langle \tau_{\text{ex}} \rangle$ as a function of M measured from the LBPM for different system sizes $L = 25$ (\square), $L = 35$ (\diamond), $L = 50$ (∇), and $L = 70$ (\ominus). Inset shows a snapshot of a planar travelling wave emerging at mobilities around $M = 7.3 \cdot 10^{-3}$. Remaining parameters are $C = 25$, $\mu = 1$, and $\sigma = 1$.



time, which rises by several orders of magnitude. This increase is as expected due to the emergence of stabilising spiral waves. As opposed to the large mobility regime, the mean extinction time in the spiralling state remains dependent on the mobility and increases with decreasing mobility. This can be explained by the dependence of the spiral's wavelength λ on the mobility M , c.f. Eq. (2.48): With decreasing mobility the extent of the spirals decreases as well and the number of spirals that cover the lattice increases. The fluctuations that are responsible for eventual extinction must thus become ever larger to destroy all spirals are therefore less frequent.

Right before the onset of the step rise of $\langle \tau_{\text{ex}} \rangle$ due to the emergence of spirals, an unexpected region with increased mean extinction time arises. Looking at the individual realisations of the system reveals that this non-monotonic behaviour occurs because of the emergence of *planar travelling waves* (see inset of Fig. 2.9). For the considered range of parameters, planar waves occur with a small probability (at maximum $\lesssim 2\%$ for $L = 70$ in the simulations presented in Fig. 2.9), but they can increase the mean time to extinction by several orders of magnitude.

Their appearance at $M \simeq 7.3 \cdot 10^{-3}$ can be understood from the measured dependence of the spiral's wavelength λ on the mobility M . Since the planar travelling wave covers the whole lattice, its wavelength is $\lambda_{\text{pl}} = 1$. Considering the dependence of $\lambda(M)$ for

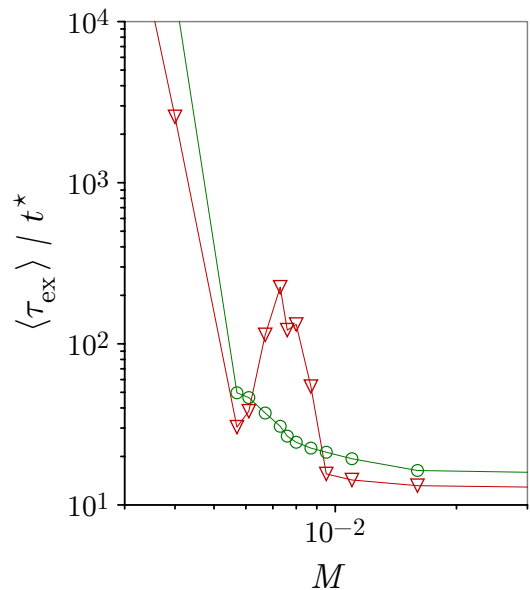


Figure 2.10: Comparison between the dependence of $\langle \tau_{\text{ex}} \rangle$ (∇) and t^* (\ominus) on M . $L = 70$, $C = 25$, and $\mu = \sigma = 1$.

travelling spiral waves in Fig. 2.6, the best algebraic fit to the measured wavelength of the spirals reveals that the wavelength would reach $\lambda = 1$ for $M_{\text{pl}} = 7.15 \cdot 10^{-3}$. The emergence of planar travelling waves can thus be understood from the analysis from Sec. 2.2.3. However, the fact that their appearance coincides with the onset of the emergence of travelling spiral waves poses a crucial problem:

The average time until extinction occurs $\langle \tau_{\text{ex}} \rangle$ should not be used to study the emergence of spiral waves because its dependence on the mobility M is significantly influenced by the emergence of planar waves.

The low probability of the emergence of travelling planar waves hints to a solution of this problem: The 95%-quantile of the c.d.f. \mathcal{P}_{ex} is unaffected by the planar travelling waves since they occur with probability $< 5\%$. Defining t^* as the 95%-quantile gives a robust measure to study the effect of the emergence of travelling spiral waves on the extinction properties of system. Fig. 2.10 shows a comparison of $\langle \tau_{\text{ex}} \rangle$ and t^* and confirms this expectation.

The typical time until extinction occurs t^* is unaffected by the effect of planar waves and is thus used to study the effect of the emergence of spiral waves.

In the remainder of this chapter, t^* will therefore be used as a measure for the typical time until extinction occurs.

2.3.2 Scaling with the System's Size N

Frey and Reichenbach (2011) have adapted the concept of stability to stochastic systems (see Sec. 2.1). In their classification the coexistence of species is called *stable* if the typical time t^* until extinction occurs grows with the system size $N = L \times L$ faster than any power of N . This usually implies that t^* grows exponentially with N , i.e. $t^* \propto e^N$. On the other side, a system is called *unstable* if it grows slower than any power of N , which usually implies that it grows logarithmically with N , i.e. $t^* \propto \ln(N)$. If t^* grows with some power of N , $t^* \propto N^\theta$, the coexistence is called *marginally stable*.

Measuring t^* in dependence on N for the LBPM should therefore reveal whether the classification of coexistence of spatially and cyclically competing species in the presence of a non-unit carrying capacity C can serve to discriminate the spiralling and the well-stirred state. The findings in Reichenbach et al. (2007a) give grounds for the expectation to find a stable and an unstable regime that corresponds to the spiralling and the well-stirred state, respectively.

Fig. 2.11 shows $t^*(N)$ for various mobilities, ranging from the extreme case of very high mobilities over intermediate values of the mobility to the extreme case of very low mobilities. In the well-stirred state, for high mobilities, the expectation that the system is quickly driven towards extinction is very well confirmed. $t^*(N)$ shows nearly no deviation from the logarithmic dependence for mobilities $M \geq 3.2 \cdot 10^{-2}$. This implies that coexistence is unstable in this mobility regime. In the other extreme, for

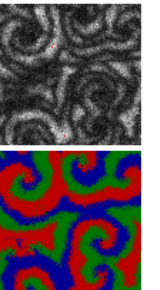
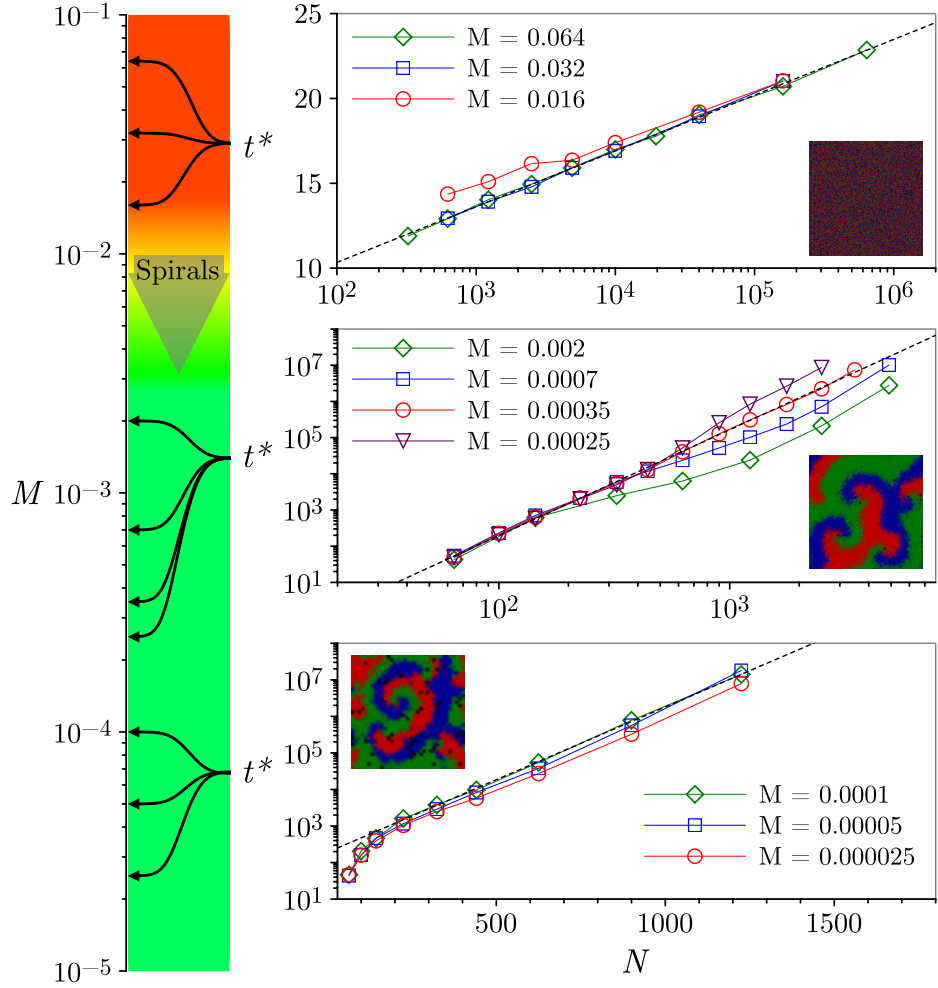


Figure 2.11: Dependence of the typical time to extinction t^* in dependence on the mobility M (coloured solid lines). Left bar indicates the range of mobility values shown. **Upper right:** Mobilities from the well-stirred state together with a logarithmic function for orientation, which implies unstable coexistence. **Middle and lower right:** Mobilities from the spiralling state together with an algebraic (middle figure) and an exponential function (lower figure) for orientation, implying stable and marginally stable coexistence, respectively. Inset show snapshots from the respective simulations. Remaining parameters are $C = 25$, $\sigma = 1$, and $\mu = 1$.



very low mobilities in the spiralling state, the expectation that coexistence is stable is also very well confirmed. Except for very small system sizes ($N \lesssim 150$), $t^*(N)$ can be described by an exponential function.

The typical time until extinction t^* exhibits a logarithmic and exponential dependence on the system size N for high and low mobilities, respectively. Coexistence can, thus, be classified as unstable and stable in the respective mobility regimes.

This seems to confirm the general expectation to find two regimes corresponding to the spiralling and the well-stirred state. However, for intermediate values of the mobility, t^* can neither be described by a logarithmic dependence nor by an exponential dependence on the system size N . Although t^* does not show a clear algebraic dependence like $t^* \propto N^\theta$, the behaviour of the typical time to extinction hints at marginal stability of coexistence in this regime. Self-evidently, it cannot be precluded that t^* exhibits a logarithmic or exponential dependence on N for even larger system sizes. But these system sizes are to date computationally inaccessible.

For intermediate values of the mobility, coexistence can neither be classified as stable nor as unstable. Although spirals form in this mobility regime, the dependence of t^* on N suggests that coexistence is only marginally stable.

The range of mobilities for which coexistence cannot uniquely be classified as stable or unstable is not negligible as it covers approximately a decade of values. Looking at snapshots from the simulation shows that the aforesaid regime belongs to the spiralling state. This surprising observation has an important consequence: The spiralling state

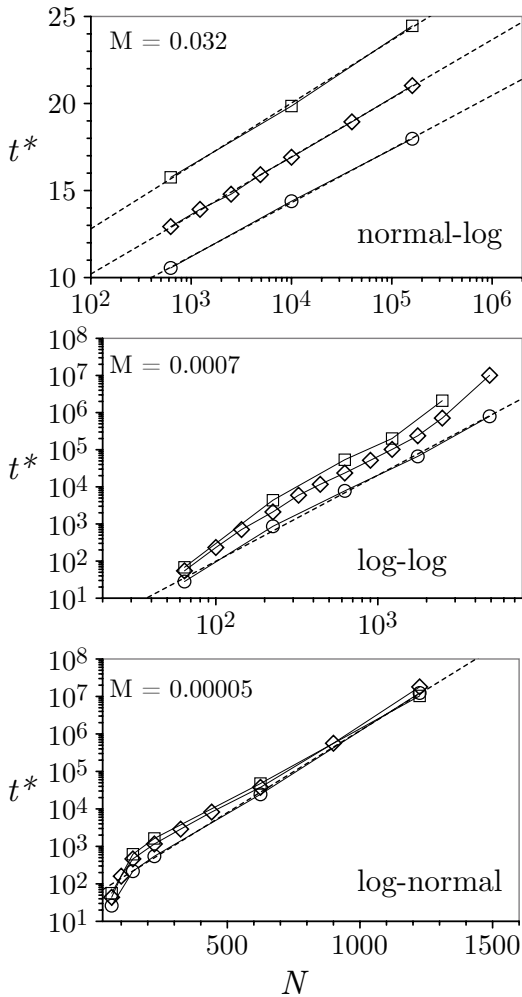


Figure 2.12: Same as Fig. 2.11 for $\sigma = 0.5$ (\square), $\sigma = 1.0$ (\diamond), and $\sigma = 2.5$ (\circ) for representative mobilities from the well-stirred regime (top row) and the spiralling regime (middle and lower row).

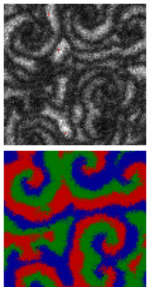
cannot be equated with stable coexistence. Instead, the spiralling state is stable only for very small mobilities and becomes marginally stable when the individual's mobility is increased. The well stirred state, in contrast, is indeed unstable for all considered mobilities.

To check whether the described behaviour is robust against changes in the parameters, Fig. 2.12 shows t^* in dependence on N for various values of σ . μ is set to 1 to fix the timescale. The ambiguous behaviour for intermediate values of the mobility apparently persists also for $\sigma \neq 1$ just as the logarithmic and exponential behaviour for large and small mobilities, respectively.

In order to use the classification of coexistence to characterise the transition between the spiralling and the well-stirred state, it would be necessary to determine the mobility where the logarithmic dependence of $t^*(N)$ changes into the ambiguous dependence for intermediate mobilities. However, there are two caveats. First, the ambiguous behaviour is... well... ambiguous and thus not clearly defined. Secondly, even if there was a clear algebraic behaviour $t^* \propto N^\vartheta$ where ϑ was a function of M , it would in general still be a tedious enterprise to determine the transition between a logarithmic behaviour and an algebraic dependence with *some* exponent ϑ . The classification according to the stability of coexistence

can thus only be used to a limited extent to characterise the transition between the spiralling and the well-stirred state.

At this point it is important to note that increasing the system size N has two distinct



effects: On the one hand, increasing N increases the spatial resolution of the system L^{-1} . On the other hand, increasing N also increases the overall number of individuals living on the lattice. The newly introduced carrying capacity C , in contrast, allows to vary the overall number of individuals without influencing the spatial resolution of the system.

2.3.3 Scaling with the Carrying Capacity C

The classification of coexistence by Frey and Reichenbach (2011) considers the “system size”, which was equated with the spatial size $N = L \times L$ in the previous sections. With the introduction of the carrying capacity C the notion *system size* becomes, however, ambiguous, since now there is the spatial extent N as well as the population size, which can be controlled by varying C .

To check that the carrying capacity C is indeed suited to tune the overall number of individuals without changing the spatial extent, the dependence of the spatial average $\langle s(x, y) \rangle_{x, y}$ of the local populations on C must be measured. Fig. 2.13 shows $\langle s(x, y) \rangle_{x, y}$ as a function of C in the spiralling regime. The average population is a monotonically increasing function of the carrying capacity that grows unboundedly for the considered range of parameters. This means (i) that any value of $\langle s(x, y) \rangle_{x, y}$ corresponds uniquely to a value of C and (ii) that any large value of $\langle s(x, y) \rangle_{x, y}$ can be obtained by varying C . This confirms that the overall population can be regulated by setting C .

To learn about the impact of C on the extinction process, it is instructive to consider $\mathcal{P}_{\text{ex}}(t)$ for different values of C . Fig. 2.14 shows $\mathcal{P}_{\text{ex}}(t)$ from the well-stirred regime and from the intermediate, ambiguous regime. Recalling that $\mathcal{P}_{\text{ex}}(t)$ can be roughly described as a superposition of the c.d.f. of the spiralling state and the c.d.f. of the well-stirred state with the probability f governing the division between the two, the effect of C on $\mathcal{P}_{\text{ex}}(t)$ can be studied separately for these three components. The right part in Fig. 2.14 shows that the lifetime of the c.d.f. of the spiralling solutions grows with increasing C . Fig. 2.14 shows furthermore that the probability f of exhibiting spirals also increases with C . This supports the intuition that a larger population is more stable because fluctuations that are large enough to make the population go extinct are less frequent for an increasing population size. The left part of Fig. 2.14, however, also shows that the c.d.f. of the well-stirred regime is shifted to the left for larger C . This means that coexistence is lost earlier for larger population sizes. While this observation might be surprising at first glance, the analysis in Sec. 2.2.4 provides an explanation: For large mobilities the system can be described as being effectively one large spatially homogeneous population. In this limit, the temporal evolution of

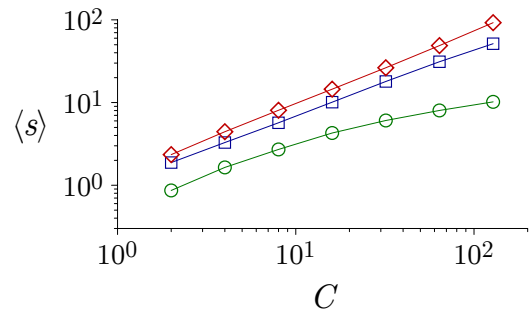


Figure 2.13: Average population number $\langle s(x, y) \rangle_{x, y}$ in dependence on C for $\mu = 0.1$ (\circ), $\mu = 1$ (\square), and $\mu = 10$ (\diamond) in the spiralling regime ($M = 5 \cdot 10^{-5}$). Remaining parameters are $L = 100$ and $\sigma = 1$.

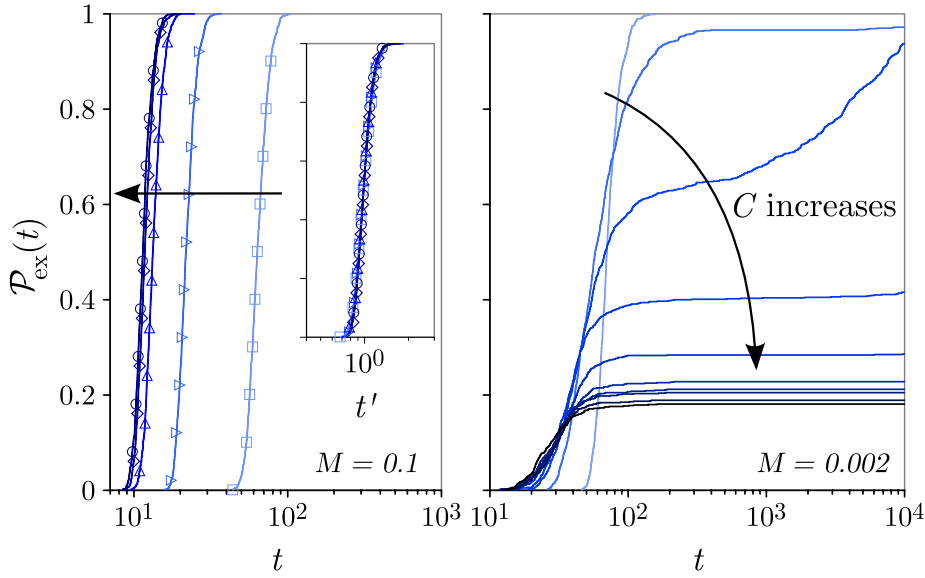


Figure 2.14: $\mathcal{P}_{\text{ex}}(t)$ from the well-stirred (left) and the intermediate regime (right) for various values of the carrying capacity ranging from $C = 2$ to $C = 800$ (left) and $C = 1600$ (right), respectively. Darker lines indicate higher C . Inset shows $\mathcal{P}_{\text{ex}}(t')$ from the well-stirred regime for the rescaled time $t' := \frac{t}{\langle \tau_{\text{ex}} \rangle}$. Symbols only visualise the collapse. Parameters are $L = 50$, $\mu = 1$, and $\sigma = 0.4$.

the scaled overall population $\mathbf{u} = \frac{1}{N} \sum_{x,y} \mathbf{s}(x,y)$ can be described by the stochastic differential equation (2.56) with the associated noise amplitude Eq. (2.57). Since no species ever goes extinct in the noise free, i.e., deterministic version of the non-spatial Rock-Paper-Scissors game, the noise term in Eq. (2.56) is the only mechanism that drives the species to extinction. The noise amplitude, however, turns out to be a monotonically *increasing* function in C . As described in Sec. 2.2.4 this originates from the fact that the rate of competitive reactions scales as C^2 . If C increases, the noise amplitude Eq. (2.57) thus increases as well, which in turn accelerates the extinction process in the well-stirred regime.

Enlarging the population by increasing the carrying capacity C reduces the typical time until extinction occurs and hence shortens the duration of coexistence in the well-stirred regime.

Apparently, the carrying capacity only affects the mean extinction time $\langle \tau_{\text{ex}} \rangle$ and not the shape of the c.d.f. in the well-stirred regime: Rescaling the time axis according to $t' := \frac{t}{\langle \tau_{\text{ex}} \rangle}$ makes all curves collapse roughly to an universal function that is independent of C (see inset in Fig. 2.14).

The comparison of the noise amplitude and the inverse mean time to extinction is suitable to check the validity of the analytical description of the well-stirred state from Sec. 2.2.4. This is because the stochastic part in Eq. (2.56) becomes $\langle \tau_{\text{ex}} \rangle g_i(\mathbf{u}) \Gamma_i(t')$ by rescaling time according to $t' = \frac{t}{\langle \tau_{\text{ex}} \rangle}$. Since the extinction process in the rescaled time frame is independent of C (see inset of Fig. 2.14), the stochastic part – the only driving force towards extinction – must be constant with respect to C , i.e., $g_i(\mathbf{u}) \propto \langle \tau_{\text{ex}} \rangle^{-1}$.

By approximating the noise amplitude $g_i(\mathbf{u})$ by the noise amplitude in the vicinity of the reactive fixed point of the non-spatial dynamics Eq. (2.25) it is possible to compare $g_i(C)$ as a function of C to $\langle \tau_{\text{ex}} \rangle^{-1}$. Fig. 2.15 shows that the noise amplitude and the inverse mean time to extinction coincide remarkably well with a proportionality

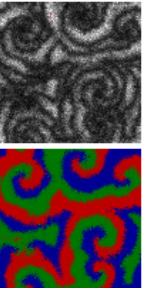
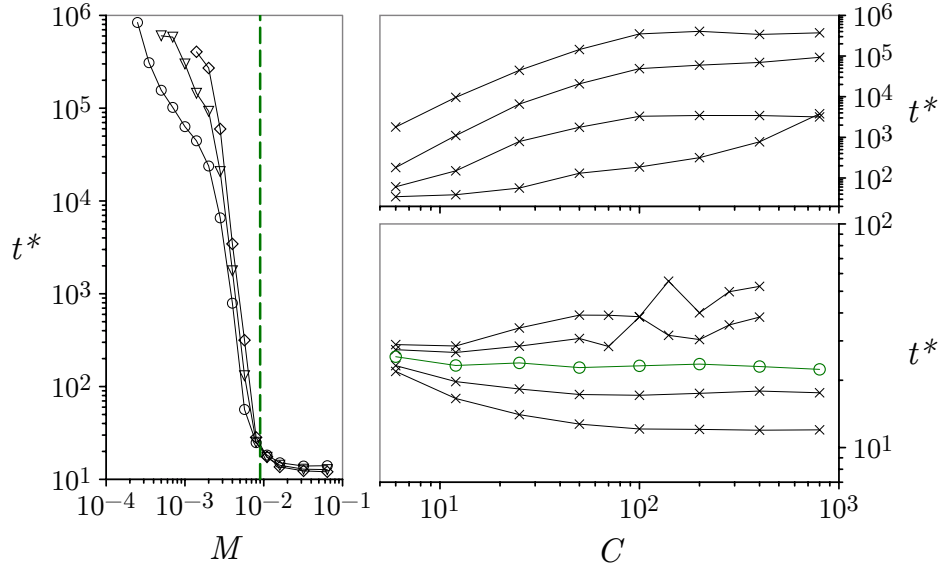


Figure 2.16: Dependence of t^* on the C . **Left:** t^* as a function of M for $C = 25$ (\circ), $C = 50$ (∇), and $C = 200$ (\diamond). Green dashed line indicates $\widetilde{M}_c = 0.009$. **Right:** t^* as a function of C for different mobilities M (\times) from the spiralling regime (top), $M = 0.0014, 0.0028, 0.004,$ and 0.0057 (from top to bottom), and from the intermediate and the well-stirred regime (bottom), $M = 0.007, 0.0076, 0.009$ (\circ), $0.011, 0.064$ (from top to bottom). Remaining parameters are $L = 35, \sigma = 1,$ and $\mu = 1$.



factor of ≈ 0.5 for the chosen set of parameters. This confirms that Eq. (2.56) is the appropriate description of the temporal evolution of \mathbf{u} in the well-stirred regime. The observation that the carrying capacity destabilises coexistence in the well-stirred regime of the spatial Rock-Paper-Scissors game reveals that the scaling behaviour of t^* cannot fit into the categories of coexistence classification (Frey and Reichenbach, 2011). However, the fact that C has a stabilising effect in the spiralling state suggests that there must be a mobility where the dependence of the typical time to extinction on C changes from negative to positive.

The right part of Fig. 2.16 shows the dependence of t^* on C for different values of M ranging from the spiralling state to the well-stirred state. For large mobilities, t^* strongly depends on C and raises steeply to saturate at a finite value. This agrees with the observation made before that C acts to stabilise coexistence in the spiralling regime. For low mobilities, t^* decreases with C , as expected.

In between, t^* changes from a negative to a positive dependence on C in a remarkable fashion: t^* becomes approximately independent of C . Physically speaking, this means that the destabilising effect from the well-stirred regime and the stabilising effect from the spiralling regime just compensate each other on average. This makes it possible to devise an alternative definition of the critical mobility. The spiralling state and the well-stirred state of the spatial Rock-Paper-Scissors game with a nonunit carrying

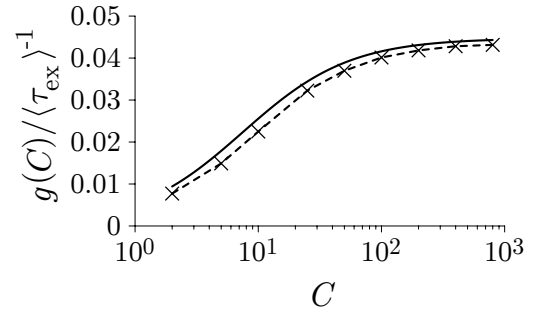


Figure 2.15: Comparison between the noise amplitude in the vicinity of the reactive fixed point (solid line) and the inverse mean time to extinction (\times) (multiplied with a scaling factor of 0.5) in the well stirred-state. Parameters are $L = 50, M = 0.1, \sigma = 0.4,$ and $\mu = 1$.

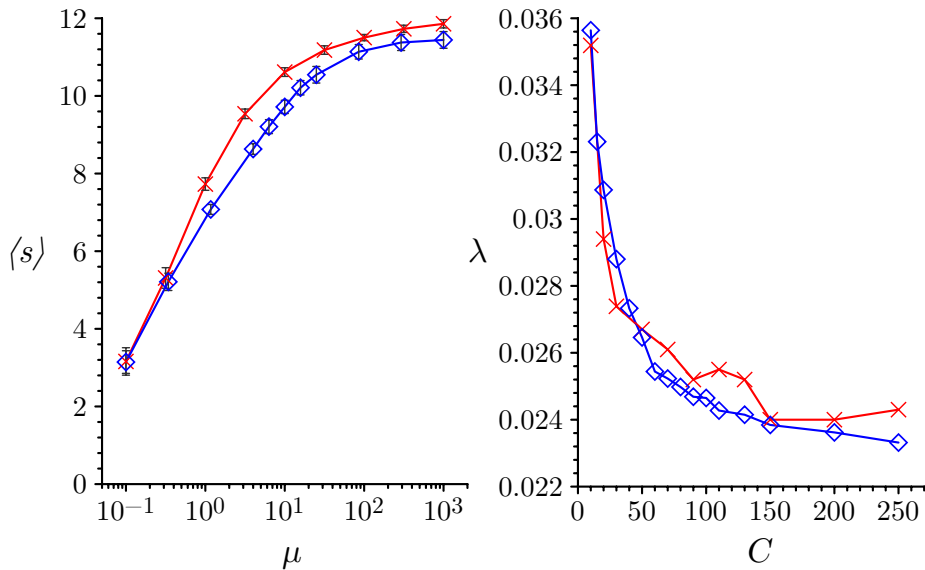


Figure 2.17: Comparison of sequential and parallel update schemes. **Left:** Average overall population per site $\langle s \rangle$ in dependence on the reproduction rate μ for the sequential update scheme ($-x-$) and the parallel update scheme ($-\diamond-$) as described in the main text. Parameters are $L = 100$, $C = 10$, $\sigma = 1$, and $M = 5 \cdot 10^{-5}$. **Right:** Same as Left for the wavelength of the spirals in dependence on the carrying capacity C . Parameters are $L = 1000$, $\mu = 5$, $\sigma = 1$, and $M = 10^{-5}$.

capacity can be discriminated by considering their influence on the typical time to extinction. At the critical mobility \widetilde{M}_c both states influence t^* equally strong while above it the well-stirred state dominates the dependence of t^* on C and below it the spiralling state dominates the dependence of t^* on C .

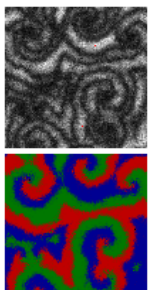
It is possible to discriminate the well-stirred state from the spiralling state by exploiting the observation that increasing C destabilises coexistence in the well-stirred state and stabilises coexistence in the spiralling state. The critical mobility \widetilde{M}_c is thus the mobility at which the typical time until extinction occurs neither grows nor decreases with C .

The left part of Fig. 2.16 illustrates the transition between the well-stirred state and the spiralling state. The critical mobility, separating the two, is found to be $\widetilde{M}_c = 0.009$ for the chosen set of parameters.

The crucial advantage of this alternative definition of the critical mobility is the property that it can be applied to finite systems. The usual scaling analysis requires the consideration of the asymptotic scaling behaviour of the typical time to extinction with regard to N . As a consequence, it suffers from a broad ambiguous regime that stems from the fundamental inaccessibility of infinite system sizes. The new method, in contrast, is able to sharply determine the critical mobility irrespective of the system size.

2.4 Sequential and Parallel Update Schemes

A peculiarity of the update scheme described in Sec. 2.2 is that the reactions of all individuals in each single update step are chosen simultaneously. This so-called *par-*



allel update scheme constitutes a significant computational advantage. The model by Reichenbach et al. (2007a) employs a sequential update scheme where in each update step one individual is chosen at random to perform one reaction. To equal one parallel update step, the sequential scheme thus requires $\propto C \times L^2$ update steps. Since the sequential update scheme needs approximately $C \times L^2$ times more calls to a random number generator to choose the individuals that are updated, the computational advantage of the parallel update scheme becomes crucial for large systems.

Nonetheless, both update schemes lead to the same dynamical system Eq. (2.24) because the relation between microscopic reaction schemes and the corresponding master equation is not unique. Consider for example the average concentration x of particle type X undergoing the bidirectional reaction $X \leftrightarrow 2X$. Its temporal evolution is then governed by $\partial_t x \propto x(1-x)$. The temporal evolution of the concentration x is, however, the same for a reaction scheme $X + Y \rightarrow 2X$ where Y is a second kind of particle with $x + y = 1$. Beyond the temporal evolution of the average concentrations, parallel and sequential update schemes can lead to markedly different results (Caron-Lormier et al., 2008). If the results of simulations depend on the update scheme while the resulting dynamical systems are identical, the differences must be considered to be spurious.

An apparently spurious pattern that emerges when the parallel update scheme is employed is the so-called checkerboard invariant (Chopard and Droz, 1998) shown in Fig. 2.18. When individuals are located on a fully populated lattice site and are surrounded only by individuals of the same species, they are

forced to move by the update scheme. In principle, this should not be expected to be a problem since individuals of the same kind are indistinguishable. However, the checkerboard pattern is invariant under application of two update steps - which is not true if the update steps are performed sequentially. To understand this phenomenon, imagine a real but infinite checkerboard whose white fields are empty and whose black fields are occupied by some large number of individuals. The update step then forces all individuals to move which results in all black fields being empty. Since all white

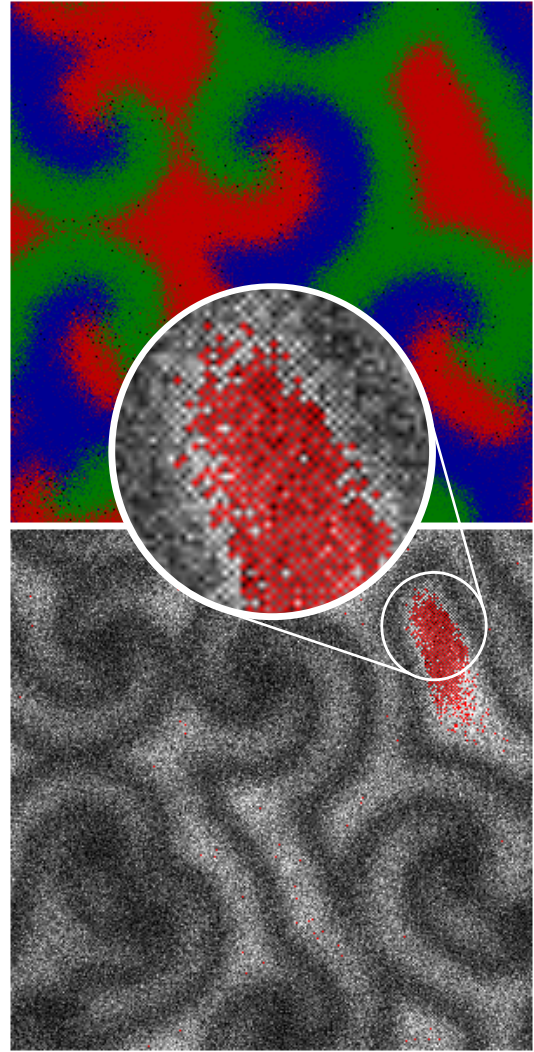


Figure 2.18: Example of the checkerboard pattern that appears because of the parallel update scheme. When individuals can neither reproduce nor die due to competition, the checkerboard is the stable pattern of motion.

fields are now occupied by a fourth of the populations of each of its four neighbouring black fields, all white fields are now occupied by the same large number of individuals on average. In the next update step the same procedure is repeated which leads to the initial configuration where all black sites are occupied and all white sites are empty. To check whether the checkerboard pattern influences the system, it is imperative to compare basic quantities obtained from simulations with the parallel update scheme to those obtained from sequential update schemes. To this end a sequential update scheme is employed that resembles the one used by Reichenbach et al. (2007a). In the sequential scheme used here, each update step consists of randomly choosing a lattice site and a single individual from that lattice site. This individual then undergoes one of the three reactions, migration, competition, or reproduction according to the probabilities Eq. (2.12). $C \cdot L^2$ of these update steps correspond to one parallel update step. Fig. 2.17 shows simulation results from the parallel and the sequential update scheme for two basic quantities, the average population size per site $\langle s \rangle$ and the wavelength of the spirals λ . The left part of Fig. 2.17 shows that, except for small reproduction rates μ , the average overall population size $\langle s \rangle$ is systematically larger for the sequential update scheme than for the parallel update scheme. However, this difference can be considered to be of minor importance since it does not even amount to one individual on average. More importantly, the right part of Fig. 2.17 shows that there is no systematic difference between the wavelength of the spirals obtained by using the parallel update scheme and by using the sequential update scheme.

In conclusion, the parallel update scheme constitutes a significant computational advantage while central observables of the system exhibit no relevant difference to a sequential update scheme.

The computational advantage of the parallel update scheme is crucial for the numerical analysis presented in this work. All results presented in the preceding sections are thus obtained by employing the parallel update scheme, described at the beginning of this section.

2.5 More than Three Species

The analysis of the changing stability properties of cyclically competing species contributes to the understanding of a mechanism that *preserves* biodiversity. However, the question how non-hierarchical competition is *established* remains open. Self-evidently, a necessary ingredient is speciation, the creation of new species from existing ones. But this raises the question whether a system of three cyclically competing species is stable against speciation. This suggests to study under which conditions a system of four species collapses to a non-transitive, i.e., cyclic, three species system.

To approach this question, it is necessary to generalise the Rock-Paper-Scissors game. In fact, the Rock-Paper-Scissors game is a so-called tournament of three strategies. Generally speaking, a *tournament* is a set of n nodes (in this case strategies or species) whereof each pair of distinct nodes is connected by a directed link pointing from the

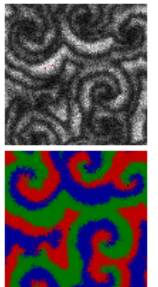
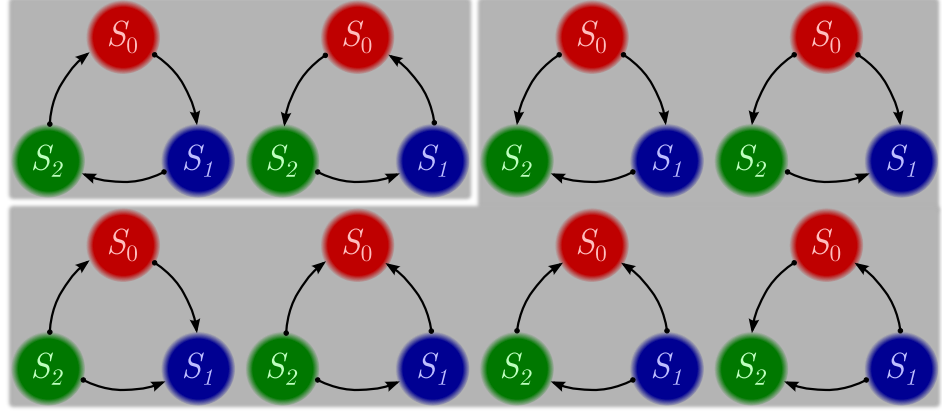


Figure 2.19: All eight possible tournaments with three nodes (strategies). The two grey shaded areas enclose tournaments with the same structure, viz., the cyclic structure (upper left) and the hierarchical structure (bottom and right).



superior strategy to the inferior one (Harary, 1969). A *tournament matrix* \mathcal{T} (or adjacency matrix) defines a tournament such that if strategy i is beaten by strategy j , $\mathcal{T}_{ij} = 1$ and zero else (the usual notation defines the tournament matrix as \mathcal{T}^T , cf. *ibid*). For the Rock-Paper-Scissors game this matrix is

$$\mathcal{T} = \begin{pmatrix} 0 & 0 & 1 \\ 1 & 0 & 0 \\ 0 & 1 & 0 \end{pmatrix}. \quad (2.59)$$

In this notation, the temporal evolution of the species' populations in the LBPM (see Sec. 2.2) can be written for an arbitrary number of species n :

$$\partial_t \mathbf{s} = M \nabla^2 \mathbf{s} + \mathbf{s} \mu \left(1 - \frac{|\mathbf{s}|_1}{C} \right) - \sigma \mathcal{D}(\mathbf{s}) \mathcal{T} \mathbf{s} \quad (2.60)$$

$|\mathbf{s}|_1$ is the 1-norm of \mathbf{s} , as before, and $[\mathcal{D}(\mathbf{s})]_{ij} = \delta_{ij} s_i$ is the diagonal matrix with the vector \mathbf{s} on the diagonal.

The definition of the tournament matrix implies that $\mathcal{T}_{ii} = 0$ and $\mathcal{T}_{ij} = 1 - \mathcal{T}_{ji}$. A priori, there are thus $2^{\frac{n(n-1)}{2}}$ possible tournaments. However, two tournaments that are equal except for a permutation of labels are not “essentially different” (Davis, 1954). More specifically, two tournaments \mathcal{T}_1 and \mathcal{T}_2 (or graphs in general) are *isomorphic* and, hence, not essentially different if and only if there is a permutation π and the corresponding permutation Matrix P_π such that $\mathcal{T}_1 = P_\pi^{-1} \mathcal{T}_2 P_\pi$ (Harary, 1969; Davis, 1954). The set of all isomorphic tournaments is then said to have the same *structure*. Davis (1954) derived a formula to determine the number of structures, i.e., essentially different tournaments, for an arbitrary number of strategies n .

For $n = 3$ this formula yields two essentially different structures: the intransitive tournament described by Eq. (2.59) and the strictly hierarchical tournament where one of the three strategies is superior to the remaining two (see Fig. 2.19). In the latter tournament it is, however, trivial to determine the winner since one strategy is superior to any other. In more general terms, if the strategies (or nodes) of a tournament can be subdivided into two non-empty sets such that all strategies in one set are superior to all strategies in the the other set, a tournament is termed *reducible* (Davis, 1954).

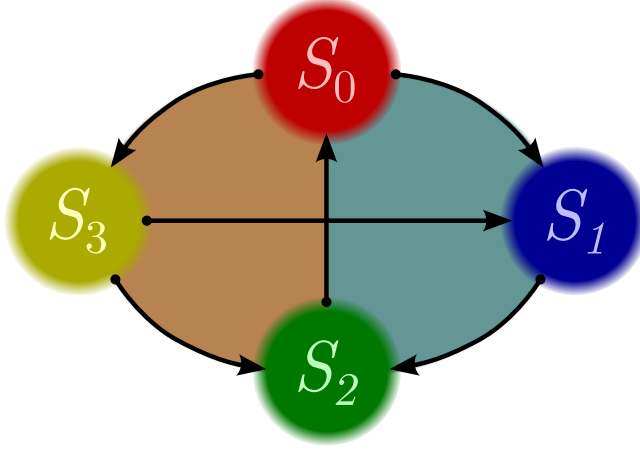


Figure 2.20: Irreducible tournament of four species. Arrows point from the superior to the inferior species in direct comparison. Shaded regions illustrate sub-tournaments of three species corresponding to the Rock-Paper-Scissors game.

In the case of $n = 4$ strategies, the formula by Davis (1954) reveals that there are 4 structures whereof, however, only one is irreducible (Moon and Pullman, 1967). Since reducible tournaments have at least a set of clear-cut winners, the answer to the initial question whether and under which conditions a system of four species collapses to a non-transitive, i.e., cyclic, three species system, is given by the structure itself. This is not so clear for the irreducible tournament shown in Fig. 2.20 which is thus studied in the following. The tournament matrix corresponding to the tournament shown in Fig. 2.20 is

$$\mathcal{T} = \begin{pmatrix} 0 & 0 & 1 & 0 \\ 1 & 0 & 0 & 1 \\ 0 & 1 & 0 & 1 \\ 1 & 0 & 0 & 0 \end{pmatrix}. \quad (2.61)$$

With this tournament matrix, Eq. (2.60) describes a spatially extended system of four species who reproduce, migrate, and compete according to the dominance scheme shown in Fig. 2.20 and becomes

$$\partial_t s_0 = M \nabla^2 s_0 + s_0 \mu \left(1 - \frac{|\mathbf{s}|_1}{C} \right) - \sigma s_0 s_2 \quad (2.62a)$$

$$\partial_t s_1 = M \nabla^2 s_1 + s_1 \mu \left(1 - \frac{|\mathbf{s}|_1}{C} \right) - \sigma s_1 (s_0 + s_3) \quad (2.62b)$$

$$\partial_t s_2 = M \nabla^2 s_2 + s_2 \mu \left(1 - \frac{|\mathbf{s}|_1}{C} \right) - \sigma s_2 (s_1 + s_3) \quad (2.62c)$$

$$\partial_t s_3 = M \nabla^2 s_3 + s_3 \mu \left(1 - \frac{|\mathbf{s}|_1}{C} \right) - \sigma s_3 s_0. \quad (2.62d)$$

Before this spatial system is studied in more detail, it is insightful to consider its non-spatial version, obtained by disregarding the $M \nabla^2$ term.

The non-spatial system has no reactive fixed point, i.e., no fixed point for which $s_i \neq 0 \forall i$. This can be seen by, e.g., dividing the equations for $\partial_t s_k = 0$ by s_k and

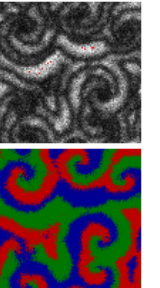
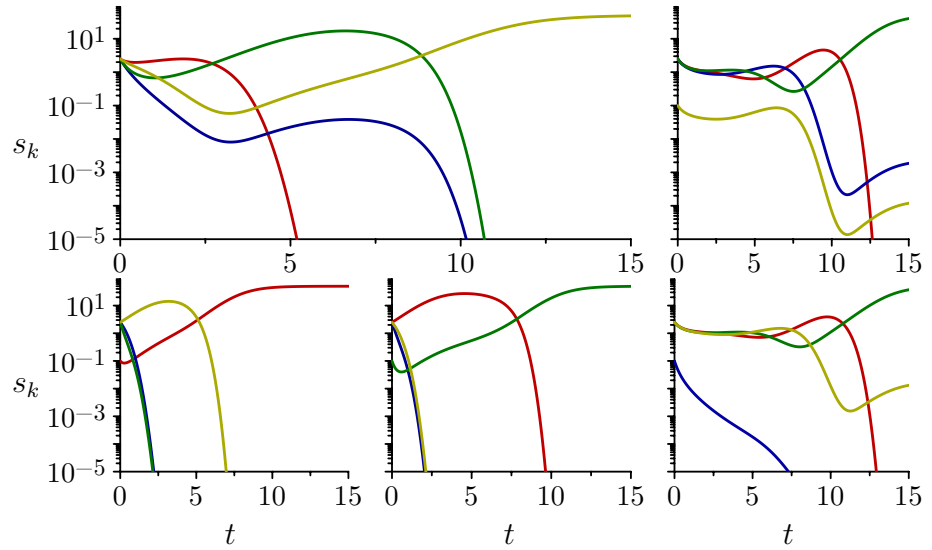


Figure 2.21: Deterministic temporal evolution of the nonspatial version of Eq. (2.62). s_0 (—), s_1 (—), s_2 (—), and s_3 (—) obtained from numerical integration. **Upper left:** Symmetric initial conditions (all $s_k = 2.5$). **Upper right and lower row:** Asymmetric initial conditions where all populations are initialised equally ($s_k = 2.5$) except for the population of one species ($s_k = 0.1$). Parameters are $\mu = 1$, $\sigma = 1$, and $C = 50$.



subtracting the equation for $k = 1$ from the equation for $k = 3$ yielding $\sigma(s_0 + s_3) = \sigma s_0$ which requires that $s_3 = 0$. Hence, a fully stochastic non-spatial version of the four species tournament quickly reduces to a three species tournament.

Yet it crucially depends on the initial condition $\mathbf{s}(t = 0)$ if species S_0 , S_1 , S_2 , or S_3 dies out first. Fig. 2.21 shows the deterministic temporal evolution of s_k for the non-spatial version of Eq. (2.62) for symmetric (all $s_k = 2.5$) and asymmetric initial conditions (all $s_k = 2.5$ except for one starting with $s_k = 0.1$). Although population sizes below one, i.e., $s_k < 1$, are limitedly meaningful, they are shown to better visualise the quick decrease: For each initial configuration, the population of at least two species quickly drop to values that correspond to extinction of that species in any population with integer valued population size (the populations described by the continuous variables s_k , in contrast, would recover from any small value for long enough times as in the non-spatial version of the Rock-Paper-Scissors game (May and Leonard, 1975)). For asymmetric initial conditions, it is interesting to observe that S_1 dies out first or simultaneously with a second species for three out of four initial configurations. On the other hand, S_0 never dies out first when the initial configuration is asymmetric. It is thus surprising to observe that S_0 is the first to die out when the initial configuration is symmetric. These findings do not depend on the amplitude of the initial conditions, i.e., the qualitatively same results are obtained by choosing $s_k = 10$ or 20 .

At this point, it is important to note that the 4-species tournament has two subsets of three species that constitute a cyclic tournament, i.e., the Rock-Paper-Scissors game, and two subsets that constitute a hierarchical tournament. In Fig. 2.20 the set of species $\{S_0, S_1, S_2\}$ and $\{S_0, S_2, S_3\}$ dominate each other in a cyclic manner (shaded areas in Fig. 2.20) while the set of species $\{S_0, S_1, S_3\}$ and $\{S_1, S_2, S_3\}$ dominate each other in a hierarchical manner (upper and lower half, respectively, of the tournament scheme Fig. 2.20). Hence, the survival of S_0 and S_2 are a necessary condition for the emergence of a non-hierarchical three species tournament from the four species tournament. When S_1 or S_3 die out, the tournament of the remaining species corresponds,

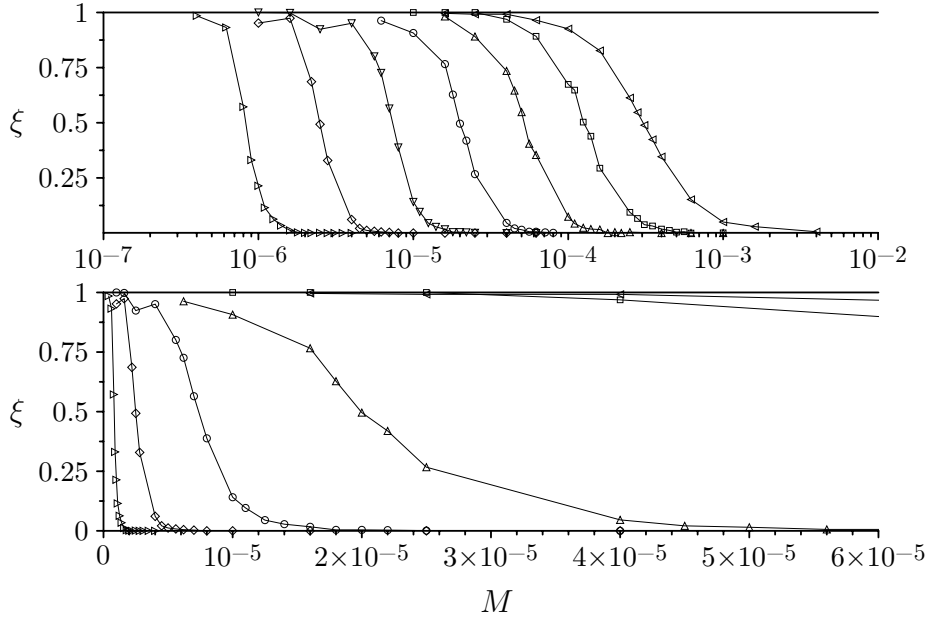


Figure 2.22: Transition from a cyclic to a hierarchical three species tournament arising from an unstable four species tournament. Probability ξ in dependence on M for different system sizes $L \times L$, $L = 50$ (\triangleleft), $L = 100$ (\square), $L = 200$ (\triangle), $L = 400$ (\circ), $L = 800$ (\diamond), $L = 1600$ (\oplus), and $L = 3200$ (\triangleright) on a logarithmic M -axis (**upper row**) and a linear M -axis (**lower row**). Parameters are $\mu = \sigma = 1$ and $C = 50$.

accordingly, to the Rock-Paper-Scissors game. When, on the contrary, S_0 or S_2 die out, the tournament of the remaining species is transitive. The initial question under which conditions a tournament of four species collapses to a non-transitive three species tournament therefore translates to the question: Under which conditions does either species S_1 or species S_3 die out first?

In the non-spatial case, the choice of the initial conditions is decisive. Since S_0 is predicted to extinct first for symmetric initial conditions, a transitive three species tournament emerges in this case. Asymmetric initial conditions, on the other hand, favour S_1 to go extinct first and thus predict the emergence of a cyclic three species tournament.

For the non-spatial four species tournament (Fig. 2.20) symmetric initial conditions (all $s_k(t = 0)$ identical $\forall k$) favour the emergence of a hierarchical three species tournament. Asymmetric initial conditions, on the contrary, favour the emergence of a cyclic three species tournament.

For the subsequent study of the spatial and stochastic version of the four species tournament, it is instructive to define the probability ξ as

$$\xi := \text{Prob}(\{S_1 \text{ goes extinct first}\} \vee \{S_3 \text{ goes extinct first}\}), \quad (2.63)$$

where $\xi = 1$ means that the system always collapses to a Rock-Paper-Scissors game while $\xi = 0$ means that the system always collapses to a hierarchical three species tournament. In fact, for each single realisation of the stochastic spatial four species tournament, the bernoulli stochastic variable Ξ is defined to be 1 if either S_1 or S_3 goes extinct first and 0 if either S_0 or S_2 goes extinct first. Hence, Ξ is 1 with probability

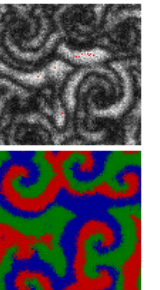
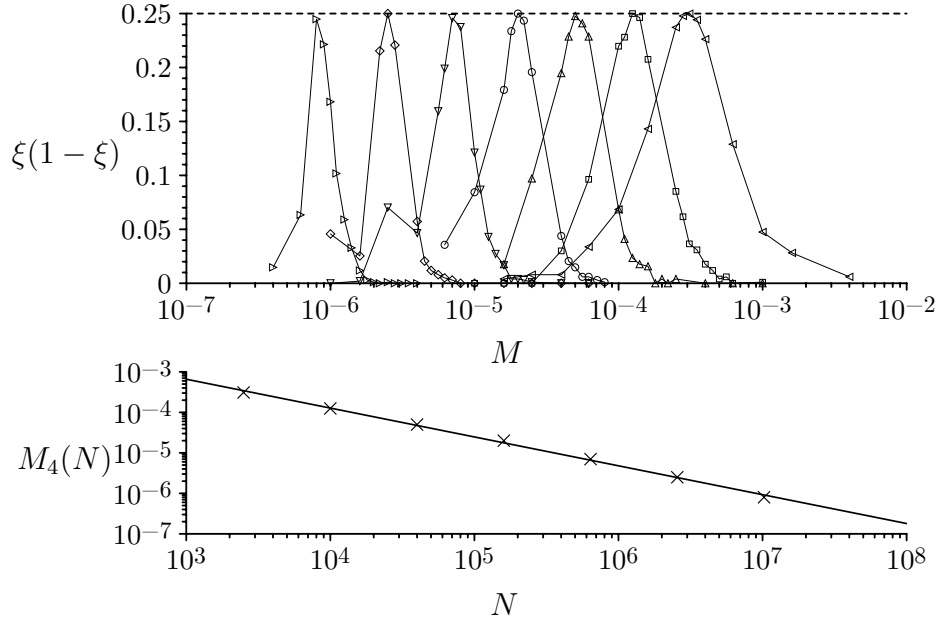


Figure 2.23: Determination of the critical mobility M_4 . **Upper row:** Variance of the order parameter Ξ for different system sizes $L \times L$ (symbols as in Fig. 2.22). Dashed horizontal line marks the maximal value of the variance of $1/4$. **Lower row:** Location M_4 of the maximum value of the variance in dependence on $N = L \times L$. Solid line is a power law fit $M_4 \propto N^{-\frac{1}{\nu}}$ with $\nu \approx 4/3$



ξ and 0 with probability $1 - \xi$. Since the sum over Ξ for different realisations is binomially distributed with parameter ξ , ξ can be computed as the average $\langle \Xi \rangle$ over many realisations.

In order to study the spatial stochastic version of the four species tournament, the lattice based population model is adapted to four species such that each individual either reproduces, dies, or migrates to an adjacent site with the respective probabilities Eq. (2.12). The only difference is the definition of $\sigma_i^*(x, y)$, which is adapted to the tournament scheme as given in Eq. (2.62). As before, the lattice is initialised with random initial condition, viz. all lattice sites are populated by a random number between 0 and 5 individuals of each species.

In the limit $M \rightarrow \infty$, every individual changes its position in the lattice so often before it reacts for the first time that fluctuations in the initial distribution of species are balanced. In that case the system resembles the nonspatial version with symmetric initial conditions and the observation that S_0 then dies out first suggests, that a transitive three species tournament emerges quickly for large mobilities, i.e., $\xi(M \rightarrow \infty) = 0$. If, on the other hand, the mobility is so small that fluctuations in the initial distribution persist, the locally asymmetric initial conditions favour the extinction of S_1 . If S_1 only survives in a small region whereas the remaining space is filled with S_0 , S_2 , and S_3 , which constitutes the Rock-Paper-Scissors game and which potentially form entangled spiral waves, S_1 cannot invade this region. On the contrary, a spiral wave consisting of S_0 , S_2 , and S_3 will take over regions formerly occupied by S_1 . This suggests that the spatial four species tournament collapses to a non-hierarchical three species tournament for low mobilities, i.e., $\xi(M \rightarrow 0) = 1$. Accordingly, it should be expected there is a transition from $\xi = 1$ for small mobilities to $\xi = 0$ for large mobilities.

To check this expectation, Fig. 2.22 shows ξ in dependence on M for various system sizes N measured from simulations of the LBPM adapted to four species. $\xi(M)$ clearly

shows a transition from $\xi = 1$ to $\xi = 0$ for growing M . This confirms the expectation that the four species tournament always collapses to a cyclic three species tournament in a spatial setting for low mobilities, while it reduces to a hierarchical three species tournament for large mobilities. The mobility M is thus decisive for the transient (i.e. the path in phase space from the unstable configuration leading to a stable configuration) on which the dynamics leaves the unstable four species state.

The upper row in Fig. 2.22 also shows that increasing the system size N shifts the curves $\xi(M)$ to smaller mobilities, implying that the probability ξ decreases for increasing N for any M . Note that N is referred to as the system's size because the number of individuals in the system is proportional to N . Yet N rather relates to the system's resolution L^{-1} because the system's linear extent is normalised to unity by the definition of M (see Sec. 2.2). Increasing N thus means that the number of lattice sites in any fixed subarea of the plane increases. The fluctuations in the initial distribution of species, i.e., the deviation from the symmetric case, accordingly decreases in

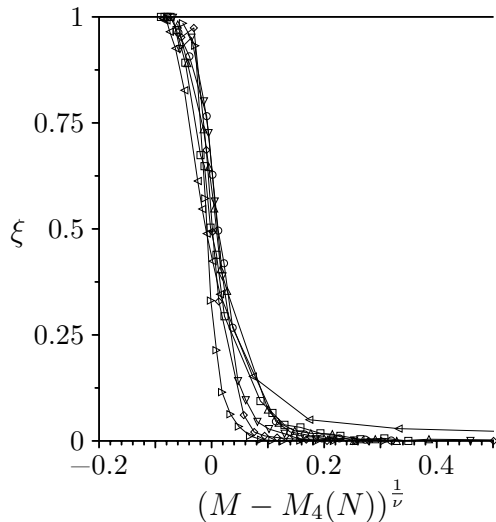
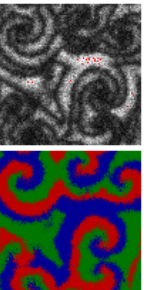


Figure 2.24: Rescaled transition of the probability ξ for a non-hierarchical three species tournament to arise from the four species tournament shown in Fig. 2.20 in a spatial environment. Labels as in Fig. 2.22.

the subarea because the standard deviation from the mean number of individuals of any species in the subarea is proportional to $1/\sqrt{N}$. In the limit $N \rightarrow \infty$ any subarea is thus initialised with the same number of individuals from each of the four species, suggesting that S_0 dies out first and a transitive three species tournament emerges, i.e., $\xi = 0$ for any M . This explains why increasing N decreases $\xi(M)$ and thus leads to a shift of the curves $\xi(M)$ to smaller mobilities. The upper row in Fig. 2.22 further suggests that the curves $\xi(M)$ for different N can be described by a universal function after an appropriate rescaling of the mobility M . To characterise the transition and particularly its dependence on the system size N it is thus helpful to determine the location of the curves $\xi(M)$. A sensible choice to determine its location is by finding the value M_4 for which $\xi = 0.5$. Conveniently, this corresponds to the maximum of the function $\xi(1 - \xi)$, which is also the variance of the stochastic variable Ξ (since $\langle \Xi \rangle = \xi$, the variance of Ξ is $var(\Xi) = \langle \Xi^2 \rangle - \langle \Xi \rangle^2 = \langle \Xi \rangle - \langle \Xi \rangle^2 = \xi(1 - \xi)$ as $\Xi^2 = \Xi$). Furthermore, it is known from finite size scaling theory that the maximum of the fluctuation of Ξ marks the critical parameter $M_4(N)$ of a phase transition for finite sizes if Ξ is an order parameter associated with a second order phase transition (Cardy, 1997). Fig. 2.23 shows the variance $\xi(1 - \xi)$ for the curves from Fig. 2.22 and the according scaling of M_4 with N . The critical mobility is well described by a power law dependency $M_4(N) = bN^{-\frac{1}{\nu}}$ with $\nu \approx 4/3$ and a scaling amplitude b , suggesting that the transition is of second order. To check whether the curves in Fig. 2.22 can be described by a

the subarea because the standard deviation from the mean number of individuals of any species in the subarea is proportional to $1/\sqrt{N}$. In the limit $N \rightarrow \infty$ any subarea is thus initialised with the same number of individuals from each of the four species, suggesting that S_0 dies out first and a transitive three species tournament emerges, i.e., $\xi = 0$ for any M . This explains why increasing N decreases $\xi(M)$ and thus leads to a shift of the curves $\xi(M)$ to smaller mobilities.

The upper row in Fig. 2.22 further suggests that the curves $\xi(M)$ for different N can be described by a universal function after an appropriate rescaling of the mobility M . To characterise the transition and particularly its dependence on the system size N it is thus helpful to determine the location of the curves $\xi(M)$. A sensible choice to determine its location is by finding the value M_4 for which



universal function after rescaling according to $\xi(M, N) \propto F[(M - M_4(N)) N^{\frac{1}{\nu}}]$ with some universal scaling function $F[.]$, Fig. 2.24 shows the curves from Fig. 2.22 as a function of the rescaled mobility $(M - M_4(N)) N^{\frac{1}{\nu}}$ (see Cardy, 1997, for more details). Although the collapse is not perfect, the similarity of the rescaled curves is remarkable compared to the unscaled curves in the lower row of Fig. 2.22. The transition of $\xi = 1$ to $\xi = 0$ can hence indeed be characterised as a phase transition of second order and the fit $M_4(N) = bN^{-\frac{1}{\nu}}$ suggests that the critical mobility is $M_4 = 0$.

There is a critical mobility $M_4(N) \propto N^{-\frac{1}{\nu}}$ with $\nu \approx \frac{4}{3}$, below which the spatial four species tournament collapses to a three species tournament of cyclically competing species. For mobilities larger than the critical mobility, the spatial four species tournament reduces to a hierarchical three species tournament.

The fact that the critical mobility $M_4(N \rightarrow \infty)$ is zero is a direct consequence of the fact that the fluctuations in the initial conditions decrease with N . Choosing initial conditions that are independent of the spatial resolution L^{-1} should thus be expected to yield a critical mobility different from 0.

In conclusion, the mobility of individuals plays a pivotal role concerning the emergence of cyclically competing species. If the mobility increases beyond the critical mobility $M_4(N)$ for a given system size, the four species tournament collapses to a hierarchical three species tournament instead of the cyclic tournament. A low mobility, hence, promotes the *emergence* of cyclic competition.

2.6 Discussion

The *lattice based population model* exhibits two dynamically distinct states, just like the original model by Reichenbach et al. (2007a): A well-stirred state, in which individuals diffuse so quickly that no spatial patterns emerge, and a spiralling state, in which the three species form entangled travelling spiral waves. The two dynamic states were supposed to correspond uniquely to two stability regimes (Reichenbach et al., 2007a); one where coexistence is stable and one where it is unstable. The observation in Sec. 2.3.2 of a broad mobility regime that is ambiguous with respect to the stability of coexistence, however, shows that the identification of the spiralling state with stable coexistence is at least not in general correct for a system of cyclically and spatially competing species that form entangled spirals. The consequence of this observation is that the transition between the spiralling and the well-stirred state can in general not be characterised by the changing stability properties.

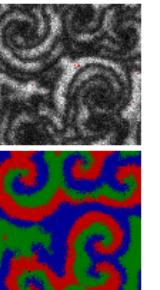
This notwithstanding, the introduction of the *carrying capacity* provides an alternative way of characterising the transition between the well-stirred state and the spiralling state. Counterintuitively, increasing the carrying capacity (and thus enlarging the population) leads to an accelerated extinction process in the well-stirred regime. Since the carrying capacity acts as to stabilise coexistence in the spiralling state, in contrast, the typical time to extinction exhibits diametrically opposite dependencies on the carrying

capacity in the two dynamical regimes. The critical mobility is therefore defined as the one where the two dynamical regimes influence the typical time until extinction occurs equally strong, rendering it independent of the carrying capacity. This is a feasible way to characterise the transition without resorting to study the asymptotic dependency of the typical time until extinction on the system size (Lamouroux et al., 2012).

The idea to relax the restriction of only one individual at maximum per lattice site has not only been followed in the present work (and Lamouroux et al., 2012, accordingly). He et al. (2010) studied a similar spatial model of the Rock-Paper-Scissors game where the global density of individuals is conserved and allowed more than one individual per lattice site. In their framework, the carrying capacity controls whether individuals can migrate to a certain site; only if the population of the target site has not yet reached the carrying capacity may individuals travel to that site. This corresponds to the situation analysed by Lugo and McKane (2008) where the density dependent migration leads to a cross-diffusion term in the deterministic equations. In that case, migration cannot simply be accounted for by the usual Laplacian. He et al. (2010) find that the introduction of the carrying capacity has no relevant impact in their framework.

The same authors (He et al., 2011) also studied the original model by Reichenbach et al. (2007a) with a fixed unit carrying capacity and measured the dependence of the mean time to extinction $\langle \tau_{\text{ex}} \rangle$ on the spatial system size N , similar to the results presented in Sec. 2.3.2. As they do not specifically consider the mobility regime of the transition between the spiralling and the well-stirred state, they do not find the ambiguous behaviour of the mean time to extinction. For the extreme cases, He et al. (2011) find, in contrast to the results from the LBPM, a linear dependence of $\langle \tau_{\text{ex}} \rangle$ on N in the well-stirred regime and the dependence $\langle \tau_{\text{ex}} \rangle \propto \frac{e^N}{N}$ in the spiralling regime. Since the two models are not identical, a direct comparison should be considered with care. However, one explanation for the different scaling behaviours might be the different lattice sizes that have been used. He et al. (2011) studied system sizes ranging from $N = 5 \times 5$ to $N = 25 \times 25$ while the results in Sec. 2.3.2 were obtained for system sizes ranging from $N = 18 \times 18$ to $N = 800 \times 800$ in the well-stirred state and $N = 8 \times 8$ to $N = 35 \times 35$ for the spiralling state. The exponential and logarithmic dependence in Fig. 2.11 are hardly visible if only system sizes up to $N = 25 \times 25$ are considered.

A model similar to the LBPM was studied by Rulands et al. (2011) in one spatial dimension. They considered a carrying capacity, which regulates reproduction, with a subtle but decisive difference to the LBPM. In the LBPM the rate of competition is proportional to the absolute number of individuals of the superior species, i.e., σs_{i+2} . This is the reason why C cannot be interpreted as a thermodynamic volume (see Sec. 2.2.1). In the model by Rulands et al. (2011), the rate of competition is $\sigma_R = \sigma s_{i+2}/C$. This, in contrast, allows to interpret the carrying capacity as a thermodynamic volume similar to the system size N . They are thus able to study the thermodynamic limit by two equivalent approaches; either by considering large system sizes or by considering large carrying capacities. The original difficulty that only a limited range of system sizes can be feasibly analysed is thus eased. However, the carrying capacity being a thermodynamic limit also allows to derive a stochastic differential equation for the local dynamics. The noise term of the local dynamics then decreases with the carrying



capacity as $1/\sqrt{C}$. As a result, the typical time to extinction t^* grows with increasing C – the system becomes more stable. In the LBPM, on the contrary, fluctuations grow with C , which is the reason for the destabilising effect of enlarging C in the well-stirred state. In the model by Rulands et al. (2011), the discrimination of the spiralling state and the well-stirred state by the respective dependence of t^* on C is thus not possible because t^* increases with C in both regimes.

To illustrate the difference between the two approaches of introducing a carrying capacity, one can imagine an experiment with bacterial strains in a petri dish. The carrying capacity in the model by Rulands et al. (2011) then corresponds to the size of the (well-stirred) dish. The fluctuations of the density of bacteria, thus, vanish by enlarging the petri dish. Contrary to this, the carrying capacity in the LBPM rather corresponds to the intensity of the nutrient solution. Increasing the intensity of the nutrient solution raises the number of bacteria in the dish without increasing the volume. As the spatial density of bacteria thus increases, competitive interactions become more frequent and therefore the corresponding fluctuations increase (cf. Lamouroux et al., 2012).

While the stability of cyclic competition among three species has attracted a considerable amount of interest, the question of the emergence thereof has been rarely addressed (Corl et al., 2010). In this respect, the study of a four species system in Sec. 2.5 is an important step in this direction. Existing studies that consider non-hierarchical competition among four species (Szabó and Sznaider, 2004) assume that at least two species do not compete with each other to ensure the existence of an equilibrium state in which all four species coexist. If there are no such *neutral pairs*, no coexistence equilibrium exists, and one species quickly becomes extinct in any finite system. The four species model studied in Sec. 2.5 is thus well suited to study under which conditions cyclic competition among three species emerges from ecosystems with more species. The analysis in Sec. 2.5 shows that there is a critical mobility for any system size below which a cyclic tournament of three species emerges while above it a hierarchical tournament emerges.

Chapter 3

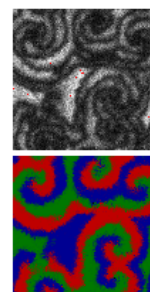
Immunity Eliciting Diseases

3.1 Introduction

Many diseases like measles, rubella, mumps, foot-and-mouth disease or influenza elicit temporal or life-long immunity upon recovery. For these diseases, susceptible, infectious, and recovered individuals exhibit similar cyclic dynamics as the three species in the Rock-Paper-Scissors game, described in the previous chapter: The number of recovered individuals increases due to the presence of infectious individuals (recovery); the number of infectious individuals increases due to the presence of susceptible individuals (infection); and the number of susceptible individuals increases because (i) all individuals are born susceptible, even those descending from infectious and recovered individuals, and because (ii) recovered individuals return to be susceptible in case that immunity is only temporal. This order causes the cyclic population dynamics and give rise to so-called *recurrent epidemics* (see Keeling and Rohani, 2008; Anderson and May, 1991).

As with any epidemic, a major goal of epidemiological modelling is to design containment strategies that aim at eradicating or at least stemming the disease. While this clearly requires the knowledge of the biological traits of the disease, the understanding of the mechanisms responsible for the proliferation of the disease on the population level is sometimes even more important. Almost a hundred years after the seminal study by Fisher (1937) and by Kolmogoroff et al. (1937), spatial aspects have been recognised as one of the most important ingredient in epidemiological modelling.

For recurrent epidemics, spatial heterogeneity influences the disease dynamics in a manifold manner. One of the earliest problems that required the inclusion of spatial aspects, and which still attracts a lot of attention, is the *persistence* of recurrent epidemics (Bartlett, 1957). The finiteness of any individual population can cause the disease to become extinct when the number of infectious individuals passes through a trough of its oscillation. Non-spatial models, however, usually fail to explain the comparably small observed *critical community size*, needed for a disease to persist (Bartlett, 1957). The interplay between different communities, embedded in a so-called *metapopulation*, however, can substantially increase the persistence of a disease due to mutual reintroduction of the disease (Grenfell, 1992; Keeling, 2000; Hagenaars et al., 2004;



Jesse et al., 2008; Liu et al., 2009).

In the strive for optimal vaccination strategies, the consideration of heterogeneously distributed populations has shown quite early that ignoring heterogeneity can lead to vaccination strategies that do not eradicate the disease (May and Anderson, 1984; Hethcote and van Ark, 1987). The interplay of vaccination strategies and spatial heterogeneity can further act as to synchronise the populations (Rohani et al., 1999), which is also seen for a sufficiently large coupling between the individual populations (Lloyd and May, 1996; Lloyd and Jansen, 2004). In any case, synchrony increases the probability of global extinction of the disease because all populations simultaneously pass through the troughs of the recurrent epidemic.

An important characteristic property of a recurrent epidemic is its *endemic state*: For long enough times, the case numbers settle to a stationary value, in which case the epidemic is called *endemic*. The endemic state is not only important to understand the long term dynamics of infectious diseases, though. It is also important for the design of containment measures like, e.g., vaccination strategies, which aim at shifting the endemic state such that the case numbers drop to zero. The endemic state for general systems of spatially segregated populations is, thus, well studied concerning its existence and stability (Post et al., 1983; May and Anderson, 1984; Hethcote and van Ark, 1987). However, most studies that go beyond these questions and quantitatively assess properties of metapopulation models assume that the infection rate of the disease is the same in every population (May and Anderson, 1984; Hethcote and van Ark, 1987; Grenfell, 1992; Lloyd and May, 1996; Keeling, 2000; Xia et al., 2004; Hagenaars et al., 2004). It was noted quite early, though, that “Subpopulations can be determined not only on the basis of disease-related factors [...] but also on the basis of social, cultural, economic, demographic, and geographic factors” (Hethcote and van Ark, 1987) and Grenfell and Bolker (1998) found that empirical observations are consistent with the assumption that infection rates are higher in urban centres than in rural areas. However, spatially varying infection rates have only very rarely been used (an example is the study by Grassly et al., 2005). Yet there is no work to the best knowledge of the author that explicitly considers the impact of spatial coupling on the endemic states of the subpopulations if the infection rate varies between them. Such situations, however, arise naturally in modern times, where the world becomes ever more interconnected. If different countries obey different health regulations or face different climatic conditions, the infectiousness of a disease may vary across the world. While there is an increasing interest in human migrations patterns (Brockmann et al., 2006; González et al., 2008; Simini et al., 2012) and in the spread of viruses on social or communication networks (Kuperman and Abramson, 2001; Pastor-Satorras and Vespignani, 2001), the interplay between asymmetries in disease properties and spatial coupling has surprisingly been overlooked so far. Yet this question is not restricted to the global scale of migration. Differences in the infectiousness may occur on many spatial scales, may it be different counties, cities, municipal districts or even different public buildings.

On a similar note, this question does not only concern human communities but can also apply to animal populations or coupling in communication networks. Different farms or livestock herds may well experience different hygienic measures and thus be

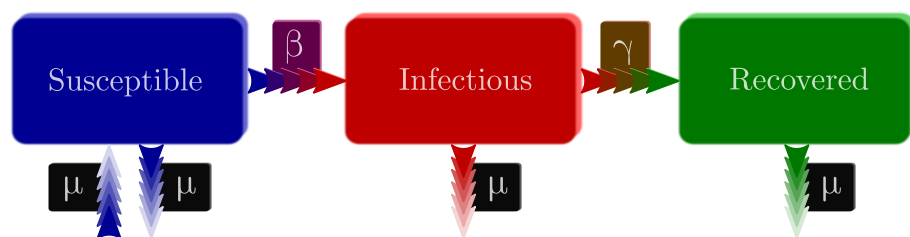


Figure 3.1: Schematic depiction of a SIR model with demography, i.e., a non-spatial compartmental model for a disease that elicits life-long immunity.

subject to varying infectiousness. Modelling all levels of heterogeneity may, however, be cumbersome - and sometimes unnecessary.

From this, two questions arise that are addressed in this dissertation. First, what is the effect of coupling on the endemic states of subpopulations if the coupled communities are subject to different infection rates? And second, which degree of spatial complexity has to be explicitly accounted for to describe the effect of coupling on a single population?

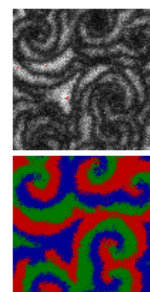
In the next sections of this dissertation, I study a metapopulation model for recurrent epidemics that considers an infectiousness that varies from subpopulation to subpopulation. I show how coupling alters the endemic states of the subpopulation in an unexpected manner with potentially severe implications for the design of travel restriction measures. I furthermore study how the spatial complexity of a metapopulation can be reduced to effectively model the impact of coupling on a single population.

3.2 A Metapopulation Model for Spatially Varying Infectiousness

Recurrent epidemics can arise from diseases that elicit temporal or life-long immunity upon recovery. From a modelling perspective, both kinds of diseases exhibit dynamically similar behaviours. For humans, diseases that elicit life-long immunity are, however, predominant compared to diseases that elicit temporal immunity and thus constitute the main part of the analysis in the next sections. In Sec. 3.3 the corresponding results for a model with temporal immunity will be derived and discussed.

3.2.1 Nonspatial Compartmental Model

The classification of individuals into groups of susceptible, infectious, and recovered individuals is clearly a simplification. In reality, the boundary between these classes are not sharp but depend on the density of the pathogen in the infected host (Keeling and Rohani, 2008). While the ability to spread the disease grows and decays continuously within each host, it is sufficient to model infectiousness as a binary property for epidemiological questions, which pertain to the spread of a disease on the population level. This kind of model, in which every individual is classified into one group out of



a discrete set of groups, is called *compartmental model*.

Before the full metapopulation model is introduced in the next section, it is instructive to consider the dynamics of an isolated population without connections to other communities. Inside such a population, the disease spreads from individual to individual by direct contacts. The rate at which a susceptible individual contracts the disease depends on two different factors; the probability for a contact with an infectious individual, $\frac{I}{N}$, and the rate of infection, β . Here, the absolute number of infectious individuals is denoted by I and the size of the population is denoted by N . The number of susceptible and recovered individuals are accordingly denoted by S and R , respectively. Once infectious, individuals recover at a constant rate γ . It is assumed that no disease related death occurs. For simplicity, the population size is kept constant by requiring that the rate at which natural death occurs is balanced by the rate at which offspring is produced. Both is denoted by μ . All offspring is born susceptible to the disease. The temporal evolution of S , I , and R is thus governed by

$$\partial_t S = -\beta S \frac{I}{N} - \mu S + \mu(S + I + R) \quad (3.1a)$$

$$\partial_t I = \beta S \frac{I}{N} - \mu I - \gamma I \quad (3.1b)$$

$$\partial_t R = -\mu R + \gamma I. \quad (3.1c)$$

For obvious reasons, this model is referred to as the SIR model with demography (see Anderson and May, 1991; Keeling and Rohani, 2008). Since S , I , and R are integer number, these equations are only illustrative. However, for $N \rightarrow \infty$ the equivalent equations for the fractions $x := \frac{X}{N}$ for $X \in \{S, I, R\}$ describe the exact temporal evolution:

$$\partial_t s = -\beta si + \mu(1 - s) \quad (3.2a)$$

$$\partial_t i = \beta si - (\mu + \gamma) i \quad (3.2b)$$

Here, and in the following, the equation for r is omitted, since $S + I + R = N$ or equivalently $s + i + r = 1$. It is also possible to rigorously derive Eq. (3.2) from the master equation for the microscopic reactions in the limit $N \rightarrow \infty$ (see box **Interlude II: Stochastic description of birth-death processes** on page 8). For brevity, this derivation is not shown here since it provides no further insight.

When a disease appears for the first time, e.g., by a mutation of an earlier pathogen, the entire population is susceptible to the disease. Whether a disease can invade such a population, depends on the *basic reproductive ratio* $R_0 := \frac{\beta}{\gamma + \mu}$. Setting $s \approx 1$ in Eq. (3.2) shows that an infinitesimal fraction of infectious individuals grows with rate $\beta - \gamma - \mu$. Only if $R_0 > 1$, can the infection thus spread in the population.

Without external perturbation, a disease that can be described by the SIR model settles to the endemic state in the long run. The endemic state of a disease is nothing else than the fixed point of Eq. (3.2). The fraction of susceptible and infectious individuals in the endemic state are, hence, (Anderson and May, 1991; Keeling and Rohani, 2008)

$$s^E = \frac{1}{R_0} \quad \text{and} \quad i^E = \frac{\mu}{\gamma + \mu} (1 - s^E). \quad (3.3)$$

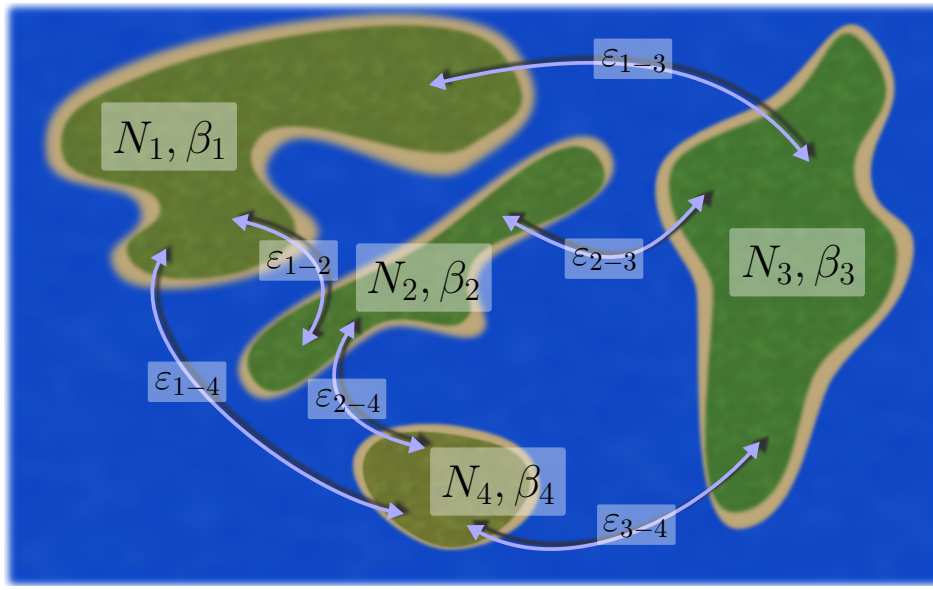


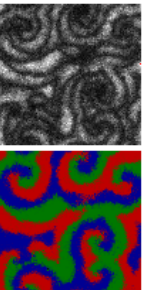
Figure 3.2: Illustration of the metapopulation concept. The metapopulation comprises four different, spatially segregated subpopulations of sizes N_1, \dots, N_4 , that are nonetheless interconnected to each other by the symmetric travelling rate $\varepsilon_{k-\ell}$. In the metapopulation model considered here, the subpopulations additionally differ in their respective infection rates β_1, \dots, β_4 due to, e.g., climatic, socio-cultural or economic reasons.

The disease free state $i = 0, s = 1$ is also a fixed point of Eq. (3.2). Linearising Eq. (3.2) around the endemic state Eq. (3.3) and the disease free state reveals that they are stable and unstable, respectively, if and only if $R_0 > 1$ (Keeling and Rohani, 2008). For $R_0 < 1$, however, the endemic state is disease free itself. The SIR model physically resembles a damped oscillator. Starting from any point (s, i) in phase space the system performs damped oscillations towards the endemic state with frequency $\nu \approx \frac{2\pi}{\sqrt{\mu(\gamma+\mu)(R_0-1)}}$ (Keeling and Rohani, 2008).

Eq. (3.2) shows that the properties of the endemic state of an isolated population are essentially determined by the basic reproduction ratio R_0 . In a set of isolated populations with the same disease unrelated birth/death rate μ and the same infectious duration γ^{-1} , the endemic states, hence, vary according to the variation in the (local) infection rate β .

3.2.2 Metapopulation Model

The metapopulation concept bases on the idea that species live in spatially separated and locally confined habitats that together constitute the global population. Interaction between individuals occurs correspondingly on two scales: The immediate interaction like predation or competition for resources takes place inside the local populations, which can be considered to be well-stirred. The indirect interaction like migration or the colonisation of empty habitats takes places on the metapopulation level (see Hanski, 1998, and references therein). The original metapopulation model goes back to Levins (1969), who modelled the individual populations as being either populated or empty and omitted the local dynamics. In epidemiology, the metapopulation is usually modelled by explicitly considering the local dynamics of the individual populations, who are then coupled to the dynamics of the other populations (Post et al., 1983; May and Anderson, 1984; Hethcote and van Ark, 1987; Grenfell, 1992; Lloyd and May, 1996;



Keeling, 2000; Lloyd and Jansen, 2004; Hagenaars et al., 2004; Xia et al., 2004; Jesse et al., 2008). Usually the coupling is realised as an effective coupling that does not explicitly consider the migration of individuals from population to population. The consequences of this effective coupling will be discussed in Sec. 3.2.5.

The metapopulation model that is introduced in this section consists of M individual populations with size N_k ($k \in \{1, \dots, M\}$). The dynamics of each population can be described by the SIR model from Sec. 3.2.1 with group sizes S_k , I_k , and R_k . The birth/death rate μ and the recovery rate γ are assumed to be independent of the location of the respective individual. The infection rate β_k , however, depends on the common location of the susceptible and infectious individual. Accordingly, the basic reproductive ratio $R_{0,k}$ also varies across the subpopulations. This implies that any susceptible individual can only contract the disease from an infectious individual located in the same population. In addition, individuals travel from population k to population ℓ irrespective of their health state with rate $\varepsilon_{\ell k}$. Including the coupling into the temporal evolution, Eq. (3.1) becomes

$$\partial_t S_k = -\beta_k S_k \frac{I_k}{N_k} + \mu(N_k - S_k) + \sum_{\ell=1}^M (S_\ell \varepsilon_{k\ell} - S_k \varepsilon_{\ell k}) \quad (3.4a)$$

$$\partial_t I_k = \beta_k S_k \frac{I_k}{N_k} - (\gamma + \mu)I_k + \sum_{\ell=1}^M (I_\ell \varepsilon_{k\ell} - I_k \varepsilon_{\ell k}) \quad (3.4b)$$

Again, these equations are only illustrative as S_k and I_k cannot evolve continuously. Meaningful equations arise in the limit $N_k \rightarrow \infty$ for the fractions $s_k := \frac{S_k}{N_k}$ and $i_k := \frac{I_k}{N_k}$.

$$\partial_t s_k = -\beta_k s_k i_k + \mu(1 - s_k) + \sum_{\ell=1}^M \left(s_\ell \frac{N_\ell}{N_k} \varepsilon_{k\ell} - s_k \varepsilon_{\ell k} \right) \quad (3.5a)$$

$$\partial_t i_k = \beta_k s_k i_k - (\gamma + \mu)i_k + \sum_{\ell=1}^M \left(i_\ell \frac{N_\ell}{N_k} \varepsilon_{k\ell} - i_k \varepsilon_{\ell k} \right) \quad (3.5b)$$

For any set of finite populations $\{N_1, \dots, N_M\}$, Eqs. (3.5) describe the temporal evolution of the expectation value of s_k and i_k around which fluctuations due to the finite populations arise.

To ensure that the size of the individual populations N_k is conserved also in the metapopulation, the number of outgoing and incoming individuals per unit time has to balance, i.e., $\sum_\ell N_k \varepsilon_{\ell k} = \sum_\ell N_\ell \varepsilon_{k\ell}$. This can be achieved by imposing a detailed balance condition for each connection, i.e., $N_k \varepsilon_{\ell k} = N_\ell \varepsilon_{k\ell}$. Given the population sizes N_k , this relation uniquely determines $\varepsilon_{\ell k}$ from $\varepsilon_{k\ell}$, and vice versa. It is thus possible to define the *symmetric travelling rate* between population ℓ and k as $\varepsilon_{\ell-k} \equiv \varepsilon_{k-\ell} := \frac{1}{2} (\varepsilon_{\ell k} + \varepsilon_{k\ell})$. With $\varepsilon_{k\ell} \frac{N_\ell}{N_k} = \varepsilon_{\ell k}$ and $\varepsilon_{\ell k} = \frac{2N_\ell}{N_\ell + N_k} \varepsilon_{\ell-k}$, Eq. (3.5) admits

the form:

$$\partial_t s_k = -\beta_k s_k i_k + \mu(1 - s_k) + \sum_{\ell=1}^M \frac{2N_\ell}{N_k + N_\ell} \varepsilon_{\ell-k} (s_\ell - s_k) \quad (3.6a)$$

$$\partial_t i_k = \beta_k s_k i_k - (\gamma + \mu)i_k + \sum_{\ell=1}^M \frac{2N_\ell}{N_k + N_\ell} \varepsilon_{\ell-k} (i_\ell - i_k) \quad (3.6b)$$

Eq. (3.6) constitutes a $2M$ -dimensional system of nonlinear partial differential equations. The next section considers the special case of two coupled populations ($M = 2$) and analyses the impact of coupling on the endemic states of the two individual populations for $\beta_k \neq \beta_\ell$. In Sec. 3.2.4 a more general case is considered and a method to effectively reduce the spatial complexity, embodied in the metapopulation, is devised.

3.2.3 Paradoxical Effects of Coupling

What is the effect of coupling if the coupled communities exhibit different infection rates? The simplest case in which this question can be answered is a metapopulation that consists of two populations, i.e. $M = 2$. For two communities, Community 1 and Community 2, Eq. (3.6) reduces to an effectively four dimensional system:

$$\partial_t s_1 = -\beta_1 s_1 i_1 + \mu(1 - s_1) + \frac{2N_2}{N_1 + N_2} \varepsilon_{1-2} (s_2 - s_1) \quad (3.7a)$$

$$\partial_t i_1 = \beta_1 s_1 i_1 - (\gamma + \mu)i_1 + \frac{2N_2}{N_1 + N_2} \varepsilon_{1-2} (i_2 - i_1) \quad (3.7b)$$

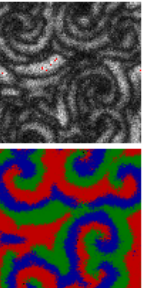
$$\partial_t s_2 = -\beta_2 s_2 i_2 + \mu(1 - s_2) + \frac{2N_1}{N_1 + N_2} \varepsilon_{1-2} (s_1 - s_2) \quad (3.7c)$$

$$\partial_t i_2 = \beta_2 s_2 i_2 - (\gamma + \mu)i_2 + \frac{2N_1}{N_1 + N_2} \varepsilon_{1-2} (i_1 - i_2) \quad (3.7d)$$

For $\varepsilon_{1-2} = 0$, this system reduces to two isolated populations that each settle to their respective known endemic state Eq. (3.3). The first thing to study is, hence, how the endemic states change with a non-zero travelling rate ε_{1-2} . To assess the quality of the change, two quantities are employed that measure the epidemiological gravity of a disease:

- The *prevalence* π , describing the dissemination of a disease. The prevalence equals the fraction of infectious individuals, i.e., $\pi_k \equiv i_k^E$.
- The *incidence rate* φ , describing the rate at which new contagions occur per unit time and population size. The incidence rate is $\varphi_k := \frac{\beta_k s_k^E i_k^E}{N_k} \equiv \beta_k s_k^E i_k^E$.

In general, π and φ are time dependent quantities, but the incidence rate and the prevalence of the endemic state considered here are constant properties of the system described by Eq. (3.7). To learn how the prevalence and the incidence rate of a community in the endemic state are influenced by coupling to another community, it



is necessary to analyse the dependence of s_k^E and i_k^E on ε_{1-2} .

Without loss of generality, it is assumed that the infection rate in Community 1 is higher than the infection rate in Community 2, i.e. $\beta_1 > \beta_2$ or equivalently $R_{0,1} > R_{0,2}$. In the uncoupled case $\varepsilon_{1-2} = 0$, the prevalence and the incidence rate of the two communities are implicitly given by Eq. (3.3):

$$\pi_k(0) = \frac{1}{\gamma + \mu} \frac{\mu}{R_{0,k}} (R_{0,k} - 1) \quad (3.8a)$$

$$\varphi_k(0) = \frac{\mu}{R_{0,k}} (R_{0,k} - 1) \quad (3.8b)$$

Since $\frac{R_{0,k}-1}{R_{0,k}}$ is a strictly monotonically increasing function in $R_{0,k}$, Community 1 has the higher prevalence and also the higher incidence rate. Intuitively, it should be expected that coupling acts as to reduce the differences between the communities and that the prevalences and the incidence rates strictly converge. Illustratively speaking, coupling Community 1 to Community 2, which has higher health standards and therefore a lower incidence rate and prevalence, should be beneficial for Community 1 and deleterious to Community 2.

For a general coupling strength ε_{1-2} , the endemic states of the two communities cannot be found directly by scrutinising Eq. (3.7). However, for large ε_{1-2} as well as for small ε_{1-2} , approximations can be obtained analytically. To validate or invalidate the expectation that the prevalence and incidence rate of the two communities monotonically converge to an average value, the limit of very strong coupling and the limit of weak coupling are, thus, considered separately.

Strong coupling limit

To find the endemic states for $\varepsilon_{1-2} \rightarrow \infty$ a power series ansatz in the inverse coupling strength $\kappa := 1/\varepsilon_{1-2}$ can be employed:

$$s_k^E(\kappa) = s_{k,\infty}^{(0)} + \sum_{p=1}^{\infty} s_{k,\infty}^{(p)} \kappa^p \quad (3.9a)$$

$$i_k^E(\kappa) = i_{k,\infty}^{(0)} + \sum_{p=1}^{\infty} i_{k,\infty}^{(p)} \kappa^p \quad (3.9b)$$

Here, $s_{k,\infty}^{(p)}$ and $i_{k,\infty}^{(p)}$ denote the coefficients of order p . It is implicitly assumed that there is a κ_c such that for all $\kappa < \kappa_c$ the series Eq. (3.9) converges. The idea behind such an ansatz is that truncating the series at some order p constitutes an approximation of the full series around $\kappa = 0$, whose precision increases with p . Truncating the series at $p = 0$ gives an approximation that is only valid for $\varepsilon_{1-2} \rightarrow \infty$ or equivalently $\kappa \rightarrow 0$. $s_{k,\infty}^{(0)}$ and $i_{k,\infty}^{(0)}$ thus denote the endemic states in the strong coupling limit.

Inserting Eq. (3.9) in Eq. (3.7) and performing the limit $\kappa \rightarrow 0$, gives

$$0 = -\beta_1 s_{1,\infty}^{(0)} i_{1,\infty}^{(0)} + \mu(1 - s_{1,\infty}^{(0)}) + \frac{2N_2}{N_1 + N_2} \left(s_{2,\infty}^{(1)} - s_{1,\infty}^{(1)} + \lim_{\kappa \rightarrow 0} \frac{s_{2,\infty}^{(0)} - s_{1,\infty}^{(0)}}{\kappa} \right) \quad (3.10a)$$

$$0 = \beta_1 s_{1,\infty}^{(0)} i_{1,\infty}^{(0)} + (\mu + \gamma) i_{1,\infty}^{(0)} + \frac{2N_2}{N_1 + N_2} \left(i_{2,\infty}^{(1)} - i_{1,\infty}^{(1)} + \lim_{\kappa \rightarrow 0} \frac{i_{2,\infty}^{(0)} - i_{1,\infty}^{(0)}}{\kappa} \right). \quad (3.10b)$$

The analogous equations for Community 2 can be obtained by exchanging the subscripts 1 and 2. Since $s_{k,\infty}^{(0)}$ and $i_{k,\infty}^{(0)}$ are independent of κ by definition, the last terms in Eqs. (3.10) require that $s_{2,\infty}^{(0)} = s_{1,\infty}^{(0)}$ and $i_{2,\infty}^{(0)} = i_{1,\infty}^{(0)}$ for Eq. (3.10) to well be defined. Otherwise no solution can be obtained as the last terms diverge to infinity.

The two populations thus become identical in the fully coupled limit, confirming the expectation that the two populations behave as one large population for $\varepsilon_{1-2} \rightarrow \infty$.

To eliminate the terms of first order, $s_{k,\infty}^{(1)}$ and $i_{k,\infty}^{(1)}$, the equations for Community 1 and Community 2 have to be added weighted with the populations sizes N_1 and N_2 , respectively. Defining $s_\infty := s_{2,\infty}^{(0)} = s_{1,\infty}^{(0)}$ and $i_\infty := i_{2,\infty}^{(0)} = i_{1,\infty}^{(0)}$, this yields:

$$i_\infty s_\infty (N_1 \beta_1 + N_2 \beta_2) = \mu(1 - s_\infty)(N_1 + N_2) \quad (3.11a)$$

$$i_\infty s_\infty (N_1 \beta_1 + N_2 \beta_2) = i_\infty (N_1 + N_2)(\gamma + \mu) \quad (3.11b)$$

Defining the weighted arithmetic mean of the infection rates

$$\bar{\beta}_a := \frac{N_1 \beta_1 + N_2 \beta_2}{N_1 + N_2}, \quad (3.12)$$

Eq. (3.11) can be cast into

$$0 = -\bar{\beta}_a i_\infty s_\infty + \mu(1 - s_\infty) \quad (3.13a)$$

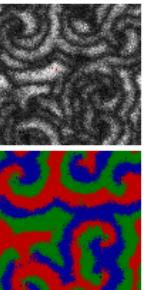
$$0 = \bar{\beta}_a i_\infty s_\infty - i_\infty(\gamma + \mu). \quad (3.13b)$$

This, however, are the known equations for the endemic state of a single well-stirred population. The solution, hence, is:

$$s_\infty = \frac{\gamma + \mu}{\bar{\beta}_a} \quad \text{and} \quad i_\infty = \frac{\mu}{\gamma + \mu} (1 - s_\infty) \quad (3.14)$$

In the fully coupled limit, the endemic states of the two populations can thus be described as a single population with a weighted average infection rate.

Fig. 3.3 shows an example of the fully coupled and uncoupled endemic states of two communities in the $s - i$ -plane. With the knowledge of the endemic cases in the two



extreme cases, the prevalence and incidence rate in these cases can be compared. The prevalence of the two communities in the fully coupled limit is, according to Eq. (3.14), $\pi_\infty = \frac{\mu}{\bar{R}_0(\gamma+\mu)} (\bar{R}_0 - 1)$ with $\bar{R}_0 := \frac{\bar{\beta}_a}{\gamma+\mu}$. As expected, it lies in between the two uncoupled values: $\pi_2(0) < \pi_\infty < \pi_1(0)$ (cf. Fig. 3.3). This is because $\frac{R_{0,k}-1}{R_{0,k}}$ is a strictly monotonically increasing function in $R_{0,k}$ and $R_{0,2} < \bar{R}_0 < R_{0,1}$, which follows from \bar{R}_0 being simply the weighted average of the basic reproduction ratios of the two communities. From Eq. (3.14), the incidence rates in the fully coupled limit can be calculated, yielding $\varphi_{k,\infty} = \frac{\mu R_{0,k}}{\bar{R}_0^2} (\bar{R}_0 - 1)$. Contrary to the prevalence, the incidence rate in the fully coupled limit are apparently different in Community 1 and Community 2 due to the different infection rates.

Apart from the individual populations, a natural question is whether the metapopulation as whole is in a better state when fully coupled or when uncoupled. The prevalence of the metapopulation as a whole $\pi_M(\varepsilon_{1-2}) := \frac{N_1 i_1^E + N_2 i_2^E}{N_1 + N_2}$ and the incidence rate $\varphi_M(\varepsilon_{1-2}) := \frac{N_1 \varphi_1 + N_2 \varphi_2}{N_1 + N_2}$ can be calculated from Eq. (3.3) and Eq. (3.14) for the uncoupled and fully coupled case, respectively. The prevalence in the fully coupled limit is implicitly given by Eq. (3.14) and it is straightforward to show that the prevalence in the uncoupled case is

$$\pi_M(\infty) = \frac{\mu}{\gamma + \mu} \left(1 - \frac{\gamma + \mu}{\bar{\beta}_a} \right) \quad \text{and} \quad \pi_M(0) = \frac{\mu}{\gamma + \mu} \left(1 - \frac{\gamma + \mu}{\bar{\beta}_h} \right), \quad (3.15)$$

respectively, where $\bar{\beta}_a$ is the weighted arithmetic mean and $\bar{\beta}_h$ is the weighted harmonic mean $\bar{\beta}_h := \frac{N_1 + N_2}{N_1/\beta_1 + N_2/\beta_2}$. Since in general, the harmonic mean is smaller than the arithmetic mean, $\bar{\beta}_h < \bar{\beta}_a$, the prevalence in the uncoupled case ($\varepsilon_{1-2} = 0$) is smaller than in the fully coupled limit ($\varepsilon_{1-2} \rightarrow \infty$), i.e., $\pi_M(0) < \pi_M(\infty)$. Similarly, calculating the incidence rate from Eq. (3.3) and Eq. (3.14) in the uncoupled case and the fully coupled limit, respectively, yields

$$\varphi_M(\infty) = \mu \left(1 - \frac{\gamma + \mu}{\bar{\beta}_a} \right) \quad \text{and} \quad \varphi_M(0) = \mu \left(1 - \frac{\gamma + \mu}{\bar{\beta}_h} \right). \quad (3.16)$$

This implies that the incidence rate of the metapopulation as a whole is also smaller in the uncoupled case than in the fully coupled limit, i.e. $\varphi_M(0) < \varphi_M(\varepsilon_{1-2} \rightarrow \infty)$.

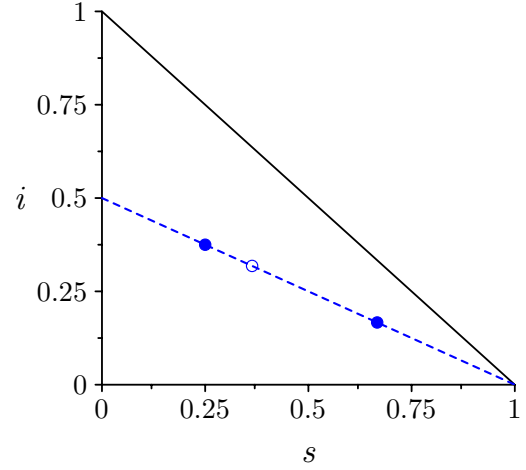


Figure 3.3: Endemic states of two communities in the uncoupled state (●) and in the fully coupled limit (○). Dashed line (---) indicates the relation $i = \frac{\mu}{\gamma+\mu} (1-s)$ (see Eq. (3.3)). $\mu = \gamma = 1$, $\beta_1 = 8$, $\beta_2 = 3$, and $N_1 = N_2$.

Considering the metapopulation as a whole, the uncoupled state ($\varepsilon_{1-2} = 0$) is preferable to the fully coupled state ($\varepsilon_{1-2} \rightarrow \infty$) as, both the incidence rate and the prevalence are higher in the latter.

The comparison between the fully coupled limit and the uncoupled case seems to support the intuition that coupling brings the two communities dynamically closer together. However, the two extreme cases do not unravel the full complexity of the system.

Weak coupling limit

To study the onset of coupling, i.e., how a small coupling strength ε_{1-2} alters the uncoupled endemic states Eq. (3.3), again a power series – now in ε_{1-2} – is chosen as ansatz:

$$s_k^E(\varepsilon_{1-2}) = s_k^{(0)} + \sum_{p=1}^{\infty} s_k^{(p)} \varepsilon_{1-2}^p \quad (3.17a)$$

$$i_k^E(\varepsilon_{1-2}) = i_k^{(0)} + \sum_{p=1}^{\infty} i_k^{(p)} \varepsilon_{1-2}^p \quad (3.17b)$$

Here, the terms of zeroth order are the known endemic states of the uncoupled case, $s_k^{(0)} = 1/R_{0,k}$ and $i_k^{(0)} = \mu(1 - 1/R_{0,k})/(\gamma + \mu)$. The terms of first order, $s_k^{(1)}$ and $i_k^{(1)}$, are equivalent to the derivation of $s_k^E(\varepsilon_{1-2})$ and $i_k^E(\varepsilon_{1-2})$, respectively, at $\varepsilon_{1-2} = 0$. They thus describe the effect of the onset of coupling. For their determination, Eq. (3.17) is inserted in Eq. (3.7) and terms of second and higher order in ε_{1-2} neglected. This yields a four dimensional system of linear equations in $(s_1^{(1)}, i_1^{(1)}, s_2^{(1)}, i_2^{(1)})$:

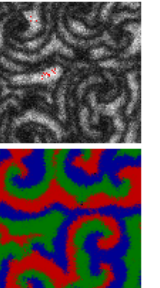
$$0 = \frac{\beta_1 \mu}{\gamma + \mu} s_1^{(1)} + (\gamma + \mu) i_1^{(1)} + \frac{2N_2}{N_1 + N_2} \frac{(\gamma + \mu)(\beta_2 - \beta_1)}{\beta_1 \beta_2} \quad (3.18a)$$

$$0 = \left(\frac{\beta_1}{\gamma + \mu} - 1 \right) s_1^{(1)} + \frac{2N_2}{N_1 + N_2} \frac{\beta_2 - \beta_1}{\beta_1 \beta_2} \quad (3.18b)$$

Again, the analogous equations for Community 2 can be obtained by exchanging the subscript 1 and 2. Eq. (3.18) shows that to linear order in ε_{1-2} , the equations for $(s_1^{(1)}, i_1^{(1)})$ are independent from the equations for $(s_2^{(1)}, i_2^{(1)})$. Hence, the four dimensional system of linear equations actually decomposes into two two dimensional systems of linear equations. The solution to Eq. (3.18), expressed in terms of $R_{0,k}$, is

$$s_1^{(1)} = \frac{2N_2}{N_1 + N_2} \frac{R_{0,1} - R_{0,2}}{R_{0,1} R_{0,2} (R_{0,1} - 1)(\gamma + \mu)} \quad (3.19a)$$

$$i_1^{(1)} = \frac{2N_2}{N_1 + N_2} \frac{(R_{0,1} - R_{0,2}) \left(\frac{R_{0,1} \gamma}{\gamma + \mu} - 1 \right)}{R_{0,1} R_{0,2} (R_{0,1} - 1)(\gamma + \mu)} = s_1^{(1)} \left(\frac{R_{0,1} \gamma}{\gamma + \mu} - 1 \right) \quad (3.19b)$$



where the analogous equations can be obtained by exchanging the subscript 1 and 2. For the weak coupling limit, the fraction of susceptible and infectious individuals are, hence, approximated by $s_k^E(\varepsilon_{1-2}) \approx s_k^{(0)} + s_k^{(1)}\varepsilon_{1-2}$ and $i_1^E(\varepsilon_{1-2}) \approx i_k^{(0)} + i_k^{(1)}\varepsilon_{1-2}$, respectively.

Eq. (3.19a) shows that $s_1^{(1)}$ is always positive, provided that $R_{0,1} > R_{0,2}$, which was assumed without loss of generality. The dependence of the fraction of susceptible individuals on the coupling strength thus behaves as expected: When Community 1 couples to Community 2, which has a lower infection rate and thus a higher fraction of susceptible individuals, the fraction of susceptible individuals increases in Community 1.

Eq. (3.19b) shows that the sign of $i_1^{(1)}$ depends on the term $\frac{R_{0,1}\gamma}{\gamma+\mu} - 1$, provided that $R_{0,1} > R_{0,2}$. This stands in contrast to the expectation: When Community 1 couples to Community 2, which has a lower infection rate and thus a lower fraction of infectious individuals, the fraction of infectious individuals should always be expected to decrease in Community 1. However, this expectation is not met if

$$R_{0,1} > 1 + \frac{\mu}{\gamma}. \quad (3.20)$$

In that case, the fraction of infectious individuals, i.e., the prevalence in Community 1 increases upon coupling to Community 2 although Community 2 has a lower fraction of infectious individuals. Analogously, if $R_{0,2} > 1 + \frac{\mu}{\gamma}$ the fraction of infectious individuals in Community 2 decreases upon coupling although it couples to a community with a higher fraction of infectious individuals.

For diseases whose basic reproductive ratio R_0 exceeds the threshold Eq. (3.20), the prevalence in a community – the level of infection – paradoxically increases upon coupling to another community that has a lower prevalence (i.e. a lower R_0). In the same way, it decreases upon coupling to a community that has a higher prevalence (i.e. a higher R_0).

Considering the incidence rates φ_k in the weak coupling limit, a similar paradoxical effect occurs. From Eq. (3.17) it is clear that the incidence rate of the individual populations is determined to linear order in ε_{1-2} by $\varphi_k(\varepsilon_{1-2}) = \beta_k s_k^{(0)} i_k^{(0)} + \beta_k (s_k^{(0)} i_k^{(1)} + s_k^{(1)} i_k^{(0)}) \varepsilon_{1-2}$. Eq. (3.3) and Eq. (3.19) yield for the incidence rate in Community 1

$$\varphi_1(\varepsilon_{1-2}) = \mu \left(1 - \frac{1}{R_{0,1}} \right) + \frac{2N_2}{N_1 + N_2} \frac{(R_{0,1} - R_{0,2}) \left(R_{0,1} - 1 - \frac{\mu}{\gamma+\mu} \right)}{R_{0,1} R_{0,2} (R_{0,1} - 1)} \varepsilon_{1-2}, \quad (3.21)$$

and the incidence rate for Community 2 is obtained by exchanging the subscripts. Again, whether φ_1 increases or decreases depends on a threshold, provided that $R_{0,1} > R_{0,2}$. The incidence rate in Community 1 increases if the threshold

$$R_{0,1} > 1 + \frac{\mu}{\gamma + \mu} \quad (3.22)$$

is exceeded. In this case, the incidence rate in Community 1 increases although it couples to Community 2 with a lower incidence rate. Analogously, if $R_{0,2} > 1 + \frac{\mu}{\gamma+\mu}$, the incidence rate in Community 2 decreases upon coupling to Community 1 although Community 1 has a higher incidence rate. This threshold Eq. (3.22) for the incidence rate is virtually identical to the threshold for the prevalence Eq. (3.20), since usually the rate at which individuals recover is much higher than the rate at which they reproduce and thus $\frac{\mu}{\gamma+\mu} \approx \frac{\mu}{\gamma}$.

For diseases whose basic reproductive ratio R_0 exceeds the threshold Eq. (3.22), the incidence rate in a community – the rate of new contagions – paradoxically increases upon coupling to another community that has a lower incidence rate (i.e. a lower R_0). In the same way, it decreases upon coupling to a community that has a higher incidence rate (i.e. a higher R_0).

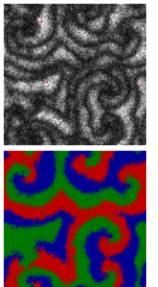
A surprising observation is that the condition for the occurrence of the paradoxical effect (Eq. (3.20) and Eq. (3.22)) in each of the two populations is independent from the other population. Hence, depending on the values of $R_{0,1}$ and $R_{0,2}$, either both populations exhibit the paradoxical effect, one of the two or none of the populations. There are thus three cases:

- **Fully paradoxical case:** If both populations exhibit the paradoxical effect, i.e. $R_{0,1} > R_{0,2} > 1 + \frac{\mu}{\gamma}$, Community 1 is put at a disadvantage from the onset of coupling, although it couples to Community 2, which has a lower prevalence. Community 2, on the contrary, profits from the onset of coupling although it couples to Community 1, which has a higher prevalence.
- **Detrimental case or semi-paradoxical case:** If only Community 1 exhibits the paradoxical effect, i.e. $R_{0,1} > 1 + \frac{\mu}{\gamma} > R_{0,2}$, both communities are put at a disadvantage from the onset of coupling. Community 1 is paradoxically put at a disadvantage as it couples to a community with a lower prevalence and Community 2 is put at a disadvantage since it does not exhibit the paradoxical effect and thus coupling to a community with a higher prevalence is disadvantageous.
- **Intuitive case:** If neither community exceeds the threshold for the paradoxical effect, i.e. $1 + \frac{\mu}{\gamma} > R_{0,1} > R_{0,2}$, all expectations are fulfilled. Community 1 profits from the onset of coupling as it couples to Community 2 with a lower prevalence and Community 2 is put at a disadvantage as it couples to a community with a higher prevalence.

The equivalent classification holds for the incidence rate and is obtained by replacing the threshold $1 + \frac{\mu}{\gamma}$ by $1 + \frac{\mu}{\gamma+\mu}$.

General coupling strength

Fig. 3.4 illustrates the three cases with regard to both the prevalence and the incidence rate. It shows the endemic states of two coupled populations and the respective



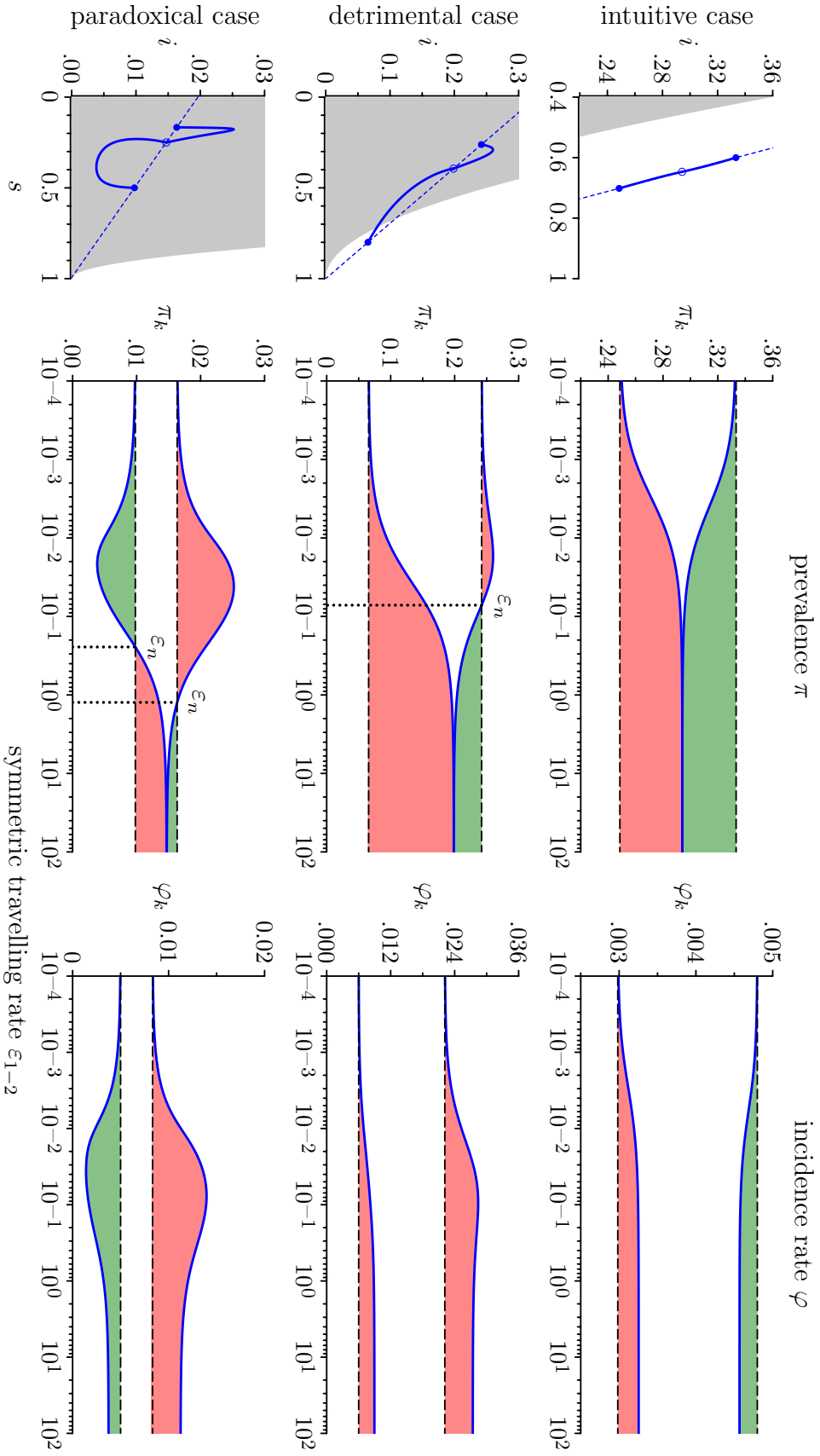


Figure 3.4: Effect of coupling two populations with different infection rates β_k : Intuitive case (top row), detrimental case (middle row), and paradoxical case (lower row). **Left column:** Uncoupled endemic states (—) and endemic states in the fully coupled limit (\circ) of the two populations in the $s - i$ -plane. Dashed lines (---) indicate the relation $i = \frac{\beta_k}{\gamma + \beta_k}(1 - s)$ (see Eq. (3.3)). Grey shaded regions indicate the positions of uncoupled endemic states of populations for which the threshold $R_0 > 1 + \frac{L}{\gamma}$ is exceeded. **Middle column and right column:** Prevalence (middle, —) and incidence rate (right, —) of the two populations in dependence of the symmetric travelling rate ε_{1-2} . Dashed black lines (---) denote the prevalence level and the incidence rate level of the uncoupled state. Green and red shaded regions indicate coupling strengths which the communities profit from and which put the communities at a disadvantage, respectively. ε_n denotes the neutral coupling strength for which the effect of coupling on the prevalence vanishes. Parameters ($R_{0,1}, R_{0,2}, \frac{L}{\gamma}$) for top, middle, and lower row are (1.6, 1.425, 5), (3.825, 1.25, 0.4878), and (6, 2, 0.02), respectively.

prevalence levels π_k and incidence rates φ_k in dependence on the symmetric travelling rate ε_{1-2} . The endemic states for $\varepsilon_{1-2} = 0$ and $\varepsilon_{1-2} \rightarrow \infty$ and the respective incidence rates and prevalence levels are computed from Eq. (3.3), Eq. (3.14), Eq. (3.16), and Eq. (3.15), respectively. The results for finite ε_{1-2} are obtained by numerically integrating Eq. (3.7) until the stationary state is reached, from which the prevalence and the incidence rate is consecutively computed. Fig. 3.4 confirms the prediction of the paradoxical effect. In the intuitive case (top row in Fig. 3.4), the two populations ‘attract’ each other in the $s - i$ -plane and correspondingly the prevalence and the incidence rate monotonically converge. On the other side, in the fully paradoxical case (lower row in Fig. 3.4), the two populations apparently ‘repel’ each other for small coupling strengths, as predicted by Eq. (3.19). Accordingly, the difference in the prevalence and the incidence rate thus initially increases. In between, in the detrimental case (middle row in Fig. 3.4), Community 2 behaves as intuition suggests and monotonically approaches Community 1, but Community 1, being in the paradoxical regime, is ‘repelled’ by Community 2. Hence, the incidence rate and the prevalence increase initially in both populations.

Illustratively speaking, the paradoxical effect consists in the counter-intuitive behaviour of the endemic states of two populations not to approach each other when they are coupled.

Neutral coupling strength

While the dependence of the incidence rate and the prevalence on the symmetric travelling rate ε_{1-2} (Fig. 3.4) is qualitatively the same, there is a marked difference concerning their asymptotic convergence. Eq. (3.14) predicts that the incidence rates $\varphi_1(\varepsilon_{1-2})$ and $\varphi_2(\varepsilon_{1-2})$ converge to different limits $\varphi_k(\infty) = \beta_k s_\infty i_\infty$ because of the different infection rates. Whether the respective limit lies above or below the uncoupled level depends on the choice of parameters (see Fig. 3.4). On the contrary, Eq. (3.14) predicts that the prevalences $\pi_1(\varepsilon_{1-2})$ and $\pi_2(\varepsilon_{1-2})$ converge to the common limit π_∞ , which lies in between the levels of the two uncoupled populations, i.e., $\pi_2(0) < \pi_\infty < \pi_1(0)$, independent of the choice of parameters. In the paradoxical regime, the prevalence of Community 1, thus, increases upon coupling and then decreases to π_∞ . Analogously, the prevalence of Community 2 decreases for small coupling strengths and then increases to π_∞ in the paradoxical regime. This implies that...

There is a neutral coupling strength for each population for which the prevalence is the same as in the uncoupled case.

This *neutral coupling strength* $\varepsilon_{n,k}$ for the k^{th} population can be found by determining the endemic state of Eq. (3.7) under the constraint that i_k is set to the uncoupled value from Eq. (3.3), $i_k(\varepsilon_{n,k}) = \frac{\mu}{\gamma+\mu} + \frac{\mu}{\beta_k}$. The calculation yields the trivial solution $\varepsilon_{n,k} = 0$ and

$$\varepsilon_{n,k} = \frac{\gamma}{2} \left(R_{0,k} - 1 - \frac{\mu}{\gamma} \right). \quad (3.23)$$

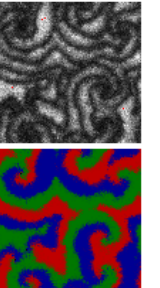
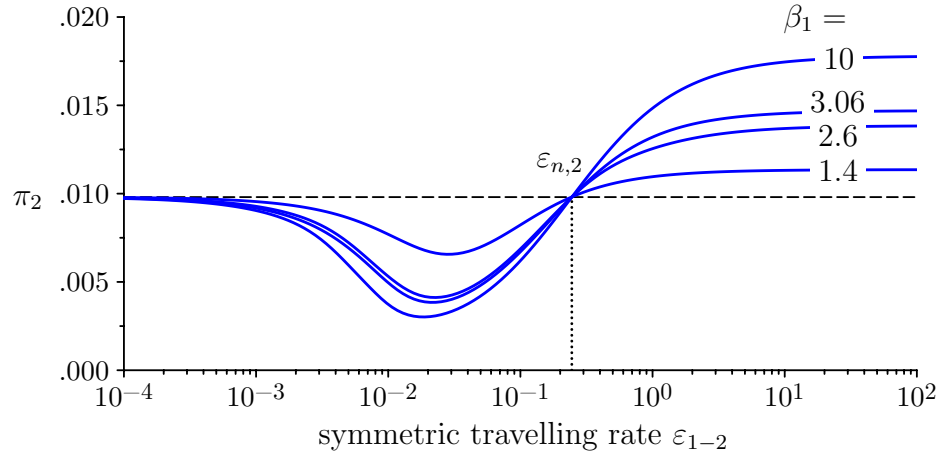


Figure 3.5: Illustration of the neutral coupling strength, being independent of properties of the coupled population. Prevalence π_2 of Community 2 in dependence on ε_{1-2} for different values of the infection rate in Community 1. The neutral coupling strength is $\varepsilon_{n,2} = 0.245$ in any case. Remaining parameters are $\beta_2 = 1.02$, $\gamma = 0.5$, and $\mu = 0.01$.



The neutral coupling strength for the respective population is shown in Fig. 3.4 and is confirmed by results from the numerical integration. Since $\varepsilon_{n,k}$ is determined by finding the root of a quadratic equation, Eq. (3.23) together with the trivial solution $\varepsilon_{n,k} = 0$ constitute all coupling strengths that satisfy $i_k(\varepsilon_{1-2}) = i_k(0)$. Hence, the neutral coupling strength ε_n denotes the limit up to which the paradoxical effect – that the prevalence of a population does not approach the prevalence of a population to which it couples – persists. The neutral coupling strength separates two coupling regimes. Recalling the assumption $R_{0,1} > R_{0,2}$, the separation has an inverse meaning for the two populations. For Community 1, $\varepsilon_{n,1}$ separates the regime in which the community is put at a disadvantage ($\varepsilon_{1-2} < \varepsilon_{n,1}$) from the regime in which the community profits from coupling ($\varepsilon_{1-2} > \varepsilon_{n,1}$). For Community 2, this order is reversed and $\varepsilon_{n,2}$ separates the regime in which the community profits from coupling ($\varepsilon_{1-2} < \varepsilon_{n,2}$) from the regime in which the community is put at a disadvantage ($\varepsilon_{1-2} > \varepsilon_{n,2}$) (shaded red and green, respectively, in Fig. 3.4).

The paradoxical effect of the prevalence persists for coupling strengths smaller than the neutral coupling strength, i.e., $\varepsilon_{1-2} < \varepsilon_n$. For coupling strengths larger than the neutral coupling strength, i.e., $\varepsilon_{1-2} > \varepsilon_n$, the paradoxical effect disappears.

The neutral coupling strength of a population surprisingly is independent of the properties of the population to which it couples. In particular, the neutral coupling strength is independent of the infection rate of the coupled population. Fig. 3.5 shows the prevalence π_2 of Community 2 for different values of the infection rate β_1 in Community 1. The neutral coupling strength, which is $\varepsilon_{n,2} = 0.245$ according to Eq. (3.23), is clearly independent of β_1 , as predicted.

Explanation of the paradoxical effect

In order to understand the occurrence of the paradoxical effect, it is necessary to consider the simplest case where an external interaction with a population gives rise to

this effect. For small coupling strengths, the connection to another population can be seen as a constant external input of susceptible and infectious individuals, disregarding the feedback on the other population that is involved in the process of coupling. The simplest case in which the paradoxical effect arises is when the input of the infectious individuals is neglected and only the input of susceptible individuals is considered:

$$\partial_t s \stackrel{!}{=} 0 = -\beta s^E i^E + \mu(1 - s^E) + \mathcal{J}_{\text{in}} \quad (3.24a)$$

$$\partial_t i \stackrel{!}{=} 0 = \beta s^E i^E - (\gamma + \mu) i^E \quad (3.24b)$$

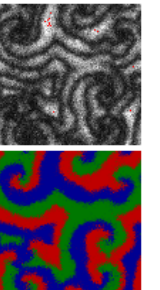
\mathcal{J}_{in} denotes the external input, which should be expected to be inhibitory since the addition of susceptible individuals should ease the epidemic rather than exacerbate it. Coupling to a population with a lower infection rate then corresponds to $\mathcal{J}_{\text{in}} > 0$ while coupling to a population with a higher infection rate corresponds to $\mathcal{J}_{\text{in}} < 0$. Eq. (3.24b) shows that the fraction of susceptible individuals in the endemic state remains unchanged by the external input: $s^E = \frac{\gamma + \mu}{\beta}$. Solving for i^E then gives:

$$i^E = \frac{\mu}{\gamma + \mu} \left(1 - \frac{\gamma + \mu}{\beta} \right) + \frac{\mathcal{J}_{\text{in}}}{\gamma + \mu} \quad (3.25)$$

The fraction of infectious individuals thus increases with a positive external input of susceptible individuals. Clearly, this simplifying model does not capture the complexity of the full model Eq. (3.7), but it clarifies the mechanism that is responsible for the paradoxical effect: It is not the input of infectious individuals that is responsible for the paradoxical effect but the input of susceptible individuals. To understand this counter-intuitive effect of the input of susceptible individuals, it is helpful to envisage that the SIR model is basically a predator-prey system in which the susceptible individuals can be equated with prey and the infectious individuals can be equated with predators. Creating a steady influx of prey eventually leads to an increase in the number of predators.

The origin of the paradoxical effect is the positive or negative net flux of susceptible individuals into the population, which acts an accelerant or extinguisher, respectively, for the epidemic.

A comparable paradoxical effect was found in the external modulation of inhibitory interneurons (Tsodyks et al., 1997). Tsodyks et al. (1997) study a model of two coupled populations of excitatory neurons and inhibitory neurons, respectively. While excitatory neurons increase the activity of connected neurons, inhibitory neurons decrease the activity of connected neurons. This is similar to an epidemic in a population consisting of infectious and susceptible individuals, where a larger number of infectious individuals mean a more severe epidemic (excitatory population) while a higher number of susceptible individuals supposedly mitigate the epidemic (inhibitory population). Similarly to Eq. (3.24), Tsodyks et al. (1997) find that an external and positive input onto the inhibitory neurons, like \mathcal{J}_{in} , can cause the activity of these very inhibitory cells to decrease. While in their model the paradoxical effect consists in the equilibrium activity of the inhibitory population to decrease, the similar paradoxical effect in the present work consists in the ‘excitatory’ population to increase.



3.2.4 Reduction of Spatial Complexity

In their famous city and villages example, May and Anderson (1984) consider a central population that is surrounded by several villages to design optimal vaccination strategies in spatially distributed populations. The vaccination strategy they devise, like the strategy devised in a similar example by Hethcote and van Ark (1987), presupposes a spatially homogeneous infection rate. When the infection rates vary spatially, the endemic states of the individual populations vary as well and alter the requirements for a vaccination strategy. It would thus be desirable if the effect of coupling on an individual population could be *efficiently* predicted when more than two populations are involved. The question in the city and villages example is then whether the collection of villages has to be modelled explicitly to account for the effect of coupling on the central city or whether the villages can be modelled as a single ‘surrounding population’.

As a starting point, the endemic state of a metapopulation as a whole, consisting of M individual populations (like the villages), is studied. The fraction of susceptible and infectious individuals in the global endemic state are:

$$\bar{s}(\mathcal{E}) = \frac{\sum_k S_k^E}{\sum_k N_k} = \frac{\sum_k N_k s_k^E(\mathcal{E})}{\sum_k N_k} \quad \text{and} \quad \bar{i}(\mathcal{E}) = \frac{\sum_k I_k^E}{\sum_k N_k} = \frac{\sum_k N_k i_k^E(\mathcal{E})}{\sum_k N_k} \quad (3.26)$$

Here, \mathcal{E} is the set of all $\frac{1}{2}M(M-1)$ coupling strengths $\{\varepsilon_{k-\ell}\}$. Although the dependence of \bar{s} and \bar{i} on \mathcal{E} is in general not known, a relation between \bar{s} and \bar{i} can be established. To determine this relation, Eqs. (3.6) must be employed, which determine the endemic states (s_k^E, i_k^E) by setting its left-hand sides to 0. The sum of Eq. (3.6a) and Eq. (3.6b) multiplied by N_k then yields

$$0 = \mu(N_k - S_k) - (\gamma + \mu)I_k + \sum_{\ell=1}^M \frac{2N_\ell N_k}{N_k + N_\ell} \varepsilon_{\ell-k} \left(\frac{S_\ell}{N_\ell} - \frac{S_k}{N_k} + \frac{I_\ell}{N_\ell} - \frac{I_k}{N_k} \right) \quad (3.27)$$

The last term is asymmetric under permutation of ℓ and k and therefore vanishes after summation over k . This summation and subsequent weighting by $\sum_k N_k$ yield equations in \bar{s} and \bar{i} and lead to the already known relation

$$\bar{i} = \frac{\mu}{\gamma + \mu} (1 - \bar{s}) . \quad (3.28)$$

The relation between the fraction of infectious individuals and susceptible individuals of a metapopulation as a whole in the endemic state is thus the same as for a single population, irrespective of the set \mathcal{E} . This was not true for the individual populations, being embedded in a metapopulation (see Fig. 3.4). The endemic state of the metapopulation can be, thus, described by defining the global basic reproductive ratio $\hat{R}_0 := 1/\bar{s}$ or equivalently the effective infection rate $\hat{\beta} := (\gamma + \mu)/\bar{s}$. The endemic fraction of infectious and susceptible individuals is then given by $\bar{s} = 1/\hat{R}_0$ and $\bar{i} = \mu/\gamma + \mu (1 - 1/\hat{R}_0)$ – just like the endemic state of a single population with the basic reproductive ratio \hat{R}_0 .

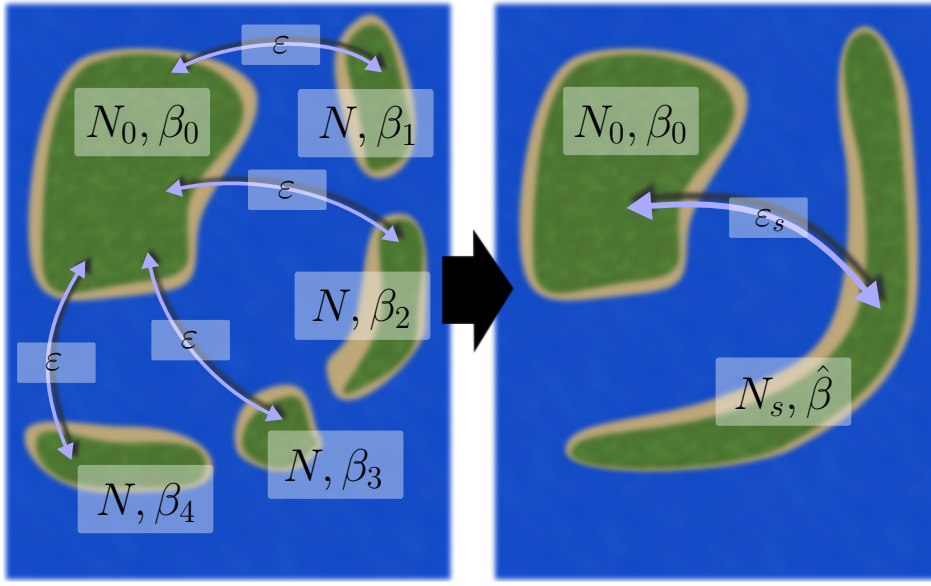


Figure 3.6: Effective model of a city and villages example. **Left:** Full model, in which a central population N_0 couples with strength ϵ to four equally large populations among which coupling is negligible. **Right:** Effective model, in which the surrounding populations are considered as one effective population N_s , whose infection rate is given by the effective infection rate $\hat{\beta}$. The substitute coupling strength ϵ_s depends on ϵ and N .

The endemic state of a metapopulation as a whole, that consists of individual populations with parameters $(\mu, \gamma, R_{0,k})$ and $k \in \{1, \dots, M\}$, can be described as the endemic state of one single population with parameters (μ, γ, \hat{R}_0) .

The global reproductive ratio \hat{R}_0 is in general a complex function of the set \mathcal{E} that cannot be determined analytically.

Turning to the example of a central city that is surrounded by several villages, the above finding allows the conjecture that the surrounding villages can be modelled as a single ‘surrounding population’ with an infection rate given by $\hat{\beta}$. Apparently, the major challenge is that the dependence of $\hat{\beta}$ on the set \mathcal{E} is largely unknown. $\hat{\beta}$ is only known for singular sets, viz. $\mathcal{E}_0 := \{0, \dots, 0\}$ and $\mathcal{E}_\infty := \{\infty, \dots, \infty\}$. Like in the special case $M = 2$ (see Eq. (3.14) and Eq. (3.15)), it is straightforward to show that

$$\hat{\beta}(\mathcal{E}_0) = \bar{\beta}_h \equiv \frac{\sum_{k=1}^M N_k}{\sum_{k=1}^M \frac{N_k}{\beta_k}} \quad \text{and} \quad \hat{\beta}(\mathcal{E}_\infty) = \bar{\beta}_a \equiv \frac{\sum_{k=1}^M N_k \beta_k}{\sum_{k=1}^M N_k}, \quad (3.29)$$

where $\bar{\beta}_a$ and $\bar{\beta}_h$ denote the weighted arithmetic and weighted harmonic mean of the β_k ’s, respectively.

Fig. 3.6 illustrates a more general example where a central population of size N_0 with an infection rate β_0 is surrounded by four populations with infection rates β_1, \dots, β_4 and equal size N , for simplicity. The infection rates are ordered such that $\beta_1 < \beta_2 < \beta_3 < \beta_4$. In this *full model*, the four populations are assumed to couple to the central population with equal strength ϵ whereas the coupling between the four populations is negligible. Nevertheless, the four surrounding populations are indirectly coupled by their common connection to the central population. The above conjecture predicts that the effect of coupling on the central population can be approximated by an *effective model* that consists only of the central population and one substitute population with

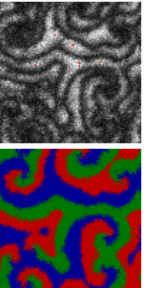
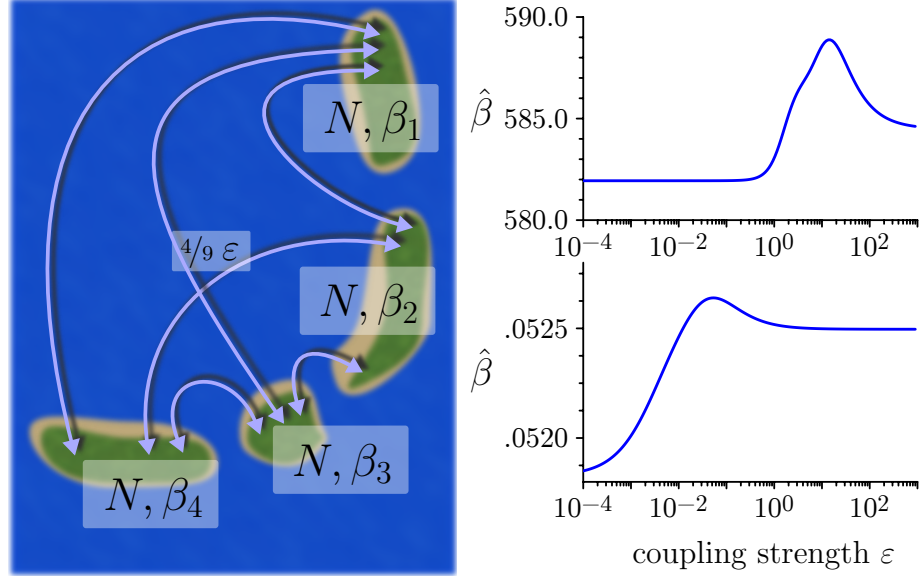


Figure 3.7: Determination of the effective infection rate $\hat{\beta}$. **Left:** Illustration of the metapopulation where a weaker direct coupling accounts for the indirect coupling in the full model (see Fig. 3.6). **Right:** Effective infection rate $\hat{\beta} = \frac{\gamma + \mu}{s}$ in dependence on ε for infection rates in the paradoxical regime (upper graph) ($R_{0,k} \in \{14.6, 15.3, 16.6, 17.3\}$ and $\gamma = 36.5$) and the intuitive regime (lower graph) ($R_{0,k} \in \{1.2, 1.3, 1.5, 1.6\}$ and $\gamma = 0.0075$). $\mu = 0.03$.



an infection rate $\hat{\beta}$. This substitute population is further described by the population size $N_s := 4N$ and a coupling strength ε_s . This coupling strength has to be chosen such that the absolute number of individuals leaving and arriving at the central population coincides in the full model and the effective model. According to the definition of the symmetric coupling strength ε_{k-l} (see paragraph preceding Eq. (3.6)), the number of individuals leaving and arriving at the central population is $8\varepsilon \frac{N_0 N}{N_0 + N}$ in the full model and $8\varepsilon_s \frac{N_0 N}{N_0 + 4N}$ in the effective model. The coupling strength between the central population and the substitute population has thus to be chosen as

$$\varepsilon_s = \frac{N_0 + 4N}{N_0 + N} \varepsilon \quad (3.30)$$

Choosing the central population to be twice as large as the surrounding populations, i.e., $N_0 = 2N$, this leads to $\varepsilon_s = 2\varepsilon$. Compared to the full model, which is a $2M$ -dimensional model with fixed parameters, the effective model is a 4-dimensional model with a parameter function $\hat{\beta} : \mathbb{R}_+^{\frac{1}{2}M(M-1)} \mapsto \mathbb{R}$.

Ideally, the dependence of $\hat{\beta}$ on ε , or equivalently ε_s , would be known. However, two principle problems arise here: First, $\hat{\beta}$ is the effective infection rate describing the metapopulation of the surrounding populations without the central population (see Fig. 3.7). It only depends on ε because of the indirect coupling via the central population. The influence of this indirect coupling on $\hat{\beta}$ is, however, not known. It has to be approximated by considering the metapopulation of the surrounding populations and mimicking the indirect coupling by a weak direct coupling. This coupling again is chosen such that the number of individuals leaving and arriving at each population coincides with the full model. Second, the dependence of $\hat{\beta}(\varepsilon)$ in the metapopulation of the surrounding populations (see Fig. 3.7) is not known analytically and thus has to be computed numerically.

Two cases are considered in the following: (i) All five populations are in the paradoxical

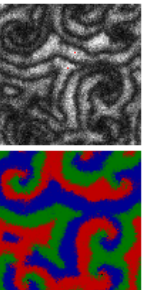
regime with regard to both the prevalence and the incidence rate, i.e., $R_{0,k} > 1 + \frac{\mu}{\gamma}$, $\forall k$. (ii) All five populations are in the intuitive regime with regard to both the prevalence and the incidence rate, i.e., $R_{0,k} < 1 + \frac{\mu}{\gamma+\mu}$, $\forall k$. The approximation of $\hat{\beta}(\varepsilon)$ is shown in Fig. 3.7 for the paradoxical (upper graph) and the intuitive case (lower graph). Since the impact of coupling on the central population is to be considered, three further subcases have to be distinguished in both the paradoxical regime and the intuitive regime. (a) The central population has the lowest infection rate, $\beta_0 < \beta_k$, $\forall k$, (b) the central population has an medium infection rate $\beta_1 < \beta_2 < \beta_0 < \beta_3 < \beta_4$, and (c) the central population has the largest infection rate $\beta_k < \beta_0$, $\forall k$.

Fig. 3.8 shows the comparison between the full model and the effective model, given the effective infection rate $\hat{\beta}$ shown in Fig. 3.7. First of all, the dependency of the fraction of infectious individuals on the coupling strength in a metapopulation of five populations shows that the paradoxical effect (that the endemic state of the central population does not approach the average endemic state of the remaining populations) persists for $M > 2$.

When the central population has the smallest or the highest infection rate, the results from the full model and the effective model almost perfectly coincide and are virtually indistinguishable, for both the intuitive and the paradoxical case. When the central population has an intermediate infection rate, the effective model reproduces the general dependency of the fraction of infectious and of susceptible individuals on the coupling strength, but the location of the maxima and minima are shifted to higher values. This is likely due to the imperfect accounting of the effect of indirect coupling on $\hat{\beta}$. When $\beta_0 \leq \beta_k$, $\forall k$, the dependency of $\hat{\beta}$ on ε is apparently well captured by the ‘direct coupling approximation’ shown in Fig. 3.7. When the central population has an intermediate infection rate, the indirect coupling via the central population alters the dependence of $\hat{\beta}$ such that the approximation becomes worse and the effective model is not capable to perfectly reproduce the dependence of the fraction of susceptible and infectious individuals on the coupling strength ε . Nonetheless, the similarity between the models is remarkable.

Hence, it is in principle possible to describe the effect of coupling on a focal population by one effective population describing the surrounding populations. When some of the surrounding populations have larger and some have smaller infection rates, the description is only approximative as long as no better way of accounting for the indirect coupling is found.

The effect of coupling that a set of populations exerts on the endemic state of a focal population can be well described by the effect of one single effective population substituting the set of populations. The effect of the substituting population is virtually indistinguishable from the effect of the full set of populations if these populations have compared to the focal population either (i) all a smaller basic reproductive ratio $R_{0,k}$ or (ii) all a larger basic reproductive ratio $R_{0,k}$.



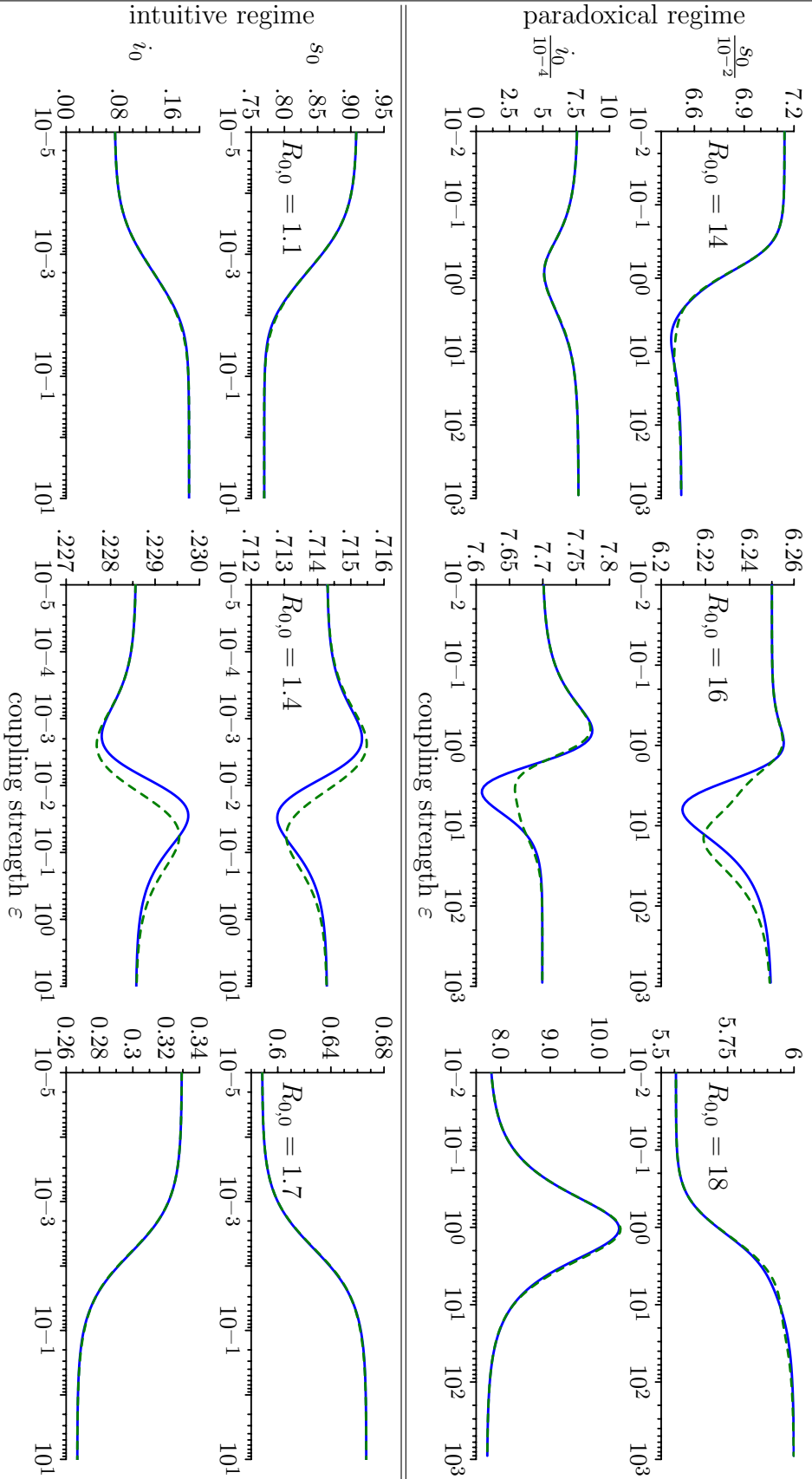


Figure 3.8: Comparison of the impact of coupling on the fraction of susceptible s_0 and infectious individuals i_0 of the central population in the full model (—), consisting of four surrounding populations and the central population, and the effective model (---), consisting only of one substitute ‘surrounding population’ and the central population. Top row shows results for all five populations being in the paradoxical regime, i.e., $R_{0,k} > 1 + \frac{\mu}{\gamma}$, $\forall k$ ($R_{0,1} = 1.2, R_{0,2} = 1.3, R_{0,3} = 1.5, R_{0,4} = 1.6$ and $\gamma = 36.5, \mu = 0.03$). Lower row shows results for all populations being in the intuitive regime, i.e., $R_{0,k} < 1 + \frac{\mu}{\gamma}$, $\forall k$ ($R_{0,1} = 14\bar{6}, R_{0,2} = 15\bar{3}, R_{0,3} = 16\bar{6}, R_{0,4} = 17\bar{3}$ and $\gamma = 0.0075, \mu = 0.03$). **Left column:** Infection rate of the central population β_0 (and correspondingly $R_{0,0}$) is smaller than the infection rates in the surrounding populations, i.e., $R_{0,0} = 14$ (upper row) and $R_{0,0} = 1.1$ (lower row). **Middle column:** β_0 is in between the infection rates of the surrounding populations, i.e., $R_{0,0} = 16$ (upper row) and $R_{0,0} = 1.4$ (lower row). **Right column:** β_0 is larger than the infection rates in the surrounding populations, i.e., $R_{0,0} = 18$ (upper row) and $R_{0,0} = 1.7$ (lower row).

3.2.5 Effective Coupling, Migration, and Home Locations

A pertinent question is which underlying model assumptions that become manifest in the model properties are responsible for the occurrence of the paradoxical effects. To answer this question, different model structures are examined in this section to identify how they relate to the model studied in the present work or to identify if they are capable to exhibit paradoxical effects.

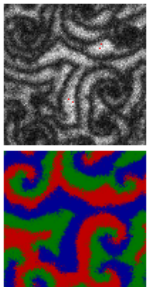
In the present work, the spread of a disease is modelled by (i) infectious individuals who migrate and infect susceptible individuals all over the metapopulation and (ii) susceptible individuals who migrate and contract the disease all over the metapopulation (see Eq. (3.6)). This migration scheme implicitly assumes that individuals migrate diffusively without memory, i.e., a movement is not correlated with any movement at an earlier point in time. For animal migration, this approach is appropriate to capture the movement patterns of individuals (Fulford and Roberts, 2002; Keeling and Rohani, 2008) but for human populations, this modelling approach omits the fact that human individuals regularly return to their home locations (González et al., 2008; Belik et al., 2011). Human migration patterns in general have attracted a lot of attention recently (Brockmann et al., 2006; Simini et al., 2012). The only recent incorporation of home locations into epidemiological modelling (see Keeling and Rohani, 2002, and references therein) has shown for example that the propagation speed of waves of infections does not unboundedly grow with the travelling rate, but that the spreading speed saturates with an increasing travelling rate of individuals (Belik et al., 2011).

In epidemiological metapopulation models, coupling is usually accounted for by a phenomenological coupling that omits the actual movement of individuals and instead only considers the effective force of infection that is caused by the movement (May and Anderson, 1984; Hethcote and van Ark, 1987; Lloyd and May, 1996; Grenfell and Bolker, 1998; Keeling, 2000; Keeling and Rohani, 2002; Hagenaars et al., 2004; Grassly et al., 2005). Broadly speaking, there are, hence, three categories of epidemiological metapopulation models: First, *home location models*, which account for home locations and model individual migration explicitly. Second, *migration models*, which model migration explicitly but disregard home locations (like the model employed in the present work). And third, *direct infection models*, which do not model individual's migration at all.

In the following, it is shown that (i) direct infection models, which do not account for migration, do not exhibit paradoxical effects and (ii) that the migration model studied in the present work is a special case of a more complex home location model.

Direct infection model

When the actual movement of individuals is omitted and susceptible individuals instead contract the disease directly from remote populations, the coupling is determined by an effective coupling parameter κ between zero and one. For two communities that are coupled in this effective way, the temporal evolution of the susceptible and infectious populations (assuming equal population sizes for simplicity) is usually modelled by (see



e.g. May and Anderson, 1984; Keeling and Rohani, 2002; Grassly et al., 2005)

$$\partial_t s_1 = \mu(1 - s_1) - \lambda_1(\kappa)s_1 \quad (3.31a)$$

$$\partial_t i_1 = -(\gamma + \mu)i_1 + \lambda_1(\kappa)s_1 \quad (3.31b)$$

$$\partial_t s_2 = \mu(1 - s_2) - \lambda_2(\kappa)s_2 \quad (3.31c)$$

$$\partial_t i_2 = -(\gamma + \mu)i_2 + \lambda_2(\kappa)s_2 . \quad (3.31d)$$

Here, $\lambda_i(\kappa)$ is the *force of infection*, which is generally a function of the fraction or number of infectious individuals in all populations (i_1 and i_2 in this case) and of the coupling parameter κ . The force of infection constitutes the only interaction between the populations and individuals cannot migrate between them.

It is directly clear by setting the left-hand side of Eqs. (3.31) to zero that for any coupling strength κ and any function $\lambda_i(\kappa)$, the fraction of susceptible and infectious individuals in the endemic states of the two populations will always fulfil the relation of the uncoupled case

$$i_k^E = \frac{\mu}{\gamma + \mu}(1 - s_k^E) . \quad (3.32)$$

This also holds for a metapopulation of any size as the size is only manifest in the force of infection. This relation implies that the endemic states of the populations lie on the line in the $s - i$ -plane connecting the endemic states of the uncoupled case (see Fig. 3.3). It also means that the endemic states cannot exhibit the paradoxical effects described in Sec. 3.2.3 and shown in Fig. 3.4 as this would require that $i_k^E \geq \frac{\mu}{\gamma + \mu}(1 - s_k^E)$ where \geq depends on whether β_k is the larger or smaller infection rate in case of two communities.

Naturally, this merely shows that this model does not exhibit the **same** paradoxical effect as the migration model. To proof that no paradoxical effect occurs in this model, it has to be shown that the endemic prevalence of a community does not increase above its uncoupled level if it couples to a community with a lower infection rate, i.e.:

$$\beta_1 > \beta_2 \Rightarrow \forall \kappa \in (0, 1] : i_1^E(\kappa) < i_1^E(0) \quad (3.33)$$

The proof of this implication is performed in two consecutive steps: First, it is shown that the endemic prevalence is either always smaller or always larger than in the uncoupled case, i.e. $\forall \kappa \in (0, 1] : i_1^E(\kappa) > i_1^E(0) \vee \forall \kappa \in (0, 1] : i_1^E(\kappa) < i_1^E(0)$. The correctness of the implication then follows in the second step by showing that $\beta_1 > \beta_2$ implies that there is some $\kappa \in (0, 1]$ for which $i_1^E(\kappa) < i_1^E(0)$ as the first step shows that this statement is equivalent to the right hand side of Eq. (3.33).

Making the legitimate assumption that $i_1^E(\kappa)$ is a continuous function of κ , the statement that $i_1^E(\kappa)$ is either always smaller or always larger than $i_1^E(0)$ is true if and only if $i_1^E(\kappa) \neq i_1^E(0) \forall \kappa \in (0, 1]$. The latter can be shown by proof by contradiction: Assuming that $i_1^E(\kappa) = i_1^E(0) = \frac{\mu}{\gamma + \mu} - \frac{\mu}{\beta_1}$ for some $1 \geq \kappa > 0$ reduces the system Eqs. (3.31) together with the relation $i_k^E = \frac{\mu}{\gamma + \mu}(1 - s_k^E)$ to two equations in one variable i_2^E :

$$0 = \mu \left(1 - \frac{\gamma + \mu}{\beta_1} \right) - \frac{\gamma + \mu}{\beta_1} \lambda_1(i_1^E(0), i_2^E, \kappa) \quad (3.34a)$$

$$0 = \mu \left(1 - \frac{\gamma + \mu}{\beta_2} \right) - \frac{\gamma + \mu}{\beta_2} \lambda_2(i_1^E(0), i_2^E, \kappa) \quad (3.34b)$$

At this point, the force of infection has to be specified to proceed. A common choice of the force of infection in a metapopulation model of this kind is:

$$\lambda_1(i_1, i_2, \kappa) = (1 - \kappa)\beta_1 i_1 + \kappa\beta_2 i_2 \quad (3.35a)$$

$$\lambda_2(i_1, i_2, \kappa) = (1 - \kappa)\beta_2 i_2 + \kappa\beta_1 i_1 \quad (3.35b)$$

Note, however, that the correctness of the proof does not depend on the exact form of the force of infection. A different choice of the functional dependence of λ_k on the fractions of infectious individuals leads to the qualitatively same results. Inserting Eqs. (3.35) into Eqs. (3.34) leads to

$$0 = (-\beta_1\mu + (\gamma + \mu)(i_2^E\beta_2 + \mu))\kappa \quad (3.36a)$$

$$0 = -(\gamma + \mu)i_2^E + \left(\frac{\gamma + \mu}{\mu}i_2^E - 1 \right) \left(i_2^E\beta_2(\kappa - 1) - \kappa\mu \left(\frac{\beta_1}{\gamma + \mu} - 1 \right) \right) \quad (3.36b)$$

For $\kappa \neq 0$ the first equation directly gives $s_2^E = \frac{\mu}{\gamma + \mu} \frac{\beta_1 - \gamma - \mu}{\beta_2}$. Plugging this into the second equation gives:

$$0 = -\frac{\mu}{\gamma + \mu} \frac{\beta_1 - \gamma - \mu}{\beta_2} (\beta_1 - \beta_2) \quad (3.37)$$

Since $\beta_1 > \gamma + \mu$, this equation implies $\beta_1 = \beta_2$ contradicting the initial assumption that $\beta_1 > \beta_2$. Thus, $i_1^E(\kappa) \neq i_1^E(0) \forall \kappa \in (0, 1]$ and hence the statement $\forall \kappa \in (0, 1] : i_1^E(\kappa) > i_1^E(0) \vee \forall \kappa \in (0, 1] : i_1^E(\kappa) < i_1^E(0)$ is true since $i_1^E(\kappa)$ is continuous.

To prove the statement $\beta_1 > \beta_2 \Rightarrow \forall \kappa \in (0, 1] : i_1^E(\kappa) < i_1^E(0)$ it remains to show that $i_1^E(\kappa) < i_1^E(0)$ for some $\kappa \in (0, 1]$ if $\beta_1 > \beta_2$. For $\kappa = 1/2$ the force of infection becomes independent of the community, i.e.,

$$\lambda := \lambda_1 \left(i_1, i_2, \frac{1}{2} \right) = \lambda_2 \left(i_1, i_2, \frac{1}{2} \right) = \frac{\beta_1 i_1^E + \beta_2 i_2^E}{2}. \quad (3.38)$$

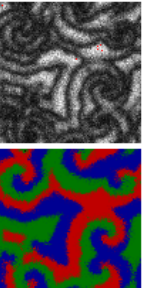
The determination of the endemic states from Eqs. (3.31) in conjunction with the relation $i_k^E = \frac{\mu}{\gamma + \mu} (1 - s_k^E)$ is then determined by

$$0 = \mu(1 - s_1^E) - \lambda s_1^E \quad (3.39a)$$

$$0 = \mu(1 - s_2^E) - \lambda s_2^E, \quad (3.39b)$$

which implies that $s_1^E = s_2^E$ and thus $i_1^E = i_2^E =: i^E$. With $\lambda = \frac{\beta_1 + \beta_2}{2} i^E$ the fraction of infectious individuals is determined to be:

$$i^E = \frac{\mu}{\gamma + \mu} - \frac{2\mu}{\beta_1 + \beta_2} \quad (3.40)$$



This is smaller than the fraction of infectious individuals in Community 1 in the uncoupled case if and only if $\beta_1 > \frac{\beta_1 + \beta_2}{2}$ which is in turn equivalent to $\beta_1 > \beta_2$. Hence, $i_1^E(\kappa) < i_1^E(0)$ for some and thus all $\kappa \in (0, 1]$ if $\beta_1 > \beta_2$, completing the proof.

A direct infection model, which does not allow for individuals to move, is not capable of exhibiting any kind of paradoxical behaviour for a reasonable choice of the force of infection.

Home locations model

Keeling and Rohani (2002) have studied the relation between a home location model and a direct infection model and answered the question in which case the latter is a good approximation for the more complex model that accounts for both home locations and migration. Their model shall be presented here to subsequently show that the model studied in the present work is a special case of the model that accounts for home locations.

The SIR model by Keeling and Rohani (2002) consists of two locations where each individual can be identified by its origin and its current location. In their nomenclature, S_{xy} refers to the absolute number of susceptible individuals originating from population x being currently in population y . Correspondingly, I_{xy} and N_{xy} denote the absolute number of infectious individuals and the absolute number of individuals, respectively, from population x currently located in population y . In their model, susceptible individuals can only contract the disease from infectious individuals located in the same population, as in the model introduced in Sec. 3.2.2, but the infection rate β is the same in both populations. Irrespective of their home location, individuals leave their home location with rate ρ and return to their home location with rate τ . With the assumption tacitly made by Keeling and Rohani (2002) that the birth and death rate μ are equal and denoting the rate of recovery by γ as before, this model is described on the mean-field level by

$$\partial_t S_{xx} = \mu(N_{xx} - S_{xx}) - \beta S_{xx} \frac{I_{xx} + I_{yx}}{N_{xx} + N_{yx}} + \tau S_{xy} - \rho S_{xx} \quad (3.41a)$$

$$\partial_t S_{xy} = \mu(N_{xy} - S_{xy}) - \beta S_{xy} \frac{I_{xy} + I_{yy}}{N_{xy} + N_{yy}} + \rho S_{xx} - \tau S_{xy} \quad (3.41b)$$

$$\partial_t I_{xx} = -(\gamma + \mu) I_{xx} + \beta S_{xx} \frac{I_{xx} + I_{yx}}{N_{xx} + N_{yx}} + \tau I_{xy} - \rho I_{xx} \quad (3.41c)$$

$$\partial_t I_{xy} = -(\gamma + \mu) I_{xy} + \beta S_{xy} \frac{I_{xy} + I_{yy}}{N_{xy} + N_{yy}} + \rho I_{xx} - \tau I_{xy} . \quad (3.41d)$$

These equations describe an 8-dimensional system since the pair $(x, y) \in \{(1, 2), (2, 1)\}$. When the return rate τ is much larger than the recovery rate γ , Keeling and Rohani (2002) show that this 8-dimensional system reduces to the 4-dimensional phenomenological direct infection model. Physically speaking, the phenomenological model is appropriate whenever the time spent in locations different from the home location is

much shorter than the duration of the infection. Keeling and Rohani (2002) have thus revealed the relationship between the phenomenological model and the more complex model that accounts for migration and home location but needs twice as many dimensions to describe its dynamics.

The model employed in the present work (see Eqs. (3.6)) lies somewhat in between these two models. It does not account for home locations but it models migration explicitly as the coupling mechanism and requires as few dimensions as the phenomenological model. The resulting question is: How does the complex model by Keeling and Rohani (2002) that accounts for home locations relates to the model employed in this work?

To answer this question it is necessary to extend the model by Keeling and Rohani (2002), Eqs. (3.41), in two ways: First, the infection rate has to be dependent on the location, i.e., $\beta \rightarrow \beta_{x/y}$. Second, the rate at which individuals leave and return to their home locations has to depend on the location, i.e., $\rho \rightarrow \rho_{x/y}$ and $\tau \rightarrow \tau_{x/y}$. With this, Eqs. (3.41) become

$$\partial_t S_{xx} = \mu(N_{xx} - S_{xx}) - \beta_x S_{xx} \frac{I_{xx} + I_{yx}}{N_{xx} + N_{yx}} + \tau_y S_{xy} - \rho_x S_{xx} \quad (3.42a)$$

$$\partial_t S_{xy} = \mu(N_{xy} - S_{xy}) - \beta_y S_{xy} \frac{I_{xy} + I_{yy}}{N_{xy} + N_{yy}} + \rho_x S_{xx} - \tau_y S_{xy} \quad (3.42b)$$

$$\partial_t I_{xx} = -(\gamma + \mu) I_{xx} + \beta_x S_{xx} \frac{I_{xx} + I_{yx}}{N_{xx} + N_{yx}} + \tau_y I_{xy} - \rho_x I_{xx} \quad (3.42c)$$

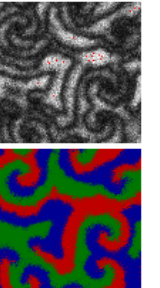
$$\partial_t I_{xy} = -(\gamma + \mu) I_{xy} + \beta_y S_{xy} \frac{I_{xy} + I_{yy}}{N_{xy} + N_{yy}} + \rho_x I_{xx} - \tau_y I_{xy} \quad (3.42d)$$

Again, the pair $(x, y) \in \{(1, 2), (2, 1)\}$. To establish the conditions for this 8-dimensional system to be equivalent to the 4-dimensional system Eqs. (3.6), the temporal evolution of the absolute number of susceptible and of infectious individuals at the two locations has to be considered, i.e., $S_x := S_{xx} + S_{yx}$ and $I_x := I_{xx} + I_{yx}$, respectively. Note that these numbers are not the numbers of susceptible and infectious individuals with x as home location but the numbers of susceptible and infectious individuals *currently* located at x . From Eqs. (3.42) the temporal evolution of S_x and I_x is

$$\partial_t S_x = \mu(N_x - S_x) - \beta_x S_x \frac{I_x}{N_x} + \tau_y S_{xy} - \rho_x S_{xx} + \rho_y S_{yy} - \tau_x S_{yx} \quad (3.43a)$$

$$\partial_t I_x = -(\gamma + \mu) I_x + \beta_x S_x \frac{I_x}{N_x} + \tau_y I_{xy} - \rho_x I_{xx} + \rho_y I_{yy} - \tau_x I_{yx} \quad (3.43b)$$

Here, the current population size at x is denoted by $N_x := N_{xx} + N_{yx}$. If the temporal evolution of S_x and I_x is supposed to depend only on quantities like S_x , I_x , and N_x and not on quantities like S_{xy} , the rate at which individuals leave a certain location must be independent from their home location, i.e., $\rho_x = \tau_x$ for $x \in \{1, 2\}$. This requirement is evidently fulfilled when individuals do not possess a home location. But strictly speaking, the requirement only means that the rate at which an individual leaves a certain location only depends on his current location and not on his home location. An example for this situation are different municipal districts, where individuals spent



half their (awake) day at work in one district and the other half at home in a different district. In that case the rate at which they leave work equals the rate at which other individuals living in that district leave their homes for work. Irrespective of the reason, Eqs. (3.43) become

$$\partial_t S_x = \mu(N_x - S_x) - \beta_x S_x \frac{I_x}{N_x} - \rho_x S_x + \rho_y S_y \quad (3.44a)$$

$$\partial_t I_x = -(\gamma + \mu) I_x + \beta_x S_x \frac{I_x}{N_x} - \rho_x I_x + \rho_y I_y \quad (3.44b)$$

if $\rho_x = \tau_x$. By equating ρ_x with ε_{yx} and considering the fractions $s_x := \frac{S_x}{N_x}$ and $i_x := \frac{I_x}{N_x}$, these equations yield

$$\partial_t s_x = \mu(1 - s_x) - \beta_x s_x i_x + 2\varepsilon_{x-y} \frac{N_y}{N_x + N_y} (s_y - s_x) \quad (3.45a)$$

$$\partial_t i_x = -(\gamma + \mu) i_x + \beta_x s_x i_x + 2\varepsilon_{x-y} \frac{N_y}{N_x + N_y} (i_y - i_x) \quad (3.45b)$$

where ε_{x-y} is used as defined in Sec. 3.2.2. This, however, is exactly the system described by Eqs. (3.6) for $M = 2$. This analysis, hence, shows that the epidemiological model by Keeling and Rohani (2002), which accounts for home locations of individuals, reduces to the model introduced in the present work when the rate at which individuals leave a certain location is independent of whether this location is their home location or not. This includes but is not limited to the case where individuals have no home location.

This finding completes the relation between the three models: The model by Keeling and Rohani (2002) can be approximated by the direct infection model in the limit of very short stays away from home (as shown in Keeling and Rohani, 2002) and reduces to the migration model introduced here when the travelling rates of individuals only depend on their current location.

The migration model introduced in Sec. 3.2.2 is a special case of the home locations model by Keeling and Rohani (2002). The paradoxical effects observed in the migration model can thus be expected to persist in more complex models for at least a finite range of parameters.

The major advantage of the direct coupling model over the home locations model is that it requires only half as many dimensions to study a spatially extended metapopulation. The migration model, introduced in Sec. 3.2.2, however, shares this advantage without disregarding the mobility of individuals.

3.3 Waning Immunity

The SIR model, as specified in Sec. 3.2.1, describes diseases that exhibit recurrent epidemics. These diseases elicit life-long immunity upon recovery and the fact that every newborn is born susceptible gives rise to the irregular oscillation of the fraction of

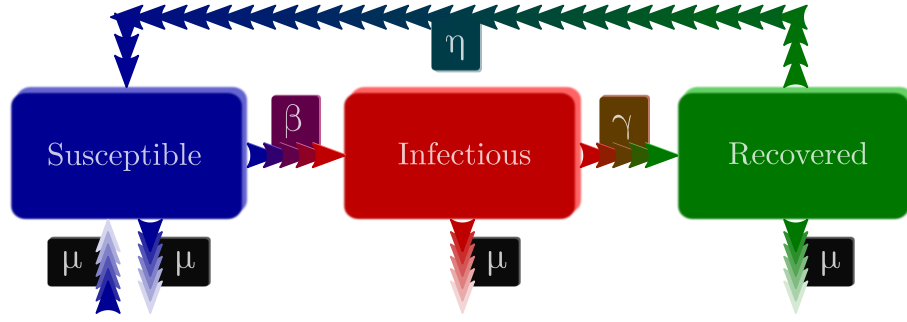


Figure 3.9: Schematic depiction of a SIRS model with demography, i.e., a nonspatial compartmental model for diseases that elicit temporal immunity.

infectious individuals. Another class of diseases that exhibit recurrent epidemics elicit only temporal or waning immunity (see Keeling and Rohani, 2008). In this case, the dominant mechanism that causes the irregular oscillations is the transition of recovered individuals to the class of susceptible individuals (see Fig. 3.9). This model is therefore referred to as the SIRS model. For this class of diseases the same paradoxical effect as in the SIR model can be observed. The corresponding results shall be presented in the following.

The infection and the recovery process are identical to the SIR model (see Sec. 3.2.1) and occur with rates β and γ , respectively. The rate at which individuals die equals the rate at which they produce offspring and are identically to the SIR model denoted by μ . In contrast, immunity, which is acquired during the infection, is lost with rate η . A derivation, corresponding to the one performed in Sec. 3.2.1, shows that the nonspatial compartmental SIRS model is thus described by

$$\partial_t s = -\beta si + \mu(1 - s) + \eta(1 - s - i) \quad (3.46a)$$

$$\partial_t i = \beta si - (\gamma + \mu)i \quad (3.46b)$$

Recalling the basic reproductive ratio $R_0 = \beta/(\gamma + \mu)$, the endemic state of the nonspatial SIRS model is (Anderson and May, 1991; Keeling and Rohani, 2008):

$$s^E = \frac{1}{R_0} \quad i^E = \frac{\mu + \eta}{\gamma + \mu + \eta} (1 - s^E) \quad (3.47)$$

The endemic state of the SIRS model with demography has thus the same form as the endemic state of the SIR model with demography Eq. (3.3). Consistently, the SIRS model reduces to the SIR model for $\eta = 0$.

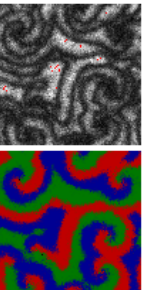
Adding the terms for the migration between two populations, yields

$$\partial_t s_1 = -\beta_1 s_1 i_1 + \mu(1 - s_1) + \eta(1 - i_1 - s_1) + \frac{2N_2}{N_1 + N_2} \varepsilon_{1-2} (s_2 - s_1) \quad (3.48a)$$

$$\partial_t i_1 = \beta_1 s_1 i_1 - (\gamma + \mu)i_1 + \frac{2N_2}{N_1 + N_2} \varepsilon_{1-2} (s_2 - s_1) \quad (3.48b)$$

$$\partial_t s_2 = -\beta_2 s_2 i_2 + \mu(1 - s_2) + \eta(1 - i_2 - s_2) + \frac{2N_1}{N_1 + N_2} \varepsilon_{1-2} (s_1 - s_2) \quad (3.48c)$$

$$\partial_t i_2 = \beta_2 s_2 i_2 - (\gamma + \mu)i_2 + \frac{2N_1}{N_1 + N_2} \varepsilon_{1-2} (s_1 - s_2) . \quad (3.48d)$$



Assuming that the first community has a higher infection rate than the second community, i.e., $\beta_1 > \beta_2$, it should be expected that the prevalence π_1 and the incidence rate φ_1 decreases as Community 1 couples to Community 2, which has a lower prevalence π_2 and incidence rate φ_2 . Accordingly, it should be expected that the prevalence and the incidence rate in Community 2 increase upon coupling.

However, as in the SIR model, the prevalence in Community 1 increases when the corresponding threshold

$$R_{0,1} > 1 + \frac{(\mu + \eta)(\gamma + \mu + \eta)}{\gamma(\gamma + \mu)} \quad (3.49)$$

is exceeded. Analogously, the prevalence in Community 2 decreases if $R_{0,2} > 1 + \frac{(\mu + \eta)(\gamma + \mu + \eta)}{\gamma(\gamma + \mu)}$. This threshold becomes identical to the threshold Eq. (3.20) for $\eta = 0$. However, for $\eta \neq 0$ this threshold is larger than the corresponding threshold in the SIR model Eq. (3.20).

The threshold to observe a paradoxical increase of the incidence rate in Community 1 φ_1 is obtained in the same way as described in Sec. 3.2.3:

$$R_{0,1} > 1 + \frac{(\mu + \eta)(\gamma + \mu + \eta)}{\gamma(\gamma + \mu) + (\mu + \eta)(\gamma + \mu + \eta)} \quad (3.50)$$

Again, this threshold becomes identical to the corresponding threshold in the SIR model, Eq. (3.22), for $\eta = 0$. The neutral travelling rate ε_n , at which the coupling leads to a prevalence level in Community 1 equal to the uncoupled case, is corresponding to Eq. (3.23)

$$\varepsilon_n = \frac{1}{2} \frac{\gamma(\gamma + \mu)}{\gamma + \mu + \eta} \left(R_{0,1} - 1 - \frac{(\mu + \eta)(\gamma + \mu + \eta)}{\gamma(\gamma + \mu)} \right). \quad (3.51)$$

Like in the SIR model, the condition for the neutral travelling rate to exist ($\varepsilon_n > 0$) is identical to the threshold for the paradoxical effect to occur. The travelling rate, too, becomes identical to its SIR counterpart Eq. (3.23) for $\eta = 0$, as expected.

The SIRS model is dynamically similar to the SIR model. The preceding results show that the paradoxical effect that the endemic states of two communities that are coupled do not approach each other is also a common feature of both models. Since the thresholds are different in the two models, the question whether typical diseases are expected to exceed these threshold and exhibit the paradoxical effects must be answered separately for the two models.

3.4 Discussion

The present work establishes a yet unknown paradigm. In stark contrast to the common believe, it is predicted that the health situation of a community (as quantified by the prevalence and the incidence rate) can paradoxically improve due to connections to communities with a worse health situation. On the contrary, the health situation can deteriorate due to coupling to communities with a better health situation.

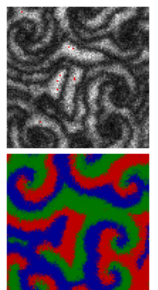
Self-evidently, the pertinent question is: “Can real diseases be expected to exhibit the paradoxical effects?” Typical human diseases that elicit life-long immunity and can thus be modelled in the SIR framework include measles, rubella, and mumps. These three diseases have basic reproductive ratios in the range 14-18, 6-16, and 14-18, respectively (see Anderson and May, 1991, and references therein). The threshold for both the prevalence and the incidence rate to exhibit the paradoxical effect for these diseases lies at around $R_0 > 1.006$ (assuming that the infectious period of the disease γ^{-1} is around a week and that the average generation time is $\mu^{-1} \approx 33$ years). The threshold is, hence, greatly exceeded, which is yet no peculiarity of these diseases. The reason for the low threshold is that the life expectancy of an individual is orders of magnitudes larger than the duration of these illnesses.

Provided that a disease exhibits the paradoxical effects in principle, the next question is which kind of connections can be expected to exhibit it. The neutral coupling strength gives an upper bound to the occurrence of the paradoxical effect (with respect to the prevalence) in terms of the symmetric travelling rate. For a disease with $R_0 = 16$ and the duration of the infectious period and the average generation time as above, the paradoxical effect persists up to travelling rates of around $375a^{-1}$. This means that for a disease like measles, rubella or mumps, the paradoxical effect will occur for any two communities between which individuals travel less often than once per day on average. This, however, applies to most human cities or villages.

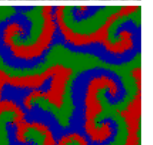
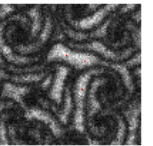
The same holds true for diseases that elicit only temporal immunity. The predominant example is mouth-and-foot disease in cloven-hoofed animals such as cows. Here, the threshold differs between different animal species because immunity wanes at different rates and the life expectancy of farm animals strongly depends on their use. In cows for example, immunity persists approximately for a year ($\eta = 1$) and the average life expectancy of a cow used for milk production is 5 years ($\mu = 0.2$). Assuming that infected cows remain infectious for about 5 days ($\gamma \approx 70$), the threshold for both the prevalence and the incidence rate to exhibit the paradoxical effect is around $R_0 > 1.02$. Although the reproductive ratio of mouth-and-foot disease varies considerably between 2-70 (Woolhouse et al., 1996), the thresholds are certainly exceeded. For these values, the corresponding neutral travelling rate lies between $0.1d^{-1}$ and $6.5d^{-1}$. The paradoxical effects of coupling infectious populations is, hence, not expected to be the exception but rather the rule.

The results in the present work, yet, depend on how coupling is introduced in the model. The finding in Sec. 3.2.5 that the present model can be considered as a special case of a model that allows for home locations of the individuals (Keeling and Rohani, 2002), raises the expectation that the results remain valid for at least a finite set of parameters in more general models. The finding in Sec. 3.2.5 that no paradoxical effects can occur in models that do not explicitly account for the migration of individuals suggests that migration is the decisive model property that is responsible for the occurrence of the paradoxical effects.

Spatial heterogeneities arise on many scales. It is therefore important to know in which cases the spatial heterogeneity has to be explicitly modelled and which cases it can be safely ignored. In this respect, the analysis in Sec. 3.2.4 shows that the impact of a



set of populations on a focal population can efficiently be modelled without explicitly accounting for the full spatial complexity of the non-focal populations when they have all either a smaller or all a larger infection rate. This suggests that regions can be grouped together when their disease parameters are well distinct from other regions. However, spatially resolved data of the infection rates is nonetheless necessary to correctly model the substitute community in this case.



Chapter 4

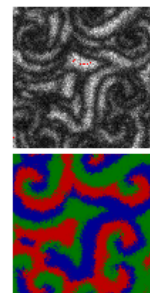
Conclusions and Outlook

In this dissertation, I studied the cyclic dynamics of spatially heterogeneous populations of three species for an ecological problem and an epidemiological problem.

In Chapter 2, the *lattice based population model* was introduced, which describes the interaction of three species that cyclically compete while they diffusively migrate and reproduce. Since it has been recognised that the mobility of individuals plays a pivotal role for the stability of coexistence, the question how to determine the critical mobility in a feasible way has become of central interest and motivated the present work.

The lattice based population model exhibits – as the original model by (Reichenbach et al., 2007a) – a transition from a spatially homogeneous, i.e., well-stirred state to a pattern forming state in which the three species form entangled and rotating spiral waves. By analysing the typical time at which one of the species becomes extinct first, I could show that this transition does not uniquely correspond to a transition from unstable coexistence to stable coexistence – as it was conjectured. I found that the typical time of extinction scales logarithmically with the system size for large mobilities, $t^* \propto \ln(N)$, and exponentially for very low mobilities, $t^* \propto e^N$, – confirming that coexistence is unstable and stable, respectively, in these two cases. However, I also found a broad regime in which the scaling of the typical time of extinction rather resembles a power law dependency, $t^* \propto N^\theta$ (see Sec. 2.3.2). This scaling implies that coexistence is only marginally stable, although spirals form in this mobility regime. Using the stability properties of coexistence is, hence, only of limited use to characterise the transition between the well-stirred and the spiralling state.

In contrast to this, the newly introduced carrying capacity allows to sharply determine the critical mobility that marks the onset of the formation of spirals. The analysis of the typical time of extinction reveals that it increases with a growing carrying capacity in the spiralling state but it decreases with a growing carrying capacity in the well-stirred state. These opposite behaviours allow to determine the critical mobility as the one for which both states influence the dependence of the typical time of extinction on the carrying capacity equally strong – turning it independent thereof (see Sec. 2.3.3). In contrast to earlier models, the introduction of the carrying capacity thus allows to



sharply discriminate the two dynamical regimes.

Apart from the question of stability, I also addressed the question of the *emergence* of cyclic competition among three species. The latticed based population model for four species allows to study under which conditions a (necessarily) unstable system of four species collapses to a system of three cyclically competing species (see Sec. 2.5). Here, I found that the probability that cyclic competition emerges after the first of the four species has become extinct exhibits a clear transition with regard to the mobility. While cyclic competition emerges for a low mobility, a mobility above a critical point ensures the emergence of a hierarchical competition. The mobility of individuals is thus not only pivotal to the stability but also to the emergence of cyclic competition among three species.

From the perspective of ecology, allowing more than one individual to coexist on a lattice site makes it possible to study more realistic and complex situations. In ecological systems, the assumption of a spatially homogenous environment for example is clearly a simplification. In general, the availability of resources will depend on local conditions like precipitation and soil fertility and will be subject to spatial stochastic fluctuations. Since the carrying capacity in the LBPM is not a property of the interacting species (like the reaction rates μ , σ , and ε) but a property of the environment, it is possible to model such a spatially heterogenous environment by introducing a space dependent carrying capacity $C(x, y)$.

From the perspective of evolutionary game theory, two player games are the simplest approach to social interactions. In general, the outcome of such interactions will depend on the strategic choices of more than two agents. The renowned Public Goods Game, being the n -person analogue of the Prisoner's Dilemma, is only one of many examples. In the LBPM the reaction rates generically depend on the make-up of the entire local population. As long as the carrying capacity is chosen to be larger than number of agents relevant to the outcome of the game, more complex games involving more than two interacting agents can easily be accounted for.

In the last years, cyclic competition in conjunction with the ability of individuals to migrate has attracted a lot of attention (Reichenbach et al., 2007a,b, 2008; Reichenbach and Frey, 2008; Peltomäki and Alava, 2008; Zhang et al., 2009; Shi et al., 2010; Wang et al., 2010; Yang et al., 2010; Ni et al., 2010; He et al., 2010, 2011; Wang et al., 2011; Rulands et al., 2011). The perhaps most relevant question that remains unsolved in this field pertains to the conditions under which three cyclically competing species form entangled travelling spiral waves. The model by Reichenbach et al. (2007a) and its consecutive studies possess the property that the overall population density is not conserved. Similar models where the overall population is conserved (e.g. Frean and Abraham, 2001) do not exhibit traveling spiral waves (Peltomäki and Alava, 2008; Reichenbach and Frey, 2008). Some authors, hence, believe that the question is settled (He et al., 2010). However, Ni et al. (2010) have employed a continuous space model of cyclic competition among species and observed the emergence of spirals even in the absence of individual mobility and despite a conserved overall population. The ques-

tion, which prerequisites are really necessary and which are sufficient for the formation of spirals thus remains open.

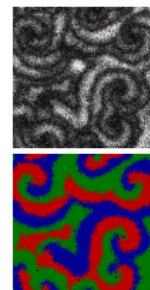
While the stability of cyclic competition among three species has attracted a considerable amount of interest, the question of the emergence thereof has been rarely addressed (Corl et al., 2010). In this respect, the study of a four species system is an important step in this direction as the emergence of cyclic competition is a promising subject for future studies.

In Chapter 3, a metapopulation model was introduced that describes spatially separated populations that are affected by a disease that elicits temporal or life-long immunity upon recovery. Since the influence of regional variations of, e.g., climatic conditions or cultural habits on the infection dynamics become ever more important in a modern world, this metapopulation model takes into account that the infection rate may vary from subpopulation to subpopulation.

In this framework, I could show that coupling two subpopulations does not necessarily cause the fraction of infectious individuals in the two subpopulations to approach each other. In contrast, coupling to a subpopulation with a higher fraction of infectious individuals can either lead to an increase or a decrease of the fraction of infectious individuals. If the infection rate of a population exceeds the threshold derived in Sec. 3.2.3 (for diseases that elicit life-long immunity) or Sec. 3.3 (for diseases that elicit temporal immunity), the fraction of infectious individuals paradoxically decreases upon coupling to a subpopulation with a higher fraction of infectious individuals. Equivalently, it increases upon coupling to a subpopulation with a lower fraction of infectious individuals. This paradoxical effect occurs as long as the travelling rate between the two populations is smaller than the *neutral travelling rate* (see Sec. 3.2.3 and Sec. 3.3). For larger travelling rates, the fraction of infectious individuals behaves as intuition suggests and approaches the level of the populations to which it couples.

This model furthermore allowed to study in which cases the dynamics of a spatially complex metapopulation can be effectively modelled as the dynamics of a single population. I could show that the influence that a set of populations exerts on a focal population can be modelled as the influence of a single substitute population if the infection rates in the populations of the set are either all smaller or all larger compared to the focal population. This suggests that regions can be grouped together when their disease parameters are well distinct from those in other regions.

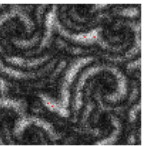
The recent threat of an influenza pandemic (Hufnagel et al., 2004) has fuelled the debate on the effectiveness of travel restrictions (Hollingsworth et al., 2006; Ferguson et al., 2006; Epstein et al., 2007; Bajardi et al., 2011). It is broadly accepted that travel restrictions alone are only capable to delay the spread of a disease up to some weeks. However, these studies all presume tacitly that the infection rate does not vary across the world. The paradoxical effects, which occur when spatial variation of the infection rate is allowed for, have potentially profound consequences for the design of such control measures. The present work shows that travel restrictions, trying to reduce travels to communities with lower health standards and to promote travels to



communities with higher health standards, can even have the opposite of the intended effect and exacerbate the health situation in the community.

Challenges that should be addressed in future works accordingly concern the design of control measures. Strategies that aim at eradicating or stemming diseases in spatially distributed populations by imposing travel restrictions should be designed with particular care with regard to a spatially varying infection rate. Most importantly, future studies should address the impact of spatially varying infection rates on the initial spread of a disease.

This work establishes that heterogeneity of the infection rate can have a profound impact on the effect of coupling on the endemic states of a disease. Since the present model omits epidemiological details like a latent phase of a disease, a temporal variation of the infection rate, or age groups, the validity of the results for different diseases remain to be established in future studies. Similarly, questions pertaining to the course of a disease or more generally the dynamics of proliferation when the infection rate depends on the location of infectious individuals, remain open and are important to be answered in the future.



Danksagung

Nach mehreren Jahren, in denen ich so viel Hilfe erfahren habe, ist es schwierig all jenen in angemessener Weise zu danken, die es verdient haben.

An erster Stelle möchte ich Theo dafür danken, dass ich diese Arbeit in seiner Abteilung anfertigen dürfte. Die Möglichkeiten, die man in der Abteilung für nichtlineare Dynamik hat, sind einzigartig. Der offene wissenschaftliche Austausch und die technischen Ressourcen sind genau so Theos Verdienst wie die Freiheit, die ich in den letzten Jahren genossen habe.

Ich möchte auch Herrn Prof. Dr. Reiner Kree dafür danken, dass er sich bereit erklärt hat, das Korreferat für diese Arbeit zu übernehmen.

Zu tiefem Dank bin ich Stephan und Jan für ihre stetige Unterstützung verpflichtet. Sie haben mich durch diese Jahre geleitet und begleitet und mich vermutlich mehr beeinflusst als ich zum jetzigen Zeitpunkt erkennen kann. Für Stephan war ich der erste Doktorand, den er betreut hat, und ich hoffe, dass er dieses erste Mal in besonderer Erinnerung behält.

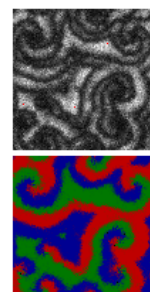
Ich danke auch Yorck, Denny und Marcus, die mir immer wieder geholfen haben, die Möglichkeiten zu nutzen, die wir in der Abteilung haben. Ohne sie wäre diese Arbeit so nicht möglich gewesen.

Genau so danke ich Jakob und Wolfgang, die mir immer wieder Tipps und kurze Einführungen gegeben haben, wie man mit Mathematica[©] umgeht.

Besonders bedanken möchte ich mich bei Ayse, Regina und Viktoryia, die täglich dafür gesorgt haben, dass ich mir keine Sorgen machen musste.

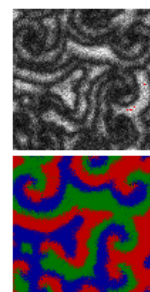
Zum Schluss habe ich die Freude, denen zu danken, die am meisten dazu beigetragen haben, dass ich diese Zeilen schreibe. Die Sicherheit und die Unterstützung in jeglicher Hinsicht, die mir meine Eltern immer gegeben haben, sind der Grund dafür, dass ich den Weg vom Beginn meines Physikstudiums in Bonn bis hierhin gehen konnte. Und auf diesem Weg hat mich vermutlich niemand mehr beeinflusst als mein Bruder. Auch wenn man es als ‘kleiner’ Bruder selten zugibt – in Teilen wird er immer mein Vorbild sein.

Vor ein paar Jahren ist Inga Teil meines Lebens geworden – ein Teil den ich nicht mehr verlieren möchte. Sie gibt mir das Gefühl, im Leben angekommen zu sein, und die Zuversicht und Gelassenheit, die ich brauchte, um diese Arbeit anzufertigen.



Bibliography

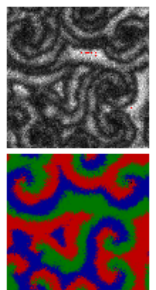
- Allesina, S. and Levine, J. M. (2011). A competitive network theory of species diversity. *Proc. Natl. Acad. Sci. USA*, 108:5638–5642.
- Anderson, R. M. and May, R. M. (1991). *Infectious Diseases of Humans*. Oxford University Press.
- Armstrong, R. A. and McGehee, R. (1980). Competitive exclusion. *The American Naturalist*, 115(2):151–170.
- Bajardi, P., Poletta, C., Ramasco, J. J., Tizzoni, M., Colizza, V., and Vespignani, A. (2011). Human mobility networks, travel restrictions, and the global spread of 2009 h1n1 pandemic. *PLoS one*, 6(1):e16591.
- Bartlett, M. S. (1957). Measles periodicity and community size. *J. R. Statist. Soc. A*, 120:48–70.
- Belik, V., Geisel, T., and Brockmann, D. (2011). Natural human mobility patterns and spatial spread of infectious diseases. *Phys. Rev. X*, 1:011001.
- Berr, M., Reichenbach, T., Schottenloher, M., and Frey, E. (2009). Zero-one survival behavior of cyclically competing species. *Phys. Rev. Lett.*, 102:048102.
- Bolker, B. and Grenfell, B. (1995). Space, persistence and dynamics of measles epidemics. *Phil. Trans. R. Soc. Lond. B*, 348:309–320.
- Brockmann, D., Hufnagel, L., and Geisel, T. (2006). The scaling laws of human travel. *Nature*, 439:462–465.
- Cameron, D. D., White, A., and Antonovics, J. (2009). Parasite-grass-forb interactions and rock-paper-scissor dynamics: predicting the effects of the parasitic plant *rhinanthus minor* on host plant communities. *J. Ecol.*, 97:1311–1319.
- Cardy, J. (1997). *Scaling and Renormalization in Statistical Physics*. Cambridge Lecture Notes in Physics. Cambridge University Press.
- Caron-Lormier, G., Humphry, R. W., Bohan, D. A., Hawes, C., and Thorbek, P. (2008). Asynchronous and synchronous updating in individual-based models. *Ecol. Model.*, 212:522–527.



BIBLIOGRAPHY

- Chopard, B. and Droz, M. (1998). *Cellular Automata Modeling of Physical Systems*. Cambridge University Press.
- Corl, A., Davis, A. R., Kuchta, S. R., and Sinervo, B. (2010). Selective loss of polymorphic mating types is associated with rapid phenotypic evolution during morphic speciation. *Proc. Natl. Acad. Sci. USA*, 107:4254 – 2459.
- Cross, M. and Greenside, H. (2009). *Pattern Formation and Dynamics in Nonequilibrium Systems*. Cambridge University Press.
- Czárán, T. L., Hoekstra, R. F., and Pagie, L. (2002). Chemical warfare between microbes promotes biodiversity. *Proc. Natl. Acad. Sci. USA*, 99(2):786–790.
- Davis, R. L. (1954). Structures of dominance relations. *Bull. Math. Biophys.*, 16:131–140.
- den Boer, P. J. (1986). The present status of the competitive exclusion principle. *Trends in Ecology & Evolution*, 1(1):25–28.
- Durrett, R. and Levin, S. (1994). The importance of being discrete (and spatial). *Theor. Popul. Biol.*, 46:363–394.
- Durrett, R. and Levin, S. (1997). Allelopathy in spatially distributed populations. *J. Theor. Biol.*, 185:165–174.
- Durrett, R. and Levin, S. (1998). Spatial aspects of interspecific competition. *Theor. Popul. Biol.*, 53:30–43.
- Dykhuisen, D. E. (1998). Santa rosalia revisited: Why are there so many species of bacteria? *Antonie van Leeuwenhoek*, 73:25–33.
- Earn, D. J. D., Rohani, P., and Grenfell, B. T. (1998). Persistence, chaos and synchrony in ecology and epidemiology. *Proc. R. Soc. Lond. B*, 265:7–10.
- Epstein, J., Goedecke, D. M., Yu, F., Morris, R. J., Wagener, D. K., and Bobashev, G. V. (2007). Controlling pandemic flu: The value of international air travel restrictions. *PLoS one*, 2(5):e401.
- Ferguson, N. M., Cummings, D. A. T., Fraser, C., Cajka, J. C., Cooley, P. C., and Burke, D. S. (2006). Strategies for mitigating an influenza pandemic. *Nature*, 442:448–452.
- Fisher, R. A. (1937). The wave of advance of advantageous genes. *Ann. Hum. Genet.*, 7(4):355–369.
- Frean, M. and Abraham, E. R. (2001). Rock-paper-scissors and the survival of the weakest. *Proc. R. Soc. Lond. B*, 268:1323–1327.
- Frey, E. and Reichenbach, T. (2011). Bacterial games. In *Principles of Evolution: From the Planck Epoch to Complex Multicellular Life*. Springer.

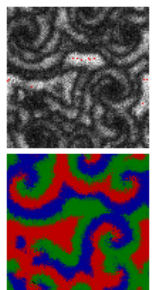
- Fulford, G. R. and Roberts, M. G. (2002). The metapopulation dynamics of an infectious disease: Tuberculosis in possums. *Theor. Popul. Biol.*, 61:15–29.
- Gardiner, C. (2009). *Stochastic Methods*. Springer Verlag, Berlin.
- Gilpin, M. E. (1975). Limit cycles in competition communities. *The American Naturalist*, 109(965):51–60.
- González, M. C., Hidalgo, C. A., and Barabási, A.-L. (2008). Understanding individual human mobility patterns. *Nature*, 453:779–782.
- Grassly, N. C., Fraser, C., and Garnett, G. P. (2005). Host immunity and synchronized epidemics of syphilis across the united states. *Nature*, 433:417–421.
- Grenfell, B. T. (1992). Chance and chaos in measles dynamics. *J. R. Statist. Soc. B*, 54(2):383–398.
- Grenfell, B. T. and Bolker, B. M. (1998). Cities and villages: infection hierarchies in a measles metapopulation. *Ecol. Lett.*, 1:63–70.
- Grenfell, B. T., Bolker, B. M., and Kleczkowski, A. (1995). Seasonality and extinction in chaotic metapopulations. *Proc. R. Soc. Lond. B*, 259:97–103.
- Hagenaars, T. J., Donnelly, C. A., and Ferguson, N. M. (2004). Spatial heterogeneity and the persistence of infectious diseases. *J. Theor. Biol.*, 229:349–359.
- Hanski, I. (1998). Metapopulation dynamics. *Nature*, 396:41–49.
- Hanski, I. and Gilpin, M. (1991). Metapopulation dynamics: brief history and conceptual domain. *Biol. J. Linn. Soc.*, 42:3–16.
- Harary, F. (1969). *Graph Theory*. Perseus Books, Reading.
- Hardin, G. (1960). The competitive exclusion principle. *Science*, 131(3409):1292–1297.
- Hassell, M. P., Comins, H. N., and May, R. M. (1991). Spatial structure and chaos in insect population dynamics. *Nature*, 353:255–258.
- Hassell, M. P., Comins, H. N., and May, R. M. (1994). Species coexistence and self-organizing spatial dynamics. *Nature*, 370:290–292.
- Hauert, C., Monte, S. D., Hofbauer, J., and Sigmund, K. (2002). Volunteering as red queen mechanism for cooperation in public goods games. *Science*, 296:1129–1132.
- He, Q., Mobilia, M., and Tauer, C. (2010). Spatial rock-paper-scissors models with inhomogenous reaction rates. *Phys. Rev. E*, 82:051909.
- He, Q., Mobilia, M., and Tauer, U. C. (2011). Coexistence in the two-dimensional may-leonard model with random rates. *Eur. Phys. J. B*, 82:97–105.



BIBLIOGRAPHY

- Heino, M., Kaitala, V., Ranta, E., and Lindström, J. (1997). Synchronous dynamics and rates of extinction in spatially structured populations. *Proc. R. Soc. Lond. B*, 264:481–486.
- Hethcote, H. W. and van Ark, J. W. (1987). Epidemiological models for heterogeneous populations: Proportionate mixing, parameter estimation, and immunization programs. *Math. Biosci.*, 84:85–118.
- Hollingsworth, T. D., Ferguson, N. M., and Anderson, R. M. (2006). Will travel restrictions control the international spread of pandemic influenza? *Nature Med.*, 12(5):497–499.
- Hufnagel, L., Brockmann, D., and Geisel, T. (2004). Forecast and control of epidemics in a globalized world. *Proc. Natl. Acad. Sci. USA*, 101(42):15124–15129.
- Hutchinson, G. E. (1959). Homage to santa rosalia or why are there so many kinds of animals? *The American Naturalist*, 93(870):145–159.
- Jackson, J. B. C. and Buss, L. (1975). Allelopathy and spatial competition among coral reef invertebrates. *Proc. Natl. Acad. Sci. USA*, 72:5160–5163.
- Jesse, M., Ezanno, P., Davis, S., and Heesterbeek, J. A. P. (2008). A fully coupled, mechanistic model for infectious disease dynamics in a metapopulation: Movement and epidemic duration. *J. Theor. Biol.*, 254:331–338.
- Kaitala, V., Ranta, E., and Lindström, J. (1996). Cyclic population dynamics and random perturbations. *J. Anim. Ecol.*, 65:249–251.
- Keeling, M. J. (2000). Metapopulation moments: coupling, stochasticity and persistence. *J. Anim. Ecol.*, 69:725–736.
- Keeling, M. J. and Rohani, P. (2002). Estimating spatial coupling in epidemiological systems: a mechanistic approach. *Ecol. Lett.*, 5:20–29.
- Keeling, M. J. and Rohani, P. (2008). *Modeling Infectious Diseases*. Princeton University Press.
- Kerr, B., Riley, M. A., Feldman, M. W., and Bohannan, B. J. M. (2002). Local dispersal promotes biodiversity in a real-life game of rock-paper-scissors. *Nature*, 418:171–174.
- Kolmogoroff, A., Petrovsky, I., and Piscounoff, N. S. (1937). Etude de l'équation de la diffusion avec croissance de la quantité de matière et son application à un problème biologique. *Moscow Univ. Bull. Math.*, 1:1–25.
- Kuperman, M. and Abramson, G. (2001). Small world effect in an epidemiological model. *Phys. Rev. Lett.*, 86(13):2909–2912.
- Lamouroux, D., Eule, S., Geisel, T., and Nagler, J. (2012). Discriminating the effects of spatial extent and population size in cyclic competition among species. *Phys. Rev. E*, 86:021911.

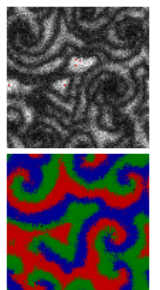
- Levins, R. (1969). Some demographic and genetic consequences of environmental heterogeneity for biological control. *Bull. Ent. Soc. Am.*, 15(3):237–240.
- Liu, Q.-X., Wang, R.-H., and Jin, Z. (2009). Persistence, extinction and spatio-temporal synchronization of SIRS spatial models. *J. Stat. Mech. Theor. Exp.*, 2009(7):P07007.
- Lloyd, A. L. and Jansen, V. A. A. (2004). Spatiotemporal dynamics of epidemics: synchrony in metapopulation models. *Math. Biosci.*, 188:1–16.
- Lloyd, A. L. and May, R. M. (1996). Spatial heterogeneity in epidemic models. *J. Theor. Biol.*, 179:1–11.
- Lugo, C. A. and McKane, A. J. (2008). Quasicycles in a spatial predator-prey model. *Phys. Rev. E*, 78:051911.
- May, R. M. and Anderson, R. M. (1984). Spatial heterogeneity and the design of immunization programs. *Math. Biosci.*, 72:83–111.
- May, R. M. and Leonard, W. J. (1975). Nonlinear aspects of competition between species. *SIAM J. Appl. Math.*, 29(2):243–253.
- Mobilia, M. (2010). Oscillatory dynamics in rock-paper-scissor games with mutations. *J. Theor. Biol.*, 264:1–10.
- Moon, J. W. and Pullman, N. J. (1967). On the powers of tournament matrices. *J. Comb. Theory*, 3:1–9.
- Murray, J. D. (1993). *Mathematical Biology*. Springer Verlag, Berlin, second edition.
- Nåsell, I. (1999). On the time to extinction in recurrent epidemics. *J. R. Statist. Soc. B*, 61:309–330.
- Ni, X., Wang, W.-X., Lai, Y.-C., and Grebogi, C. (2010). Cyclic competition of mobile species on continuous space: Pattern formation and coexistence. *Phys. Rev. E*, 82:066211.
- Novotny, V., Drozd, P., Miller, S. E., Kulfan, M., Janda, M., Basset, Y., and Weiblen, G. D. (2006). Why are there so many species of herbivorous insects in tropical rainforests? *Science*, 313:1115–1118.
- Nowak, M. A. (2007). *Evolutionary Dynamics*. Harvard University Press.
- Nowak, M. A., Bonhoeffer, S., and May, R. M. (1994a). More spatial games. *Internat. J. Bifur. Chaos*, 4(1):33–56.
- Nowak, M. A., Bonhoeffer, S., and May, R. M. (1994b). Spatial games and the maintenance of cooperation. *Proc. Natl. Acad. Sci. USA*, 91:4877–4881.



BIBLIOGRAPHY

- Nowak, M. A. and May, R. M. (1992). Evolutionary games and chaos. *Nature*, 359:826–829.
- Nowak, M. A. and May, R. M. (1993). The spatial dilemmas of evolution. *Internat. J. Bifur. Chaos*, 3(1):35–78.
- Pastor-Satorras, R. and Vespignani, A. (2001). Epidemic spreading in scale-free networks. *Phys. Rev. Lett.*, 86(14):3200–3203.
- Peltomäki, M. and Alava, M. (2008). Three- and four-state rock-paper-scissors games with diffusion. *Phys. Rev. E*, 78:031906.
- Post, W. M., DeAngelis, D. L., and Travis, C. C. (1983). Endemic disease in environments with spatially heterogeneous host populations. *Math. Biosci.*, 63:289–302.
- Ranta, E. and Vepsäläinen, K. (1981). Why are there so many species? spatio-temporal heterogeneity and northern bumblebee. *Oikos*, 36(1):28–34.
- Reichenbach, T. and Frey, E. (2008). Instability of spatial patterns and its ambiguous impact on species diversity. *Phys. Rev. Lett.*, 101:058102.
- Reichenbach, T., Mobilia, M., and Frey, E. (2007a). Mobility promotes and jeopardizes biodiversity in rock-paper-scissors games. *Nature*, 448:1046–1049.
- Reichenbach, T., Mobilia, M., and Frey, E. (2007b). Noise and correlations in a spatial population model with cyclic competition. *Phys. Rev. Lett.*, 99:238105.
- Reichenbach, T., Mobilia, M., and Frey, E. (2008). Self-organization of mobile populations in cyclic competition. *J. Theor. Biol.*, 254:368–383.
- Rohani, P., Earn, D. J. D., and Grenfell, B. T. (1999). Opposite patterns of synchrony in sympatric disease metapopulations. *Science*, 286:968–971.
- Rulands, S., Reichenbach, T., and Frey, E. (2011). Threefold way to extinction in populations of cyclically competing species. *J. Stat. Mech.*, 2011:L01003.
- Sahasrabudhe, S. and Motter, A. E. (2011). Rescuing ecosystems from extinction cascades through compensatory perturbations. *Nat. Commun.*, 2:170.
- Schipper, J. et al. (2008). The status of the world’s land and marine mammals: Diversity, threat, and knowledge. *Science*, 322:225–230.
- Schütt, M. and Claussen, J. C. (2010). Mean extinction times in cyclic coevolutionary rock-paper-scissors dynamics. arXiv:1003.2427v1.
- Shi, H., Wang, W.-X., Yang, R., and Lai, Y.-C. (2010). Basins of attraction for species extinction and coexistence in spatial rock-paper-scissors games. *Phys. Rev. E*, 81:030901(R).

- Simini, F., González, M. C., Maritan, A., and Barabási, A.-L. (2012). A universal model for mobility and migration patterns. *Nature*, 484:96–100.
- Sinervo, B. and Lively, C. M. (1996). The rock-paper-scissors game and the evolution of alternative male strategies. *Nature*, 380:240–243.
- Strogatz, S. H. (1994). *Nonlinear Dynamics and Chaos*. Westview Press.
- Szabó, G. and Czárán, T. (2001a). Defensive alliances in spatial models of cyclical population interactions. *Phys. Rev. E*, 64:042902.
- Szabó, G. and Czárán, T. (2001b). Phase transition in a spatial lotka-volterra model. *Phys. Rev. E*, 63:061904.
- Szabó, G. and Hauert, C. (2002). Phase transitions and volunteering in spatial public goods games. *Phys. Rev. Lett.*, 89(11):118101.
- Szabó, G. and Sznaider, G. A. (2004). Phase transition and selection in a four-species cyclic predator-prey model. *Phys. Rev. E*, 69(3):031911.
- Szabó, G., Szolnoki, A., and Borsos, I. (2008). Self-organizing patterns maintained by competing associations in a six-species predator-prey model. *Phys. Rev. E*, 77:041919.
- Tsodyks, M. V., Skaggs, W. E., Sejnowski, T. J., and McNaughton, B. L. (1997). Paradoxical effects of external modulation of inhibitory interneurons. *J. Neurosci.*, 17(11):4382–4388.
- van Saarloos, W. (2003). Front propagation into unstable states. *Phys. Rep.*, 386:29–222.
- Wang, W.-X., Lai, Y.-C., and Grebogi, C. (2010). Effect of epidemic spreading on species coexistence in spatial rock-paper-scissors games. *Phys. Rev. E*, 81:046113.
- Wang, W.-X., Ni, X., Lai, Y.-C., and Grebogi, C. (2011). Pattern formation, synchronization, and outbreak of biodiversity in cyclically competing games. *Phys. Rev. E*, 83:011917.
- Woolhouse, M. E. J., Haydon, D. T., Pearson, A., and Kitching, R. P. (1996). Failure of vaccination to prevent outbreaks of foot-and-mouth disease. *Epidemiol. Infect.*, 116:363–371.
- Xia, Y., Bjørnstad, O. N., and Grenfell, B. T. (2004). Measles metapopulation dynamics: A gravity model for epidemiological coupling and dynamics. *Am. Nat.*, 164:267–281.
- Yang, R., Wang, W.-X., Lai, Y.-C., and Grebogi, C. (2010). Role of intraspecific competition in the coexistence of mobile populations in spatially extended ecosystems. *Chaos*, 20:023113.



BIBLIOGRAPHY

- Zhang, F., Li, Z., and Hui, C. (2006). Spatiotemporal dynamics and distribution patterns of cyclic competition in metapopulation. *Ecol. Model.*, 193:721–735.
- Zhang, G.-Y., Chen, Y., and Qing, W.-K. Q. S.-M. (2009). Four-state rock-paper-scissors games in constrained newman-watts networks. *Phys. Rev. E*, 79:062901.

